An Investigation into Cellular Attachment and Contraction in Collagen-GAG Scaffolds with Characterized Pore Sizes

by

Andrew Michael Albers

B.S. Ceramic Engineering
Clemson University, 2001

SUBMITTED TO THE DEPARTMENT OF MATERIALS SCIENCE AND ENGINEERING IN PARTIAL FULFILLMENT OF THE REQUIREMENTS FOR THE DEGREE OF

MASTER OF SCIENCE IN MATERIALS SCIENCE AND ENGINEERING
AT THE
MASSACHUSETTS INSTITUTE OF TECHNOLOGY

SEPTEMBER 2004

Signature of Author: _____
Department of Materials Science and Engineering
July 21, 2004

Certified by: _____
Lorna J. Gibson
Matoula S. Salapatas Professor of Materials Science and Engineering
Thesis Supervisor

Accepted by: _____
Carl V. Thompson II
Stavros Salapatas Professor of Materials Science and Engineering
Chair, Departmental Committee on Graduate Students

An Investigation into Cellular Attachment and Contraction in Collagen-GAG Scaffolds with Characterized Pore Sizes

by

Andrew Michael Albers

Submitted to the Department of Materials Science and Engineering
on July 21, 2004 in Partial Fulfillment of the
Requirements for the Degree of Master of Science in
Materials Science and Engineering

ABSTRACT

Scaffolds fabricated from natural and man-made polymers have historically been used in partial- and full-thickness dermal wound beds to inhibit contraction and promote natural healing of tissue. By encouraging fibroblast migration and proliferation in the scaffolds, it is possible to reduce scar tissue formation and regenerate functioning dermis.

A series of experiments were performed to determine the effects of average pore size and available surface area in a lyophilized Collagen-GAG scaffold on the infiltration and attachment of dermal fibroblasts. An updated design of the Cell Force Monitor (CFM) was used to quantify bulk cellular contractile behavior in seeded scaffolds. The effect of scaffold geometry on fibroblast contractile behavior was also investigated with the CFM.

Results show that cellular seeding methods employed led to cellular agglomeration on the surfaces of the scaffolds, negating any possible correlation between internal available surface area and cellular attachment. It was also discovered that cell culture passaging techniques have more of an influence on cellular contractile behavior than scaffold pore size, given the seeding techniques employed in this study. No correlation was found between contractile behavior and scaffold geometry in the CFM.

Thesis Supervisor: Lorna J. Gibson
Title: Matoula S. Salapatas Professor of Materials Science and Engineering

Acknowledgements

I would like to thank the Interdisciplinary Research Cluster in Biomaterials and Tissue Engineering within the Cambridge-MIT Institute (Award #54/P) for the funding provided to complete this research. Academic funds were also provided by the Department of Materials Science and Engineering.

My gratitude goes to Drs. Debbie Chachra and Fergal O'Brien for their assistance and patience while I was getting my feet wet in the wacky world of cell culture and research in general.

I appreciate the emotional, spiritual, mental, and academic support of Abel Hastings, Megan Frary, and Robert Boyer.

Thanks also to Brendan Harley, Scott Vickers, and Tim Gordon, of the Yannas, Spector, and Grodzinsky lab groups, respectively, for their technical assistance and valuable knowledge of all things cellular, material, and mechanical.

Thanks to Katie Madden in the Division of Comparative Medicine for her fantastic support during the tissue harvest procedures. Thanks to Leslie Arnold and Michele Miele in Professor Edelman's lab for assistance in histology and cell culture.

I am grateful to Eric Soller for his assistance and expertise during the harvesting procedures. His wry humor and steady hand with a #10 blade were irreplaceable.

Thanks to Professors Ioannis Yannas and Myron Spector for their academic guidance and willingness to answer questions.

Finally, I owe many thanks to Lorna Gibson. Through the various weeks where my next best course of action was to run out of the lab screaming and pulling my hair out, Lorna's patience, kindness, and encouraging words always kept me coming back for one more try...

Table of Contents

Acknowledgements **5**

List of Figures **9**

List of Tables **11**

Chapter 1 Introduction **12**

1.1 Scaffold Characteristics 13

1.2 Tissue Harvesting 17

1.3 Scaffold Seeding 19

1.4 Cellular Contraction 23

Research Questions 29

Chapter 2 Materials and Methods **31**

2.1 Scaffold Fabrication 31

2.2 Tissue Harvesting 33

2.3 Cell Culture 35

2.4 Attachment Study: 24- and 48-hour runs 36

2.5 Embedding and Sectioning 37

2.6 SEM Imaging 38

2.7 Cell Force Monitor (CFM) 39

Chapter 3 Results **49**

3.1 Scaffold Fabrication 49

3.2 Tissue Harvesting and Cell Culture 49

3.3 Cell Culture 50

3.4 Cellular Attachment in Collagen-GAG Scaffolds, 24-and 48-Hour Trials 54

3.5 Cell Seeding on CFM Scaffolds 58

3.6 Cellular Distribution Through Scaffolds 59

3.7 SEM Imaging of Scaffolds 67

3.8 Contractile Behavior in Scaffolds 70

3.9 Aspect Ratio Results 78

Chapter 4 Discussion **82**

4.1 Scaffold Fabrication..... 82
4.2 Harvesting of Dermal Tissues..... 82
4.3 Cell Culture..... 84
4.4 Cell Seeding Considerations..... 85
4.5 SEM Image Analysis..... 89
4.6 Cell Force Monitor Considerations..... 90
4.7 Aspect Ratio Considerations..... 95

Chapter 5 Conclusions..... 96

References..... 99

Appendix 1 Dermal Fibroblast Isolation Procedure for Sprague-Dawley Rat..... 105

Appendix 2 Cell Culture Protocols..... 107

Appendix 3 Glycomethacrylate Embedding Protocol..... 110

Appendix 4 CFM Materials and Calibration..... 112

Biography..... 121

List of Figures

Figure 2.1 CFM setup for mass/force calibration..... 40

Figure 2.2 Calibration stage for proximity sensors..... 41

Figure 2.3 Dimensions for Calculation of K_{matrix} 42

Figure 2.4 Updated CFM..... 43

Figure 2.5 Updated CFM (detail)..... 44

Figure 3.1 Rat dermal fibroblast, P2..... 51

Figure 3.2 Rat dermal fibroblast, P5..... 52

Figure 3.3 Dutch Belted rabbit dermal fibroblast (P4); MC3T3 cells, same scale..... 53

Figure 3.4 Sprague-Dawley rat dermal fibroblast, P3, 5:1 split passaging..... 53

Figure 3.5 Sprague-Dawley rat dermal fibroblast, P3V ($5x10^5$/flask passaging)..... 54

Figure 3.6 24-hour rabbit dermal fibroblast cell seeding..... 55

Figure 3.7 48-hour attachment, rabbit dermal fibroblast..... 56

Figure 3.8 24-hour rat fibroblast attachment..... 57

Figure 3.9 MC3T3 through-thickness micrograph of -10 scaffold at t = 0 hr..... 60

Figure 3.10 Rat dermal fibroblast -10 scaffold, t = 0 hr. 62

Figure 3.11 Rat dermal fibroblast -10 scaffold, t = 24 hr..... 63

Figure 3.12 Rat dermal fibroblast -40 scaffold, t = 0 hr..... 64

Figure 3.13 Rat dermal fibroblast -40 scaffold, t = 24 hr..... 65

Figure 3.14 Rat dermal fibroblast -10 scaffold, t = 24 hr. ("non-shiny side")..... 66

Figure 3.15 Rat dermal fibroblast -40 scaffold, t = 0 hr. ("shiny" side)..... 66

Figure 3.16 Rat dermal fibroblast -40 scaffold, t = 24 hr. ("shiny" side)..... 67

Figure 3.17 Quenched Matrix scaffold surfaces..... 68

Figure 3.18 -10 Scaffold surfaces, uncoated..... 68

Figure 3.19 -10 Scaffold gold-coated (Images courtesy Amanda Blackwood, Olin College).... 69

Figure 3.20 -40 Scaffold, gold-coated (Images courtesy Amanda Blackwood, Olin College)... 69

Figure 3.21 -10 Scaffold, uncoated- detail of cross-section edges..... 69

Figure 3.22 Typical CFM scaffold-only response..... 71

Figure 3.23 CFM rat fibroblast-only contractile response for all -10 matrix runs (n=8)..... 72

Figure 3.24 CFM rat fibroblast-only contractile response for all -40 matrix runs (n=7)..... 72

Figure 3.25 Initial contraction rate for -10 scaffold..... 74

Figure 3.26 Initial contraction rate for -40 scaffold..... 75

Figure 3.27 1:1 aspect ratio run results, rat dermal fibroblasts (n=4)..... 78

Figure 3.28 3:1 aspect ratio run results, rat fibroblast (n=4)..... 79

Figure 3.29 1:3 aspect ratio run results, rat fibroblast (n=4)..... 79

List of Tables

Table 2.1 Freeze Drying program parameters (O'Brien, et al. 2004b) and Harley (unpublished) 32

Table 2.2 Scaffold sizes used (Note: "L" denotes length of scaffold between grips)..... 47

Table 3.1 Scaffold Physical Characteristics (O'Brien, et al. 2004a)..... 49

Table 3.2 Comparison of cellular density within scaffolds for seeding runs..... 55

Table 3.3 Cell seeding 22-hour attachment information from CFM runs..... 58

Table 3.4 Initial contractile slope, inflection point force, and 22-hour contractile per-cell force value (Significant difference denoted by *,@,#,$ for respective groups)..... 76

Table 3.5 Inflection point force grouped by passage contractile behavior (significant difference denoted by *,$,#,@)..... 77

Table 3.6 Results for Aspect Ratio CFM runs (Note: * or $ denotes statistical significance between groups, # denotes failed variance test)..... 81

Chapter 1 Introduction

One of the goals of tissue engineering involves the replacement of missing or diseased tissues with an artificial template that facilitates re-growth of normal, functioning tissue and facilitates the healing process as much as possible.

The insertion of this artificial, but biocompatible, material into dermal wound sites is aimed at inhibiting the contraction of the wound site that is seen in "normal", uninterrupted healing. The contraction of the dermal layer during the healing process leads to the formation of scar tissue in the healed skin. The desire to minimize contraction and scar formation results from the undesirable mechanical properties of scar tissue compared to uninjured skin. The inhibition of contraction has been shown as a critical requirement for regeneration of normal dermis (Yannas 2001). The mechanics and kinetics of undisturbed dermal wound contraction depend on the cellular behavior within the extracellular matrix (ECM). Cellular behavior, including adhesion, migration, contraction, and protein expression, is influenced by physical environment (ECM), as well as signaling pathways, genetic coding, and external mechanical stimuli.

The effect of mechanical structure of the ECM on cellular behavior can be studied *in vitro* by creating artificial structures that mimic natural ECM, the environment "seen" by cells *in vivo*. This investigation focuses on the *in vitro* attachment and contractile behavior of dermal fibroblasts inside a collagen-GAG dermal regeneration template, or scaffold, with known pore size, internal surface area, and modulus.

Background

1.1 Scaffold Characteristics

Hutmacher has stated that there are four main necessities to be addressed when designing a scaffold for use in bone and cartilage tissue engineering. These principles are general enough to apply to most areas of tissue engineering, and include (i) a three-dimensional, highly porous, interconnected pore network, (ii) biocompatibility and tunable bioresorbability, (iii) surface chemistry that promotes cell attachment, proliferation, and differentiation, and (iv) mechanical properties similar to the natural surrounding tissue at the implant site (Hutmacher 2000).

Scaffold construction

Scaffolds are fabricated using a variety of materials. Since biocompatibility is a key issue in any device to be implanted in the body, different synthetic, chemically inert polymers are often blended together to form a structure with the desired rigidity and degradation characteristics. Synthetic materials used include poly(glycolic acid), poly(L-lactide), poly(glycolide-co-caprolactone), and poly (lactic-co-glycolic acid) (Grande, Halberstadt et al. 1997; Chen, Ushida et al. 2001; Yang, Magnay et al. 2002; Lee, Kim et al. 2003). Natural polymers and materials utilized include alginate, hyaluronic acid, and various forms of collagen (primarily types I and II), combined with glycosaminoglycans (GAG), that are used to further modify the structure and more accurately mimic natural ECM (Yannas, Burke et al. 1980; Sheu, Huang et al. 2001; Perets, Baruch et al. 2003; Sachlos, Reis et al. 2003). Several laboratories have also experimented with hybrid scaffolds of synthetic and natural materials in an effort to obtain the positive characteristics of both (Kisiday, Jin et al. 2002; Rhee and Choi 2002; Zhao, Yin et al. 2002).

When investigating scaffolds for tissue engineering, the method used to construct the scaffold will have an influence over all four of the design principles cited above. The fabrication

processes most often referenced and utilized in the literature include lyophilization (freeze-drying), foaming, fiber bonding, three-dimensional printing, and porogen leaching (Chen, Ushida et al. 2001; Freyman, Yannas et al. 2001; Sachlos, Reis et al. 2003). Each of these techniques can take the same base material and create a scaffold with different void fraction, pore interconnectivity, pore size, and strut thickness. The native structure of the implant site should dictate the needed properties from above, in addition to necessary mechanical strength, bulk density, and half life (dissolution rate of the scaffold). Since each fabrication technique produces scaffolds with different properties, it is important to select the process that will produce the desired characteristics.

Cellular Attachment to Scaffold

Several strategies can be found in the literature for examining the attachment characteristics of cells to different biomaterial surfaces. The physical characteristics of constructs, such as pore size and bulk sample geometry, can influence the behavior of seeded cells. Cellular migration and contraction properties have been shown to differ in constructs of differing average pore sizes. Studies have shown that fibroblasts can cover pores of smaller size individually but utilize a cooperative bridging mechanism when encountering openings larger than the cell size. This bridging, however, is highly time-dependent, with smaller pores being covered or bridged more quickly than larger pores (Salem, Stevens et al. 2002). Seeding efficiency and cellular attachment have also been shown to increase with an increase in available surface area due to a decrease in average pore size (Yang, Shi et al. 2002; O'Brien 2004). It has also been shown that matrix composition influences cellular morphology of seeded cells (Nehrer, Breinan et al. 1998). Since morphology is directly related to the migration and contractile behavior of cells, it is important to know the extent to which cells are able change morphology within a specific physical environment.

In addition to the attachment properties of cells onto a 2D or 3D surface area, the force with which the cells adhere is also an important characteristic to know when designing a scaffold. The affinity for attachment of a cell to a surface will also influence the velocity and extent of migration (Park, Park et al. 2001), as well as the ultimate contractile force achievable (Brown, Sethi et al. 2002). Several laboratories have studied the effect of surface modification on traction forces (linked to contraction) generated by migrating fibroblasts (Dembo and Wang 1999; Beningo, Dembo et al. 2001; Munevar, Wang et al. 2001; Clark, An et al. 2003).

Many groups are trying to understand the biological fundamentals of cellular attachment through investigation of the intra- and intercellular proteins and enzymes that are involved in adhesion. The attachment of cells onto biomaterial surfaces is mediated by integrin-receptor interaction. The modification of biomaterial surfaces to include or exclude certain receptors can affect the extent to which cells attach to and contract an artificial substrate (Sethi, Mudera et al. 2002). Man-made polymers (PGA, PLLA, PLGA, etc.) do not naturally contain these receptors, so they must be coated with proteins to promote cellular adhesion. Briefly, cells have certain pairs of integrins, an "α" tail and a "β" tail, that map to certain receptors. The receptors can be found in proteins and natural materials such as collagen, fibronectin, vitronectin, and laminin (Giancotti and Ruoslahti 1999). The amino sequence "RGD", signifying a specific sequence of arginine, glycine, and aspartic acid within a larger peptide chain, has been identified in many receptors and is linked to cellular adhesion in multiple cell types (Ruoslahti and Pierschbacher 1987; Hersel, Dahmen et al. 2003). Since type I collagen naturally contains the RGD sequence involved in integrin-receptor adhesion, the collagen-GAG scaffolds used in this study already contain binding sites known to be utilized by fibroblasts during attachment, migration, and contraction (Tamariz and Grinnell 2002).

GAG Functionality

The scaffolds used in the study contain ~8wt.% glycosaminoglycan (GAG) in the form of Chondroitin-6 Sulfate, in addition to the type I collagen. The GAG helps to precipitate out the native collagen from the acidic solution during the scaffold fabrication process and is involved in the partial covalent bonding of the scaffold. The extent of covalent bonding is a main determining factor in the half-life of the scaffold (Yannas and Burke 1980). The elution rate of GAG during degradation of an implanted scaffold can be tuned by altering crosslinking technique in the scaffold (Yannas, Burke et al. 1980). The addition of GAG to pure collagen also increases the elasticity and fracture energy of the scaffold, leading to greater ease of handling during implantation and *in vitro* experimentation (Yannas and Burke 1980). The negatively charged GAG side chain Chondroitin-6 Sulfate is found in differing quantities in different tissues of human and animal subjects, so biocompatibility is not a factor (Yannas 2001).

Crosslinking Techniques

Crosslinking technique also influences the physical characteristics of the scaffold. The crosslinking treatment utilized can affect degradation rate and elastic modulus of the scaffold (Lee, Grodzinsky et al. 2001). Several crosslinking techniques and chemicals are commonly used, including glutaraldehyde (GTA), 1 ethyl-3-(3-dimethylaminopropyl) carbodiimide (EDAC), ultraviolet (UV), transglutaminase, and dehydrothermal treatment (DHT) (Lee, Grodzinsky et al. 2001; Orban, Wilson et al. 2004; Pek, Spector et al. 2004). While the chemical means of GTA, EDAC, and transglutaminase require aqueous treatment of the scaffold (and sometimes subsequent dehydration, chemical-leaching, and sterilization steps), the DHT and UV techniques maintain a dry scaffold and achieve crosslinking and sterilization in a single processing step (Lee, Grodzinsky et al. 2001).

Mechanical properties of the collagen-GAG scaffold

Testing of the mechanical properties of the collagen-GAG matrix used in this study has been undertaken by Freyman (2001c) and more recently Harley [unpublished]. The effect of crosslinking on modulus and stiffness of collagen-GAG scaffolds has also been investigated by Torres, et. al (2000) and Pek, et. al (2004). The importance of creating a scaffold with elastic modulus similar to natural skin is important because dermal fibroblasts have been found to contract to a specific internal force generation (Freyman, Yannas et al. 2002). As noted by numerous studies, strain generated by fibroblasts during wound healing leads to scar formation, so inhibition of contraction, either by mechanical or chemical means, is a key to regeneration of healthy, functioning dermis (Yannas 2001; Nien, Han et al. 2003).

1.2 Tissue Harvesting

During harvesting procedures, it is critical to know the structure of the tissue type being harvested. For dermal harvesting, a general knowledge of the composition of the different layers of skin is necessary in order to ensure that the correct cell type is harvested. In short, there are five critical layers of the integument (or what is referred to in general as "skin") that need to be visualized and defined during a harvesting procedure. These layers include (described from the outer surface inward);

a) epidermis, actually a 5-layer structure itself, and is easily distinguishable from the dermis because it is non-vascularized
b) basement membrane, which has a more shiny, whitish, gummy appearance than the epidermis, and is much thinner than the epidermis
c) papillary dermis, the outer layer of dermis that has a higher cellular density than
d) reticular dermis, characterized by thicker collagen fibrils than papillary dermis
e) subcutaneous layer, often fatty, that separates the dermis from any muscular layers or internal organs (Hebel 1976; Marieb 2003).

In the case of dermal harvesting, it has been shown that the fibroblasts found in papillary dermis exhibit better proliferative capacity in cell culture compared to reticular dermis (Harper and Grove 1979), but both layers are capable of producing viable fibroblast cultures.

Harvesting Procedures

The simplest means of harvesting tissues involves removal of the entire integument layer and subsequent treatment of the explant with specific enzymes (see Digestion Techniques) to isolate and eliminate certain tissues. In order to further isolate a specific tissue type from aggregate tissue, several techniques can be employed during the harvest procedure. Troxel harvested skin from guinea pigs using a two-fold dermal separation process, with the first cut taking off the epidermis and papillary dermis and the second cut removing the reticular dermis. The first layer was vortexed to separate off the epidermis from the dermis, and then both layers of dermis were treated with a solution of Collagenase and Dispase (Troxel 1994). Freyman used an outmigration procedure in which the epidermis and dermis were separated by Dispase, the dermis minced, and pieces of tissue were placed in a flask and cells were allowed to migrate out over the course of two weeks (Freyman, Yannas et al. 2001). Other researchers have used similar procedures to remove the entire dermal layer from Sprague-Dawley rats, but have separated harvested cells from ECM with a serial digestion method utilizing graded concentrations of dissociation enzymes (Strobel, Cady et al. 1986).

Digestion Techniques

Depending on the tissue type harvested, different enzymes exist to disaggregate tissue and free cells from the surrounding ECM. Collagenase (types I-IV) and Dispase are two enzymes that are often used in explant tissue separation procedures. Trypsin can also be used to separate cells from ECM (Salzman 1961; Worthington Biochemical Corporation 2003). Collagenase works by cleaving a single peptide bond in the collagen molecule between specific amino acids

(Yannas 2003). The resulting fragments of the collagen molecule unravel and gelatinize, leading to disaggregation of the tissue and liberation of embedded cells. Dispase works by dissolving the basement membrane, effectively cleaving the epidermis from the dermis without disrupting the cell membrane (Invitrogen 2001). Trypsin is an enzyme that acts to digest nonspecific peptide bonds. It is not often used alone as a tissue dissociation enzyme, but often is used in tandem with Collagenase to liberate cells from denatured collagen/ECM fragments (Worthington Biochemical Corporation 2003).

Once a viable harvest method is established, culturing of cells can proceed until the desired passage number or quantity of cells is obtained. The effects of culturing on cells depends largely on the way in which the cellular environment changes during passaging and subculturing. Trypsin-EDTA is most often used to separate cells from the culture substrate. The use of fetal bovine serum in media can reverse the nonspecific peptide cleavage enacted by Trypsin, effectively "cleaning" the cell membrane of any detrimental or obstructive coating. Cellular contraction and attachment on a biomaterial surface has been shown to be highly dependent on the availability of both integrin and receptor sites, as discussed earlier. The assumption made throughout this study is that culture and harvest techniques, as well as biomaterial fabrication procedures, do not inhibit or eliminate integrin-receptor activity.

1.3 Scaffold Seeding

When designing biomaterial devices, it is necessary to create a construct that has ample sites for cellular attachment (surface area), interconnected pathways to promote maximum cellular infiltration and mobility (interconnectivity of pores), and degradation resistance to allow enough time for cells to migrate in and begin creating new ECM (scaffold half-life).

Work done in this lab by Pek, et. al (2004) on the degradation rates of collagen-GAG scaffolds, coupled with the results of O'Brien, et. al on pore size engineering of collagen-GAG scaffolds (2004a,b), left a need for further *in vitro* characterization of the cellular infiltration,

attachment, and contractile capabilities of the scaffolds. To accomplish this, the scaffolds previously described were seeded with dermal fibroblasts from both Dutch Belted rabbits and Sprague-Dawley rats, as detailed in Materials and Methods below.

In general, the seeding of artificial biomaterial constructs has been investigated with respect to several different tissue architectures. In the area of bone engineering, many laboratories are attempting to characterize cellular behavior in and on porous mineral scaffolds that mimic bone (Tampieri, Celotti et al. 2001; Werner, Linner-Krcmar et al. 2002). Hybrid structures also exist in polymer-ceramic composite form in an effort to obtain desirable properties of cellular interaction with both materials (Rhee and Choi 2002; Zhao, Yin et al. 2002). Laboratories have also created collagen gels and peptide hydrogels with pre-embedded cells, thus eliminating the possibility of inefficient or non-uniform seeding. These constructs hold the cells in place, allowing them to proliferate, migrate, and produce their own natural ECM over time. The cell-seeded material can be cultured for several weeks and later used for implantation or just studied *in vitro* (Hinz, Celetta et al. 2001; Kisiday, Jin et al. 2002; Hinz, Dugina et al. 2003; Nien, Han et al. 2003; Orban, Wilson et al. 2004). There also exist strategies to directly inject cell-carrying microspheres into the internal wound site, thus eliminating the need for implantation of scaffolds, seeded or unseeded (McGlohorn, Grimes et al. 2003).

When the decision is made to use an artificial scaffold in cell seeding experimentation, several variables must be decided upon. For instance, it is debated in the literature whether pre-wetting of the scaffolds is necessary. Some reviews maintain that pre-wetting is necessary for all scaffold types in order to displace the air inside the bulk to maximize available cellular attachment sites (Vunjak-Novakovic 2003). Some studies have shown that pre-wetting does not affect the contractile behavior of seeded cells (Nehrer, Breinan et al. 1997). Still other studies require pre-wetting in a specialized solution in order to facilitate cellular attachment to receptor-deficient biomaterials. When pre-wetting is carried out, several different liquids have been utilized; pure serum (to reduce the hydrophobicity of nylon scaffolds) (Grande, Halberstadt et al.

1997), collagen solution (to enhance cellular attachment to PLLA scaffolds) (Yang, Magnay et al. 2002), complete media (Nehrer, Breinan et al. 1997; Freyman, Yannas et al. 2002; Zhao, Yin et al. 2002; Vunjak-Novakovic 2003), phosphate-buffered saline solution (PBS) (Marty-Roix, Bartlett et al. 2003), and even distilled water (Lee, Grodzinsky et al. 2001). The hydration incubation time of scaffolds varied in the studies from 30 minutes to 24 hours.

Scaffolds were not pre-wet in all cases before seeding. Dry-seeded scaffolds were used in experimentation in several cases (Grande, Halberstadt et al. 1997), including the previous study done by members of this laboratory that served as the basis for the current research (O'Brien 2004).

Once the question of pre-wetting is answered, the next step is to determine the actual method of seeding the cells onto or into the scaffold. Of the various techniques found in the literature, the most popular methods include static seeding, rocker tube seeding, spinner flask seeding, and centrifugal seeding.

Static seeding involves the pipetting of the cells onto the surface of a dry or pre-hydrated scaffold and allowing attachment to commence in an incubator for a set amount of time before *in vitro* experimentation (Grande, Halberstadt et al. 1997; Nehrer, Breinan et al. 1997; Torres, Freyman et al. 2000; Sheu, Huang et al. 2001; Yang, Magnay et al. 2002; Zhao, Yin et al. 2002). In a similar technique, cell suspensions were not pipetted onto the dry surface of the scaffolds, but rather injected into the dry interior of the scaffolds and incubated for a set period of time to facilitate attachment before *in vivo* implantation (Lee, Kim et al. 2003).

Rocker/roller tube seeding is a dynamic seeding technique that involves adding a cell suspension to a centrifuge tube or multi-well plate containing a pre-wet scaffold. The tube or multiwell plate is placed on a rocker/shaker or tube roller for a set amount of time to facilitate attachment (Lee, Grodzinsky et al. 2001; Zeltinger, Sherwood et al. 2001). The inert surface of the polyethylene centrifuge tubes precludes the attachment of cells onto the tube walls, so only the scaffold itself contains cell binding sites.

In spinner flask seeding, scaffolds are either suspended or free-floating in a flask. A cell suspension is added to the flask and a stir bar is used to keep the cells in suspension for the duration of the seeding experiment (Vunjak-Novakovic 2003). The time required for effective seeding when using the spinner flask method (sometimes as high as 24 hours) is one of the main drawbacks of this technique (Vunjak-Novakovic, Obradovic et al. 1998).

In another technique, centrifugal force is used to embed cells in scaffolds. Essentially, cells are pipetted onto the top surface of a scaffold and then subjected to a centrifugal force for a set amount of time. The centrifugal force encourages migration of the cells through the thickness of the scaffold. In studies conducted with low cell concentrations, the centrifugation method was found to produce higher seeding efficiencies compared to other seeding techniques (Yannas, Lee et al. 1989; Godbey, Hindy et al. 2004).

Cellular Density Considerations

The cellular seeding density within the scaffold can affect the contractile behavior, mitotic activity, and extent of migration of seeded cells. For many *in vitro* experiments, the cellular seeding density is much lower than in natural *in vivo* skin. Cellular extraction numbers in guinea pig dermis has been reported to be on the order of $5x10^5$ cells/mm^3 (Yannas, Lee et al. 1989). It should be noted that the particular harvest procedure used in the study contained epidermal, basal, and dermal cells. In bovine articular cartilage, the cellular density has been observed to range from between $3x10^8$ cells/cm^3 to $1 x10^8$ cells/cm^3 ($3 x10^5$ - $1 x10^5$ cells/mm^3) (Williamson, Chen et al. 2001).

Results of seeding experimentation in scaffolds have been reported for cellular concentrations of 1,100, 1,700, 2,500, 9000, 10,000, 25,000 per mm^3 (Grande, Halberstadt et al. 1997; Freyman, Yannas et al. 2001; Lee, Grodzinsky et al. 2001; Sheu, Huang et al. 2001; Zhao, Yin et al. 2002). Results show that higher cell seeding concentration can lead to increased seeding efficiency and linearly increased contractile response (Freyman, Yannas et al. 2001).

Studies have also shown that a threshold level of cellular density is needed in order to elicit a bulk contractile response (Tamariz and Grinnell 2002).

Cell Residence Time

The last important parameter considered in cellular seeding is incubation time. The effect of time on cellular attachment to a substrate or a construct has been studied by many groups. In most cases, increasing residence time of cells on a treated surface or scaffold leads to increased adhesion strength and seeding efficiency (Freyman 2001; Freyman, Yannas et al. 2001; Reyes and Garcia 2003). Contractile force generation has also been shown to be highly time-dependent, with asymptotic force generation levels in published systems occurring only after several (6-12) hours of incubation after the initial seeding period (Delvoye, Wiliquet et al. 1991; Eastwood, Mcgrouther et al. 1994; Brown, Prajapati et al. 1998; Cacou, Palmer et al. 2000; Freyman, Yannas et al. 2001; Knezevic, Sim et al. 2002; Campbell, Clark et al. 2003).

1.4 Cellular Contraction

It has been more than 140 years since Langer first observed lines of tension in cadaver skin, leading to the hypothesis that cells are capable of generating mechanical force (Silver, Siperko et al. 2003). Since then, many researchers have attempted to determine the origin, extent, and reason for this contractile ability. Contractile behavior has also been observed in multiple cell types, from dermal fibroblasts to peripheral nerve cells, articular cartilage, ligament/tendon cells, and even osteoblasts (Spector 2002). The main protein that is implicated as a marker of contractile response in cells is α-smooth muscle actin (α-SMA), which can be detected by various staining procedures. The conditions that lead to the expression of α-SMA are still under investigation. It is known that transforming growth factor-β_1 (TGF-β_1) induces expression of α-SMA (Desmouliere, Geinoz et al. 1993; Malmstrom, Lindberg et al. 2004), but the exact activation pathways used by TGF-β_1 are still under investigation (Brown, Sethi et al. 2002).

One thing known for certain is that contractile behavior of dermal fibroblasts is an integral part of the healing process. In an effort to close up the wound site and prevent infection, cells generate internal tensional forces and transfer that force to the substrate they are adhered to, most commonly the extracellular matrix (ECM) *in vivo*. It is well known that generation of contractile forces has been implicated in scar formation and that the rigidity of scar tissue reduces range of motion, making it inferior to uninjured dermis.

Research undertaken in the realm of wound healing has focused on treatment of the wound bed with an artificial construct capable of mechanically inhibiting contraction and hosting migrating fibroblasts and epithelial cells (Yannas 2001; Yannas 2003). In order to create more biocompatible constructs from a chemical, structural, and geometrical standpoint, much work has been undertaken *in vitro*. The benefits of *in vitro* research include simplicity of design, cost-effectiveness, and large-scale repeatability. The drawbacks include cellular phenotype changes associated with increased residence time in culture, a lack of understanding of all the signaling pathways and proteins involved in *in vivo* cellular function, and the need for constant replenishment of nutrients and proteins in quantities that mimic body fluid composition during the healing process.

Once the decision is made to do *in vitro* work, there exist several documented setups for measuring the contractile forces generated. The main decision to be made when looking at generation of forces by cells is whether to look at bulk contraction of a construct by many cells or contraction of an individual cell.

Bulk Contraction

Measuring the bulk contraction of a scaffold or gel can give information about the general contractile response of a population of cells. The bulk response is useful because it can give a contractile response influenced by multicellular signaling and interference, either from a mechanical or chemical standpoint. The cooperative response, however, is dependent on the cell

seeding density approaching a minimum threshold necessary for cell-cell interaction. In fact, studies have shown that apoptosis can occur in less than 10 hours if cell-cell interaction is blocked or inhibited, as can be achieved by low seeding density (Bates, Buret et al. 1994). This assumes that cells are evenly distributed throughout the scaffold. A complication of looking at bulk contractile response is the difficulty in obtaining information regarding the percentage of cells that are actually involved in the contraction. When cells are grouped together, the cellular response is different than when isolated cells are attached to a scaffold strut. It has been shown in numerous studies that seeding to higher densities improves cell-cell interactions and can lead to higher bulk force generation (Freyman, Yannas et al. 2001; Dvir-Ginzberg, Gamlieli-Bonshtein et al. 2003). Several general setups exist for measuring bulk contractile behavior of cells in artificial constructs. These are described below:

Free-Floating Scaffold/Gel

In free-floating contractile studies, samples, usually round, are cut from scaffold sheets or formed individually as gels. The dimension change due to contraction of the constructs is measured over time. If the modulus of the construct is known, the cell-mediated contractile force can be calculated (Torres, Freyman et al. 2000; Kinner and Spector 2001; Lee, Grodzinsky et al. 2001; Veilleux, Yannas et al. 2004). This force is generated solely by the migration and contraction characteristics of the cells themselves, without any external mechanical stimuli, a condition that is not found *in vivo*. Because of this, several studies conclude that cellular behavior in untethered constructs is inherently different than cellular response in mechanically loaded or tethered systems and therefore the two setups can not be directly compared (Brown, Prajapati et al. 1998; Brown, Sethi et al. 2002).

Tethered Scaffold/Gel

Artificial constructs are typically tethered such that only uniaxial contractile behavior is measured (Delvoye, Wiliquet et al. 1991; Eastwood, Mcgrouther et al. 1994; Cacou, Palmer et al. 2000; Freyman, Yannas et al. 2001; Campbell, Clark et al. 2003), though some setups found in the literature utilized a biaxial system (Knezevic, Sim et al. 2002). All systems were capable of resolving bulk contraction into cell-generated contractile force. One area where the systems differed, however, was in how the gels or scaffolds were pre-loaded with a specific resistance/weight. The constructs were pre-loaded either mechanically or by altering the properties of the constructs or measuring device. The resistance was often used as an experimental parameter to determine whether the change in resistance felt by the cells affected cellular behavior. In one case, the contractile response exhibited by seeded fibroblasts was found to be independent of the resistance felt by the cells (Freyman, Yannas et al. 2002). In other cases, while the resistance felt by cells was not directly correlated to the individual cell contraction, a decrease in bulk contraction was seen with an increase in external resistance (Knezevic, Sim et al. 2002).

Individual Cellular Contraction

As an alternative to measuring bulk contractile behavior of a population of cells, the individual force generation capability of cells has been measured in several different experimental setups. By looking at the extent to which attached cells contract and wrinkle specialized, characterized substrates, it is possible to calculate the forces generated by individual cells during migration (locomotion) and contraction (Dembo and Wang 1999; Pelham and Wang 1999; Wrobel, Fray et al. 2002). In other setups, microfabricated beds of needles have been used as a substrate for cellular adhesion. The bending moment of the individual needles is used to calculate individual cell forces generated during migration and contraction (Tan, Tien et al. 2003). The advantage of individual cell contraction data is offset by the lack of cell-cell interaction, a critical

factor in ECM remodeling. Also, the results from cell-substrate interactions only quantify the 2D response of cells in culture. It has been shown in studies that cellular behavior changes when comparing 2D and 3D environments (Tamariz and Grinnell 2002; Grinnell, Ho et al. 2003). However, from a migration standpoint, the measurement of 2D forces generated can be used to predict the effectiveness of substrate/construct materials used *in vivo* in both 2D and 3D architectures.

Force Generation Quantification

Once the experimental setup is determined, the actual quantification of contractile forces generated by seeded cells can be obtained in several ways. In most setups, the force can be determined by calculating the strain induced in the gel or scaffold (by measuring the deflection of a beam or embedded particles in the construct or by measuring the bulk dimension change over time) and coupling it to the measured modulus of the construct. For the 2D substrate experiments, the buckling strength of the substrate can be calculated through characterization of the material properties and coupled to the strain generated in the substrate in order to find the force generated by attached cells. As far as individual cell force generation numbers are concerned, obtained either from substrate experiments or normalized bulk experiments, the forces reported vary up to two orders of magnitude between cell type and experimental setup. From the literature, the following values arise: 0.1- 0.6nN/cell for human dermal fibroblasts (Eastwood, Mcgrouther et al. 1994; Brown, Prajapati et al. 1998; Campbell, Clark et al. 2003), 1nN/cell for rabbit dermal fibroblasts (Freyman, Yannas et al. 2001), 1.0-1.4nN/cell for canine articular chondrocytes (Zaleskas, Kinner et al. 2004), 1.4mN/10^6 cells (corresponding to 1.4nN/cell) for rat cardiac fibroblasts (Knezevic, Sim et al. 2002), 2.0-2.2nN/cell for human dermal myofibroblasts and fibroblasts (Wrobel, Fray et al. 2002), and up to 50nN force generated by contracting cellular processes in bovine pulmonary artery smooth muscle cells (Tan, Tien et al. 2003). The numbers based on bulk contractile forces measured may actually underestimate the contribution of

individual cells to the generation of contractile force due to the fact that not all attached cells are involved in contraction at any given time (Kinner and Spector 2001).

As detailed earlier, cells attach to collagen fibrils by means of an integrin-mediated process and can begin to contract only after this attachment takes place. Given that the contraction will happen due to column buckling of these collagen fibrils, the dimensions will necessarily change as this process evolves. If the scaffold is isotropic in design and seeding is assumed to be uniform throughout the scaffold, then the overall dimension change would also be expected to progress in an isotropic fashion. In the case of uniaxial cyclic loading of scaffolds, cells have been shown to respond to the applied force by aligning themselves along the axis of principal strain in order to minimize the strain "felt" by the total body (Delvoye, Wiliquet et al. 1991; Eastwood, Mudera et al. 1998; Wang, Yang et al. 2004). In these cases, the contraction should proceed in an anisotropic fashion, with the major axis of contractile behavior being along the line of applied force. In a system without external forces applied, as with the free-floating experimentation, the cellular response appears to be more dependent on cell density and the physical properties of the scaffold (Nehrer, Breinan et al. 1998; Tamariz and Grinnell 2002; Wrobel, Fray et al. 2002; O'Brien 2004). In these cases, the contraction is observed to occur in the expected isotropic fashion. When looking at dimensional changes of an anisotropically contracting scaffold, it is not known what influence the surface and edge effects are expected to contribute to any observed contractile response. To that end, the aspect ratio of the mechanically impinged scaffold or gel may or may not play a role in contractile response. In cyclic loading setups, the aspect ratio of the construct has been shown to influence the directional alignment and contractile response of attached cells. When subjected to the same cyclic loading pattern and magnitude, the aspect ratio of the scaffold influenced the amount of strain "felt" by the cells, and the cells responded accordingly (Eastwood, Mudera et al. 1998).

Several research questions form the basis for this investigation:

1.) What is the seeding efficiency for dermal fibroblasts in collagen-GAG scaffolds with different average pore sizes (and corresponding different specific surface areas)?

2.) How does the contractile behavior of dermal fibroblasts depend on pore size and surface area in a collagen-GAG scaffold?

3.) How does the contractile behavior of dermal fibroblasts depend on the aspect ratio of mechanically impinged collagen-GAG scaffold?

The following sections detail the work undertaken in this investigation:

Chapter 1 presented a history of the processes, complications, and advances made in previous experimentation carried out in this and other laboratories.

Chapter 2 describes the materials and methods used in scaffold fabrication, tissue harvesting, and cell culture. Collagen-GAG scaffold seeding and cellular attachment quantification methodologies are also presented, as well as the setup and execution of CFM runs measuring the *in vitro* contractile response of dermal fibroblast cells in collagen-GAG scaffolds

Chapter 3 presents the results from the experiments described above, including the quantification of cell attachment percentage based on average pore size of the scaffolds used, the cellular contractile response as a function of pore size in restrained collagen-GAG scaffolds, and cellular contractile response as a function of the aspect ratio of mechanically restrained scaffold

Chapter 4 includes a discussion of the results, including the effects of passaging and culture conditions on cellular behavior *in vitro* and the effects seen on the above experimentation. It also includes an analysis of the effects of scaffold seeding technique on seeding efficiency and the mechanisms of cellular attachment in this study and the similarities and differences to *in vivo* behavior. The *in vitro* contractile response of cells seeded in artificial tissue engineering constructs and the mechanisms of cooperative behavior in cellular contraction of collagen-GAG scaffolds are discussed as well.

Chapter 5 gives brief conclusions and recommendations for future related research work.

Chapter 2 Materials and Methods

2.1 Scaffold Fabrication

Collagen-GAG slurry preparation

A mixture of collagen and chondroitin-6 sulfate in 0.05M acetic acid was prepared according to previously published protocols (Yannas, Lee et al. 1989; O'Brien, Harley et al. 2004b). Briefly, 3.6 grams microfibrillar collagen from bovine tendon (Integra Life Sciences, Plainsboro, NJ) was added to 600mL of 0.05M Glacial acetic acid (Mallinckrodt-Baker, Paris, KY) and blended at 15,000rpm in a blender (IKA Works, Inc. Wilmington, NC) for 90 minutes at 4°C. In parallel, 0.32 grams of GAG in the form of Chondroitin-6 Sulfate (Sigma, St. Louis, MO) was added to another 120 mL of 0.05M acetic acid and mixed for 30 minutes on a stir plate. The GAG solution was added dropwise with a peristaltic pump to the collagen solution over 15 minutes after the initial 90-minute blending of the collagen. After the GAG was added, the slurry was mixed for another 90 minutes at 4°C. After mixing, the slurry was stored in a refrigerator at 4°C to prevent denaturing of the collagen. The slurry had a shelf life of 2 weeks before re-mixing was needed. If re-mixing was required, the slurry was re-blended at 10,000rpm and 4°C for 15 minutes and degassed again before use.

Collagen-GAG scaffold preparation

Collagen-GAG scaffold utilizing four different final freezing temperatures (corresponding to scaffolds exhibiting four different specific surface areas) was fabricated according to previously described methods (O'Brien, Harley et al. 2004b). Briefly, slurry created as detailed above was degassed for 60-90 minutes under vacuum (50mTorr) and 67.8 mL of slurry was pipetted into stainless steel pans 12.4cm x 12.4 cm on a side. Micropipette tips were used to move any remaining visible bubbles to the edges of the pan. The freeze dryer (VirTis,

Gardiner, NY) was equilibrated to room temperature (20°C) before starting the freeze-drying process. A breakdown of the programmed runs used can be found in Table 2.1 below.

Scaffold Type	-10	-20	-30	-40
t_{ramp}	5 minutes	10 minutes	10 minutes	15 minutes
T_{final}	-10°C	-20°C	-30°C	-40°C
t_{actual}	~35 minutes	~45 minutes	~55 minutes	~65 minutes
t_{hold}	60 minutes	60 minutes	60 minutes	60 minutes
$t_{hold\ vac\ 0°C}$	17 hours	17 hours	17 hours	17 hours

Table 2.1 Freeze Drying schedules, from O'Brien, et al. (2004b) and Harley (unpublished)

In the table above, t_{ramp} refers to the programmed ramp time in the freeze dryer program, while t_{actual} is the real time that elapsed during the ramp down time to the final temperature, T_{final}. As shown, t_{hold} and $t_{hold\ vac\ 0°C}$ were the same for all runs. The "hold" step was carried out to ensure that the freezing of the ice crystals in solution is complete. In fact, when doing the -10 freeze-drying runs, it was often necessary to extend the t_{hold} an extra 10-20 minutes to ensure that the entire pan was frozen before pulling a vacuum on the frozen slurry. After the 60-80 minute t_{hold}, the vacuum system was engaged and the chamber was evacuated to approximately 200mTorr. After the desired level of vacuum was achieved, the temperature was raised to 0°C and left for 17 hours (overnight). Shortly after the temperature was raised to 0°C, the vacuum continued to pull down to a final level of approximately 100mTorr. After the 17 hours had elapsed, the chamber temperature was first raised to 20°C and, once the temperature had equilibrated, the vacuum was released. The scaffold at this point was treated as clean but not sterile.

Scaffold Crosslinking Procedure

After freeze-drying, the scaffolds were placed in aluminum foil pouches to maintain cleanliness. Scaffolds were dehydrothermally treated for 24 hours at 105°C in a vacuum oven (Fisher IsoTemp 201, Boston, MA) at 50mTorr. This crosslinking step acted to create covalent bonding between the collagen and the GAG, as discussed earlier, and also sterilized the scaffolds. After 24 hours, the scaffolds (still in their aluminum foil pouches) were removed, sealed by folding over the top of the pouch, and stored in a dessicator until needed.

2.2 Tissue Harvesting

Harvesting of dermal fibroblasts was carried out on adult male and female Dutch Belted rabbits and male and female adolescent and adult Sprague-Dawley rats. For a detailed description of the harvest procedures used, see Appendix 1. Briefly, an area of skin approximately 6cm wide, centered at the base of the foreleg and extending 12cm between the ventral line and the midline, was shaved and sterilized before the surgical procedure began. When possible, the epidermis was separated first from the remaining layers of integument. As described earlier, the epidermis actually contains five distinct layers of its own. Since epidermal cells were not desired in this study, the epidermis was considered as a whole and was easily distinguishable as the non-vascularized tissue first excised from the animal. After the epidermis was removed during surgery, the dermis was separated from the underlying layer of subcutaneous tissue and/or muscle by means of scalpel slicing and the action of opposing pulling force by forceps. Once a sizable piece of dermis was obtained, usually at least 2cm x 2cm unstretched, the sample was placed in a 50mL tube filled with 30mL of sterile Dulbecco's Phosphate-Buffered Saline (DPBS) (Gibco) supplemented with 2% Antibiotic/Antimycotic (Gibco) and transported in a cooler packed with reusable ice packs. Once back in the laboratory, the tissue was treated one of three different ways;

1.) The explant outmigration procedure of Freyman, et al. (2001c) was utilized as published.

2.) The tissue was minced into roughly $1mm^3$ cubes and placed directly in a 0.25 wt.% Type I Collagenase (Sigma, St. Louis, MO) solution (approximately 1200U/mL) for 2-3 hours,

3.) The tissue was placed as a single piece with the reticular dermis side down in a 4cm x 4cm plastic weigh boat and treated with graded solutions of 0.8% wt.% Type I Collagenase for 2 x 30 minutes followed by 4 x 30 minutes in 0.25 wt.% Collagenase solution.

The Type I Collagenase solution was made by adding the desired amount of enzyme to sterile, unsupplemented Dulbecco's Modified Eagle's Medium (DMEM) and vacuum filtering through a 0.22μm tube top filter (Corning Life Sciences, Corning, NY). In both cases, the tissue/solution were placed in a 50mL tube and placed upright on a rocker tray (VWR Scientific) in an incubator at 37°C and 5% CO_2 with the cap popped to allow for oxygenation. Every 15 minutes, caps were tightened and the tubes were gently shaken by hand to further disperse tissues and allow for equal enzymatic action over the entire tissue surface. Caps were released again and returned to the rocker tray.

Collagenase solutions were made to correlate to approximately 5mL solution/in^2 of tissue. Summaries of protocols continue below;

2.) Referred to as the "vortex method". After the tissue volume was reduced in the Collagenase, the solution was vortexed on a Vortex Genie (VWR Scientific for Scientific Instruments, Inc. Bohemia, NY) for approximately 30 seconds in an effort to dislodge cells from remaining ECM pieces. The speed was adjusted such that a spinning cone was set up inside the 50mL tube, just below the threshold of turbulent flow. After vortexing, the cell suspension was passed through a 70μm cell strainer and the resulting suspension was centrifuged at 900rpm for 5 minutes. The cell pellet was resuspended in complete

DMEM, added to a T-75 vented cell culture flask (Becton-Dickinson Biosciences, Bedford, MA), and cells were cultured as described below.

3.) Referred to as the "serial digestion" method. After every 30-minute digestion interval, the Collagenase solution was replaced and the exposed solution was treated for 5 minutes with Trypsin-EDTA (Gibco), subsequently inactivated with a volume of complete DMEM equal to the existing solution volume, and centrifuged for 5 minutes at 900rpm. The pellet was washed with complete DMEM again and recentrifuged. The resulting cell pellet was resuspended in complete DMEM, added to a tissue culture flask, and cultured as described below.

2.3 Cell Culture

All cells were cultured in an incubator (NAPCO 6000, Presicion/NAPCO, Winchester, VA) at 37°C, 5% CO_2 and 95% relative humidity.

Fibroblast cells were cultured in vented, canted neck T-75 flasks in 17mL of DMEM (Gibco) supplemented with 10% FBS (HyClone, Logan, UT) and 1% Antibiotic/Antimycotic (Gibco). Media was changed every 3-4 days, and cells were passaged when 90% confluent (4-9 days).

For traditional cell passaging, flasks were split in a 5:1 ratio once 90% confluence was reached. For passaging done with "vortex method" cells, denoted with a "V" after the passage number, cells were split to new flasks at a concentration of 5E5 cells/flask. Culturing environment and passaging procedures were otherwise kept the same. See Appendix 2, Cell Culture Protocol, for a more detailed description of culture methods.

Cell Counting

All cell counting was done by hand with a hemacytometer (Hausser Scientific, Horsham, PA). In order to get more averaging of cellular concentration, most counts were done in duplicate. For a detailed description of the cell counting process, see Appendix 2.

2.4 Attachment Study: 24- and 48-hour runs

The cell attachment study was carried out according to methods previously described by O'Brien et al. (2004a). One alteration made to the original protocol involved a change in the size of scaffold used and the subsequent amount of cells seeded onto the scaffold. Due to difficulties in obtaining large cell numbers, the size of scaffold used was 15mm x 22mm x 3mm ($990mm^3$), half the size of previously published results, and cell quantity was proportionally reduced to 1.5 million cells seeded per side.

Cells were cultured in $75cm^2$ flasks (Becton-Dickinson, Franklin Lakes, NJ) in Dulbecco's Modified Eagle's Medium (DMEM) (Gibco) supplemented with 10% FBS (HyClone, Logan, UT), 1% Penicillin/Streptomycin (Gibco) and 1% Fungizone (Gibco). Cells were placed in an incubator (NAPCO 6000, Precision, Winchester, VA) at 37°C, 5% CO_2, and 95% relative humidity. Cells were fed twice a week and passaged every 6-9 days. Passages 2-6 were used in the study.

For passaging and seeding, cells were washed with 5mL Dulbecco's Phosphate Buffered Saline (Gibco) for 30 sec. and then treated with 4mL 0.05% Trypsin-EDTA (Gibco) and placed in an incubator at 37°C for 7 minutes to facilitate cell detachment. Viable cell number was determined by staining with Trypan Blue (Gibco) and counting using a Hemacytometer (Hausser Scientific, Horsham, PA).

Cells were spun down at 900rpm for 5 minutes in a lab centrifuge (Labofuge 400, Heraeus Instruments, Hanau/Germany) and re-suspended in complete DMEM at a density of 3 million cells per mL. Initial seeding of scaffolds was done in a 6-well PE tissue culture plate

(Becton-Dickinson). 1.5 million cells were seeded on the "shiny" side of the dry scaffold and placed in an incubator at 37°C for 10 minutes to facilitate attachment. After 10 minutes, the scaffolds were flipped over and placed into another 6-well PE tissue culture plate treated with 3mL of a 2 wt.% Agarose solution (J.T. Baker, Phillipsburg, NJ), seeded on the opposite side with another 1.5 million cells, and placed back in the incubator. After 10 minutes, wells were topped off with 3mL complete DMEM and placed back in the incubator for either 24 or 48 hours. After the desired time period, scaffolds were removed from the incubator and unattached cells were rinsed off by dipping scaffolds 10x in PBS. Scaffolds were digested in 5mL of a non-sterile 2.4U/mL solution of Dispase (Gibco) in a 15mL tube (Becton-Dickinson). The tubes were placed in a water bath (VWR Scientific/Sheldon Mfg., Cornelius, OR) at 37°C for thirty minutes to facilitate digestion of the collagen scaffolds. Tubes were shaken by hand every ten minutes while in the water bath. Cell counts were done with hemacytometer after 30-45 minutes of digestion and percentage attached was calculated by dividing this count by the original number of seeded cells. Counts were done in duplicate and statistical analysis was done on all tests (n = 4 or 5) using a statistical analysis software package (SigmaStat, Ver. 2.03, SPSS, Inc., Chicago, IL).

2.5 Embedding and Sectioning

The cell attachment values obtained from the original rabbit and rat fibroblast seeding runs gave different results compared to previous MC3T3 experimentation by O'Brien et al. (2004a), so additional scaffolds were seeded and embedded in order to determine the cellular penetration through the scaffolds.

Due to limited cell availability, smaller pieces of scaffold were utilized for sectioning. An 8mm dermal biopsy punch (Miltex, Bethpage, NY) was used to cut uniform pieces of scaffold from dry -10 and -40 scaffolds. Cell seeding density of 3×10^6 / mL was kept, but volume was scaled down to maintain the same cellular quantity per volume of scaffold.

Rat dermal fibroblast cells were seeded in the 8mm round scaffolds in the same manner as the previous seeding experimentation. Dry matrices were seeded on one side, incubated for 10 minutes to facilitate attachment, flipped onto Agarose-coated wells, seeded with an equal volume on the other side, and incubated for another 10 minutes to facilitate attachment. Two samples, one showing initial cellular distribution at t = 0 hr. and one showing final cellular distribution at t = 24 hr., were created for both -10 and -40 scaffolds. At either t = 0 hr. or t = 24 hr., samples were sacrificed by placing samples in 2mL of a 10% neutral buffered formalin solution for 24-48 hours. Samples were embedded according to the Glycomethacrylate (JB-4 kit, Polysciences, Warrington, PA) embedding procedure (see Appendix 3). Samples were cut to 5μm thickness on a microtome (Leica Model RM 2165, Leica Microsystems, Bannockburn, IL) and stained with a Hematoxylin and Eosin (H+E, Sigma, St. Louis, MO) staining procedure (see Appendix 3).

In order to more accurately judge behavior of different cell types within the scaffold, a -10 scaffold was seeded with MC3T3 cells from the previous study in the same manner and prepared according to the same protocols. Since the previous study found a correlation between attachment percentage and available specific surface area, the -10 scaffold was used as a baseline reference for cellular penetration through the thickness of the scaffold, with the assumption being that the scaffolds with more surface area would have a similar through-thickness distribution of cells. The sectioning results from this exercise were used as a check to measure infiltration through the thickness of the scaffold for a different cell type with previously published attachment results (O'Brien 2004a).

2.6 SEM Imaging

Scanning Electron Microscope images were obtained from two different sources. Uncoated images of the scaffold were obtained on a LEO SEM (Model 438 VP, Cambridge, England) at an accelerator voltage of 19.5-20kV using a Backscatter Electron detector, with magnification as indicated on the images presented in Chapter 3.7.

Sputter-coated images were obtained from Amanda Blackwood and Dr. Debbie Chachra at the Franklin W. Olin College of Engineering. A sputter coater (Denton Vacuum, Inc DESK-1, Moorestown, NJ) was used at a current of 50 milliamps (DC) on gauge to coat the scaffold samples with gold. The elapsed sputtering time was approximately 90 seconds. For the Olin College SEM samples, a JEOL JSM-6060LV (Peabody, MA) scanning electron microscope was used at an accelerator voltage of 5kV and magnification as indicated on the images presented in Chapter 3.7.

2.7 Cell Force Monitor (CFM)

CFM Refurbishment

The Cell Force Monitor (CFM), originally designed by Freyman (2002), was updated with new positioners and sensors. New supports were milled to replace older, corroded aluminum pieces. New grips were also made to replace older polyethylene components.

Proximity sensors (Kaman Aerospace and Instrumentation, Colorado Springs, CO) were replaced in order to gain a greater sensing distance. This was needed because of the change in collagen-GAG matrix-only contraction behavior as a result of new freeze-drying protocols (see Section 2.1). Linear positioning stages were replaced (Edmund Optics, Barrington, NJ) and rack and pinion support posts (for z-axis positioning) were also replaced (Edmund Optics). New supports were milled from common ¼" aluminum stock to hold the new, larger-diameter sensors. Also, because of the larger diameter sensors, larger Be-Cu beams (2%Beryllium-98%Copper, 24mm wide, 0.125mm thick) were ordered (Goodfellow, Berwyn, PA). New scaffold grip supports were milled from Polysulfone (McMaster-Carr, Dayton, NJ), a medical-grade plastic, to replace corroded aluminum supports. New scaffold grips were designed and fabricated from scrap Polysulfone (McMaster-Carr). See Appendix 4 for part numbers and drawings of all new parts.

CFM Calibration and Force Calculation

Two calibration factors are needed to obtain an accurate measurement of cell contractile forces, C_{mass} and C_{displ}. C_{mass} takes into account the effects of the moment of inertia of the beam on contractile forces generated by cells. C_{displ} takes into effect the stiffness of the scaffold itself on cellular contraction. By combining these two "resistances," it is possible to obtain the gross contractile force generated by the bulk of the cells seeded in the scaffolds.

C_{mass} is obtained from the slope of a calibration curve plotted by placing known masses on the beam of a rotated CFM setup and plotting values of mass vs. voltage as shown in Figure 2.1 below.

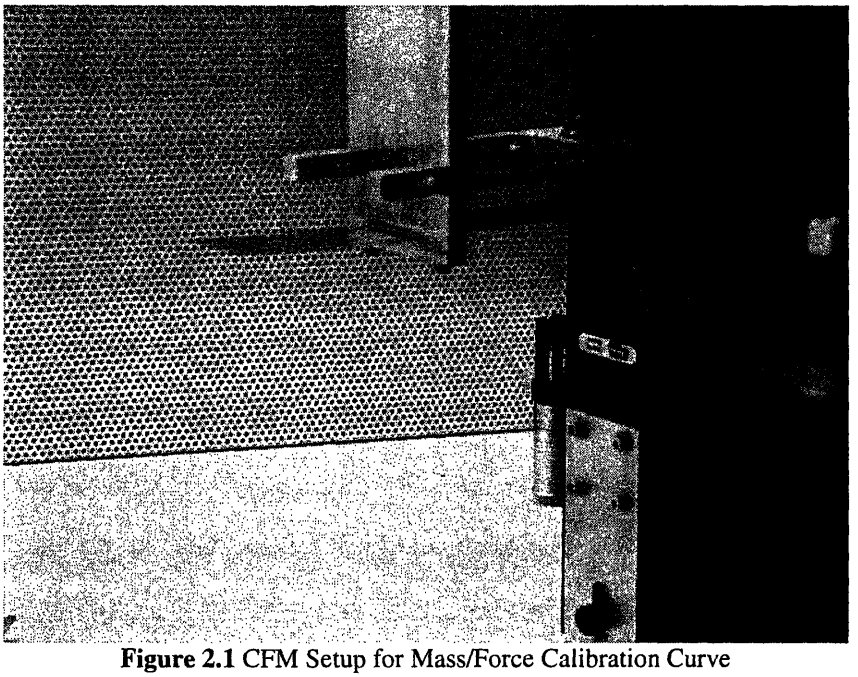

Figure 2.1 CFM Setup for Mass/Force Calibration Curve

The calibration slope for C_{displ} is obtained by measuring voltage vs. displacement of the proximity sensors when attached to a micrometer calibration stage as shown in Figure 2.2.

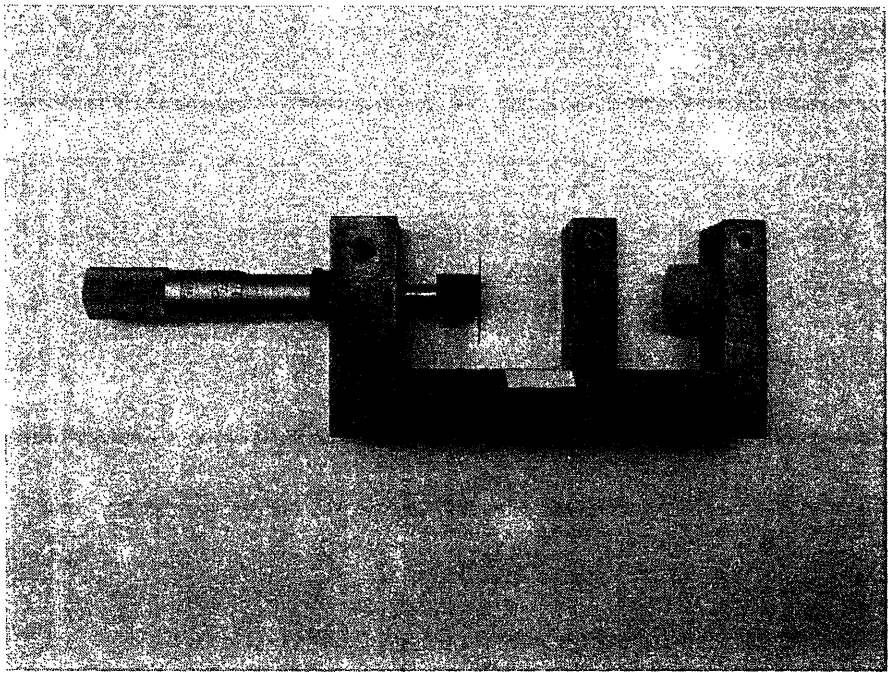

Figure 2.2 Calibration Stage for Proximity Sensors

Once these calibration factors are obtained, the general form of the force generated is calculated as shown:

The general equation for equating proximity sensor voltage (V) to cell force (F_{cell}) is shown in Equation (1) below:

$$F_{cell} = F_{beam} + F_{matrix} \tag{1}$$

where F_{beam} and F_{matrix} are derived from equations (2) and (3), respectively, containing calibration constants C_{mass} and C_{displ}, respectively, as discussed above.

$$F_{beam} = V \cdot C_{mass} \tag{2}$$

$$F_{matrix} = V \cdot C_{displ.} \cdot K_{matrix} \tag{3}$$

where K_{matrix}, as shown in Equation (4), is related to the modulus (E_{matrix}) of the hydrated scaffold,

$$K_{matrix} = (E_{matrix} \cdot A) / L \quad (4)$$

'A' is the cross-sectional area of the matrix perpendicular to the direction of measured contraction and 'L' is the length of the matrix between the two grips, as illustrated in Figure 2.3.

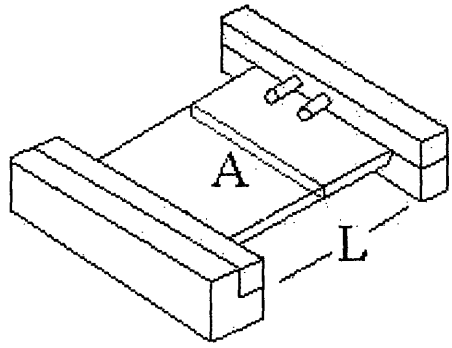

Figure 2.3 Dimensions for Calculation of K_{matrix}

The value for E_{matrix} was taken from recent research by Harley (unpublished) evaluating the modulus of hydrated matrix in different strain regimes. For a strain value of up to 15%, the modulus was calculated to be approximately 200Pa. For values above 15%, the value was calculated to be 80Pa. The value of E_{matrix} was taken as 200Pa for all experimentation in this study.

After the bulk pulling force was obtained, this number was normalized to the number of cells in each scaffold as obtained by the hemacytometer count detailed above.

CFM Setup

After replacement, calibration, and installation of all parts, the CFM still remained similar to the previous generation setup. The new CFM is shown in Figures 2.4-2.5.

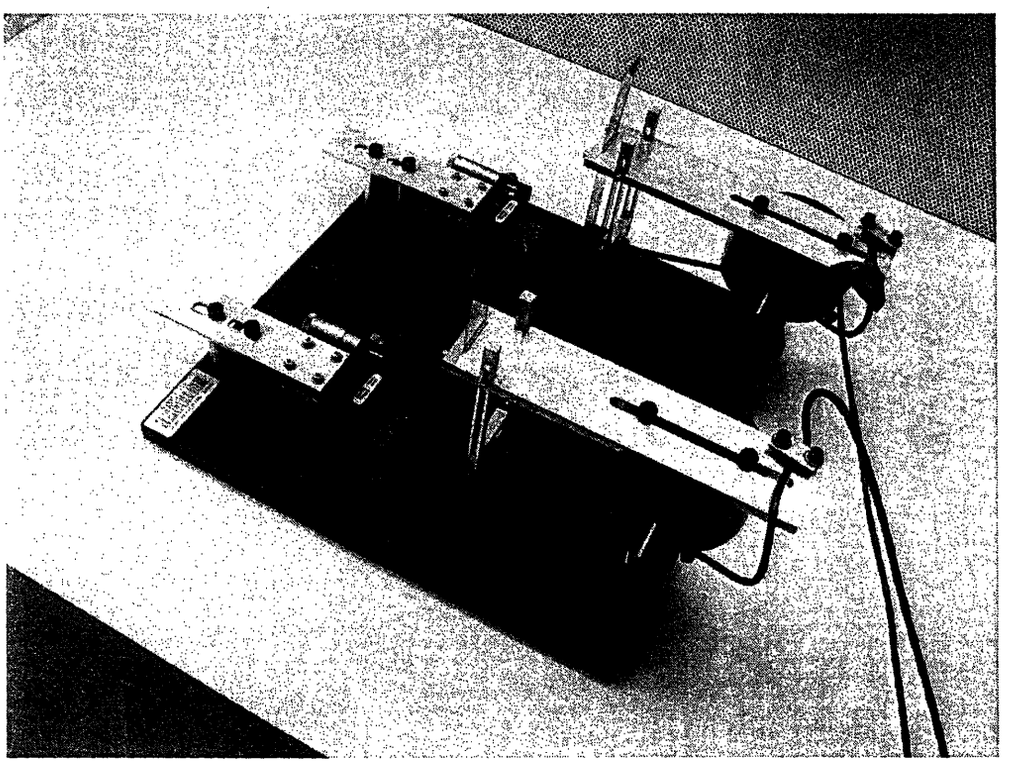

Figure 2.4 Updated CFM

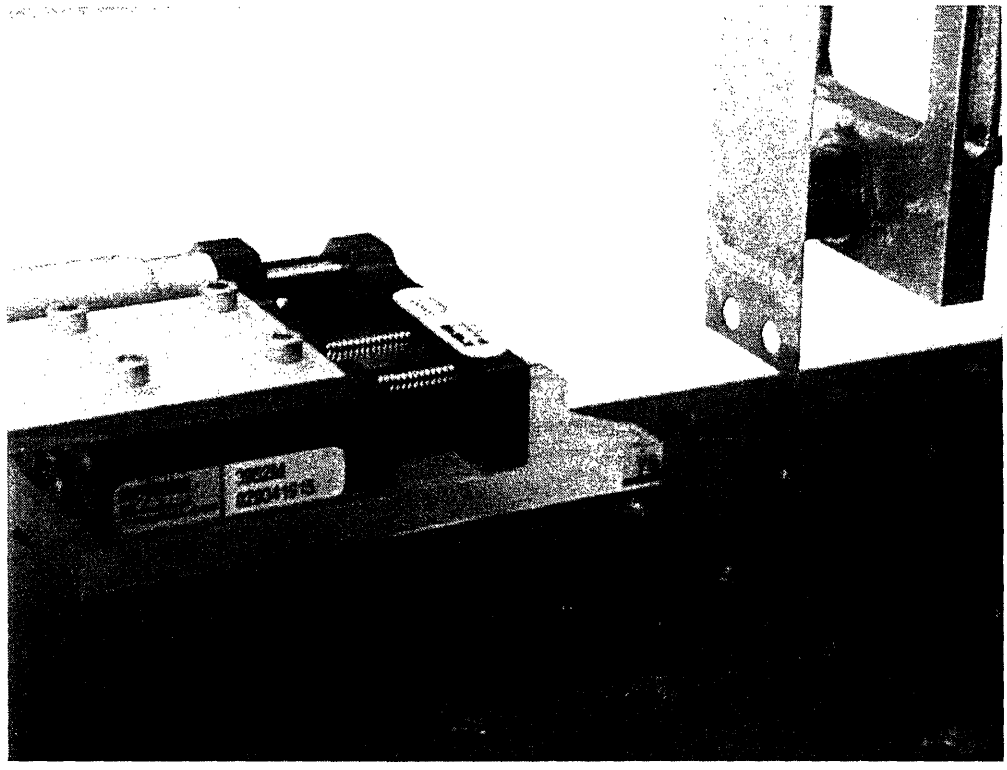

Figure 2.5 Updated CFM (detail)

Be-Cu beams were fixed in place vertically on the milled horizontal arm attached to the z-positioning stage. Position sensors were mounted on milled brackets directly behind the vertical Be-Cu beams. A fixed, single-axis linear positioning stage with integrated grip holder was attached to the optics plate in line with the beam and sensor setup with a gap adjustable from 10-45mm. The plastic grips were attached to opposite ends of a piece of scaffold cut to the desired size and shape. One grip was affixed with screws to the linear positioning stage and the other was attached to the beam with a stainless steel surgical clamp (Roboz Surgical, Rockville, MD).

CFM Run Details

A scaffold piece was cut from a sterile sheet of matrix using a template of the appropriate size and a straight-edge razorblade. The desired shape was created by making a downward, single-motion cut with the razorblade around the entire template, taking care to not create any nicks in the edges of the scaffold that were not clamped (these nicks can act as stress concentrators during testing and skew the output of contractile forces generated). The scaffold was then clamped one grip at a time, secured with screws, and placed in the polyethylene well.

While the seeding procedure for the CFM runs was initially identical to the seeded runs described above, an alternative method was developed in an effort to increase cellular infiltration within the scaffolds. The blot seeding technique used on all reported CFM runs was similar to the previous protocol, with one difference. As the scaffold was flipped over after the initial 9-minute attachment incubation, a piece of filter paper was used to blot the unseeded side in an effort to remove excess media. The filter paper was held on the scaffold for approximately 10 seconds or until the majority of the wicking had stopped. This side was then seeded with the same amount of cellular suspension as the first side and the piece was incubated for 9 minutes.

Initial CFM runs (data not reported) used a suspension of 2×10^6 cells/mL, with 0.5mL seeded per side, for a final concentration of 2×10^6 cells/scaffold. The cellular response in the scaffolds was shown to be dependent on gross cell number, determined by the cellular concentration in seeded suspension, with a threshold value being necessary to produce a repeatable contractile response. Accordingly, the cellular concentration in reported seeded CFM runs was increased to 5×10^6 cells/mL with 0.4 mL seeded per side for a total of 4×10^6 cells per scaffold in order to increase gross cellular adhesion and obtain a repeatable result. In two CFM runs (-10 P4 and -40 P4V) the gross cell number used was 3.75×10^6 cells, seeded at a density of 5×10^6 cells/mL. The difference in seeded number for these two runs was -6%; since all CFM results were normalized to a per-cell force value in all cases, the difference between these two runs and all other runs was taken to be negligible. In one other CFM run (-40 scaffold, P5 cells),

the gross cell number used was 3 x 10^6 cells, seeded at a density of 5 x 10^6 cells/mL. While this represents a 25% decrease in cellular seeding density, the value obtained for this run was still used because the run produced a characteristic curve with a large contractile response.

During the second incubation period, the CFM was placed on a hot plate in the sterile hood in an effort to reduce the temperature difference between the internal incubator environment and the CFM. After the 9 minute incubation period, the wells were removed from the incubator and 30 mL of complete media was added to the wells containing the cell seeded scaffold/grip setup. A timer was then set for 10 minutes and the grips were attached to the appropriate side of the CFM with screws or surgical clamps. The z-positioner was used to position the beam side grip just above the bottom of the polyethylene well in order to eliminate any resistance or friction between the grip and the bottom of the well. The CFM was then inserted into the incubator and the wells were topped off with media until the meniscus breached the top of the wells (20-25mL). The single-axis positioner was used to set the initial voltage to the zeroed voltage obtained from the "grip-only" run (see below). After the 10 minute timer expired, the CFM data acquisition program was started and allowed to run for 22 hours.

After the 22 hour time period, the grip/scaffold setup was removed from the CFM. Using a razorblade, the exposed area of scaffold was removed from the grips and rinsed by dipping 10x in non-sterile PBS (Gibco). The scaffolds were then placed in a 15mL centrifuge tube containing 6mL of a 2.4U/mg solution of Dispase (Gibco) for 30-45 minutes and allowed to sit in a water bath at 37°C. The tubes were gently shaken by hand every 10 minutes to accelerate the dissociation process. Attached cell numbers were obtained by hemacytometer count.

CFM Zeroing

In order to get the cell-only force, two zeroing runs were first made with each CFM. The first run determined the zero point of the setup by running the CFM for 22 hours with only the grips in the well. The baseline voltage over the course of the run was taken as the equilibrium

"grip-only" zero point and used as the set point when beginning all subsequent CFM runs. Values for grip-only voltages were adjusted to the range of 0.05-0.10 V by moving the proximity sensor closer to or further away from the beam.

A 22-hour scaffold-only run was next completed according to the above protocol. The only difference between the "cell-seeded" runs and the "matrix-only" runs involved either the inclusion or exclusion of cells in the media pipetted onto the surface. In both cases, the same amount of media and incubation time was utilized before starting the data acquisition process.

Scaffold Sizes

For the CFM contraction study, "-10" and "-40" matrix was utilized. For the aspect ratio study, "-10" matrix was used exclusively. Pieces were cut with templates to sizes as shown in Table 2.2.

Study	Scaffold	Cut size (W x L)	Exposed Size (mm^2)	Aspect Ratio (W x L)
Contraction	-10	30mm x 22 mm	20mm x 22 mm (440)	1:1
	-40	30 mm x 22 mm	20mm x 22 mm (440)	1:1
Aspect Ratio	-10	35 mm x 22 mm	35 mm x 12 mm (420)	3:1
	-10	12 mm x 45 mm	12 mm x 35 mm (420)	1:3

Table 2.2 Scaffold sizes used (Note: "L" denotes length of scaffold between grips)

As mentioned above, CFM runs measuring cellular contractile force were completed with both -10 and -40 matrix, representing the smallest and largest specific surface areas, respectively. Cells used were passage 3-5, but cells from two separate culturing techniques were used (with new passaging procedure denoted by a "V" after the passage number). Each CFM run gave two

plots of contractile response, from "CFM L" and "CFM R". The matrix-only voltage plot was subtracted from the gross cell-seeded voltage plot from respective CFM's "L" and "R" in order to obtain the cell-only contractile voltage response. At this point, the force generation curve was computed from the equations in the section above, and the resulting curve was divided by the number of cells attached at 22 hours, obtained by hemacytometer count. The resulting number was referred to as the "per-cell contractile force," or the average force generated per cell within the scaffold. It should be noted, however, that, as shown in the seeding pictures of the previous section, not all cells contributed to the contractile response. The averaging of all attached cells, as done in this study, most likely caused a decrease from the "true" per cell contractile force generated. Unfortunately, due to the Dispase-mediated dissolution necessary to perform the hemacytometer count and the lack of an easily repeatable staining procedure, a more accurate quantification of the cells involved in the actual contraction of the scaffold was not available.

Chapter 3 Results

3.1 Scaffold Fabrication

The scaffold physical properties obtained by the four different freeze-dryer program runs executed as described in Materials and Methods are shown in Table 3.1 below. Since freeze-drying runs were executed according to the protocols of O'Brien, et. al. (2004a) and used the same equipment, the pore characteristics of the four scaffolds were assumed to be the same.

Scaffold Type	**-10**	**-20**	**-30**	**-40**
Average Pore Size	150μm	121μm	110μm	94μm
Specific Surface Area (S.A./V)	0.0067/μm	0.0084/μm	0.0092/μm	0.0106/μm

Table 3.1 Scaffold Physical Characteristics from O'Brien, et al. (2004a)

In all scaffolds fabricated, the freeze-drying process produced a scaffold with qualitatively different features at the two boundary surfaces; a "shiny" side that was formed on the top surface of the slurry exposed to the chamber atmosphere and a "non-shiny" side formed on the surface exposed to the stainless steel pan. For all seeding and CFM runs, the shiny side was seeded first, as discussed earlier.

3.2 Tissue Harvesting and Cell Culture

Rabbit dermal fibroblasts were first chosen because of the ease of availability of the animal tissue at the beginning of the study. The switch in tissue source to the Sprague-Dawley rat was made because of the increasing need for a more easily and readily accessible cell source. Sprague-Dawley rats (that would otherwise be euthanized due to overpopulation of other study populations) are routinely available on short notice from MIT's animal facility. Also factored

into the decision were considerations of possible in vivo work to be done with rats by partner labs focusing on fibroblast behavior in a collagen-GAG scaffold in different sites of an animal model.

The two different harvesting procedures described above were presented because they proved to be the most successful of the numerous methods investigated. However, not all harvesting procedures executed according to the above protocols were successful. Several harvest procedures executed using the "serial method" were unsuccessful in producing any viable cells. Other procedures done with the serial method produced viable cells only from the 0.8% digestions or the 0.25% digestions, but not both. Due to the sporadic success of this method and the underlying uncertainty in the reason for failure, new protocols were explored.

It should be noted that the need to open the cap to allow for oxygenation during digestion was discovered only after several failed harvest procedures. Several more serial digestion procedures were attempted after the oxygenation issue was addressed, with only mixed success in producing viable cells.

3.3 Cell Culture

Culturing techniques were largely performed as learned from previous laboratory members. In culturing done with New Zealand White rabbit dermal fibroblasts inherited from previous laboratory members, it was observed that the cellular quantities obtained per confluent flask would decrease as passage number increased. There was much difficulty in getting a large quantity of cells from culture flasks. Even though the physical aspects of the cell appeared to remain the same, the cells would noticeably grow in size as passage number increased (images not available). For passaged NZW dermal fibroblasts, P3 - P6, the average number of cells obtained per $75cm^2$ flask was 1.2 – 1.9 million cells, with most flasks yielding ~1.3 million cells. For Dutch Belted rabbit dermal fibroblasts, the same trend was seen as passage number increased, though larger initial numbers of cells per flask were found. P2 through P6 cells used for scaffold seeding experimentation yielded 2.9×10^6 (P2) - 1.1×10^6 (P6) cells per flask. When Sprague-

Dawley rat dermal fibroblasts were harvested, the numbers were comparable to historical levels. Rat dermal fibroblast densities per confluent flask ranged from 2.3 - 1.1 million cells per flask. The same trend of decreasing cell number with increasing passage number was observed.

In all of the cases above, a nonspecific splitting ratio of 5:1 was used when passaging cells. By P6, the cells had taken on less of a stretched, bipolar fibroblast-like morphology and had spread out in multiple directions with more, but less pronounced, processes. The change in spreading morphology can be seen in a comparison of P2 and P5 rat dermal fibroblasts, as shown in Figures 3.1 and 3.2.

Figure 3.1 Rat dermal fibroblast, P2

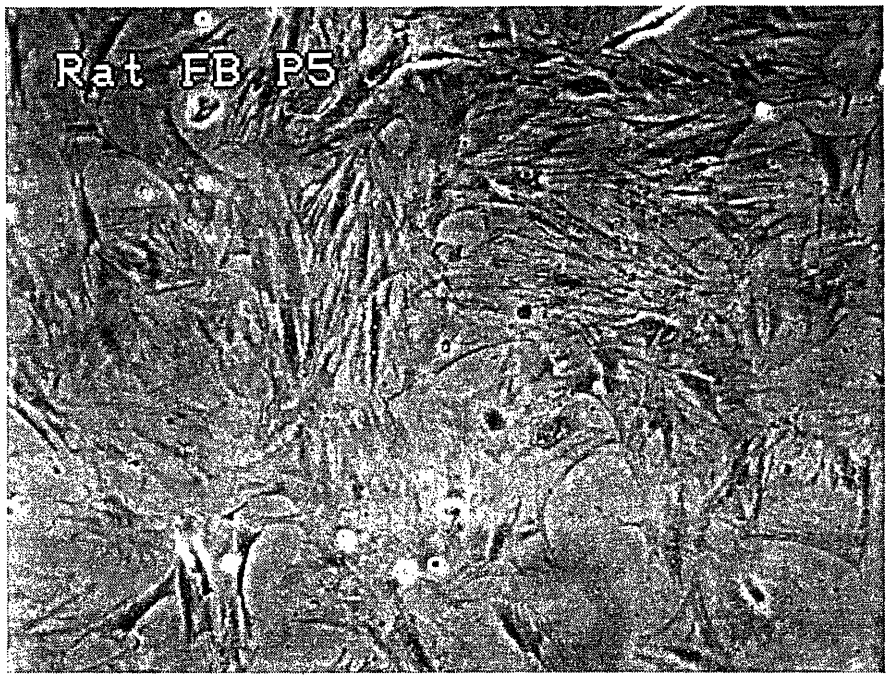

Figure 3.2 Rat dermal fibroblast, P5

(Note: glowing white marks on slides due to light reflection off of floating or partially-adhered cells.)

The cells shown in the hemacytometer exhibit a definite size difference between cell types. The specific reasons for the cellular changes observed may be explainable through a combination of mechanisms (as described below).

Images of Trypsinized cells are shown in Figures 3.3-5 for P4 Dutch Belted rabbit fibroblast, MC3T3, and Sprague-Dawley rat fibroblast from both the old (P3) and new (P3V) passaging method. Cells are shown on a hemacytometer slide.

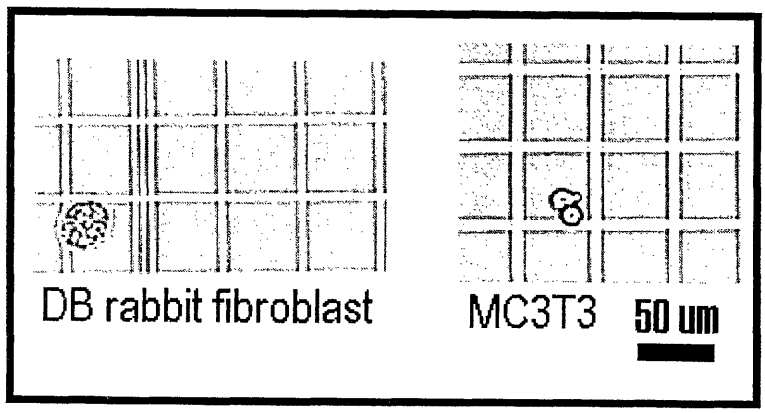

Figure 3.3 Dutch Belted rabbit dermal fibroblast (P4); MC3T3 cells, same scale

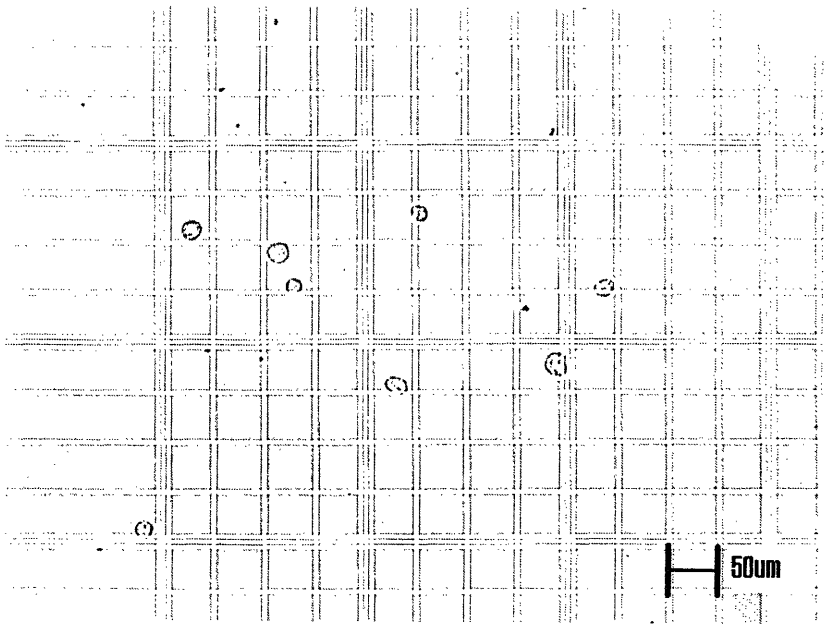

Figure 3.4 Sprague-Dawley rat dermal fibroblast, P3, 5:1 split passaging

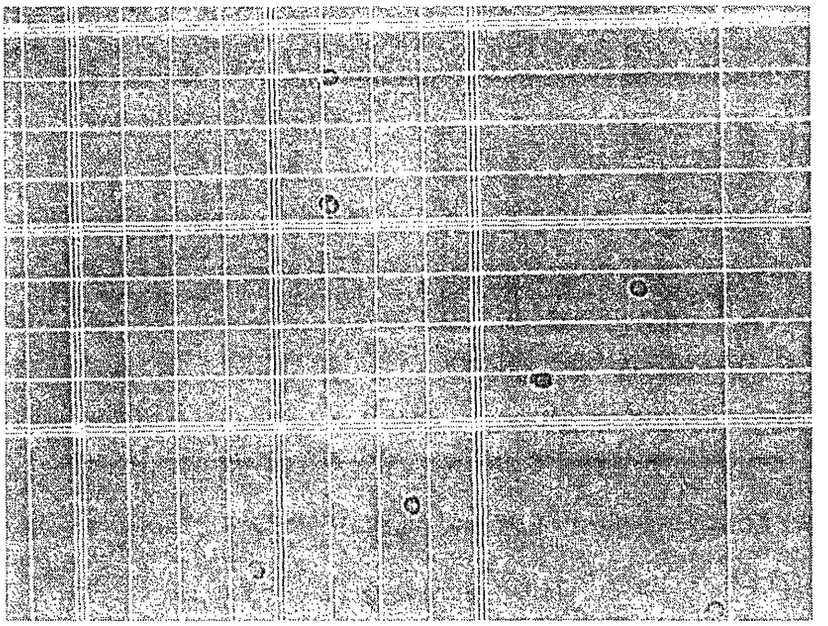

Figure 3.5 Sprague-Dawley rat dermal fibroblast, P3V ($5x10^5$/flask passaging)

When the vortex method was introduced into the harvesting protocol, the decision was made to create a cellular environment that was as similar as possible between all passages. To accomplish this, cells were not split blindly in a 5:1 ratio. Instead, as discussed in the Methods above, the cells were Trypsinized and passaged in new flasks to a density of 500,000 cells per flask, no matter the passage number. This technique has been shown to better stabilize cell counts per flask as passage number increases. The morphology of the cells with increasing passage number also seems to remain more static, though this is a qualitative observation only.

3.4 Cellular Attachment in Collagen-GAG Scaffolds, 24- and 48-Hour Trials

As shown in Table 3.2, the seeding density of cells within the scaffold is calculated by dividing the total number of cells seeded by the total volume of the scaffold.

Scaffold Size	Scaffold Volume	Cell Density	Total Cell number seeded	Cell Seeding Density
15mm x 22mm x 3mm	990 mm^3	$3x10^6$/ mL	1mL = $3x10^6$ cells	$3x10^3$cells/mm^3 scaffold
8mm round x 3mm	151 mm^3	$3x10^6$/ mL	153μL = $4.58x10^5$ cells	$3x10^3$cells/mm^3 scaffold
20mm x 22mm x 3mm (CFM)	1320 mm^3	$5x10^6$/ mL	0.8mL = $4x10^6$ cells	$3x10^3$cells/mm^3 scaffold

Table 3.2 Comparison of cellular density within scaffolds for seeding runs

24 Hour Attachment Study, Rabbit Dermal Fibroblast

Plotted percentages in Figure 3.6 are expressed in terms of percentage of seeded cells attached after 24 hours vs. the four scaffold pore sizes examined.

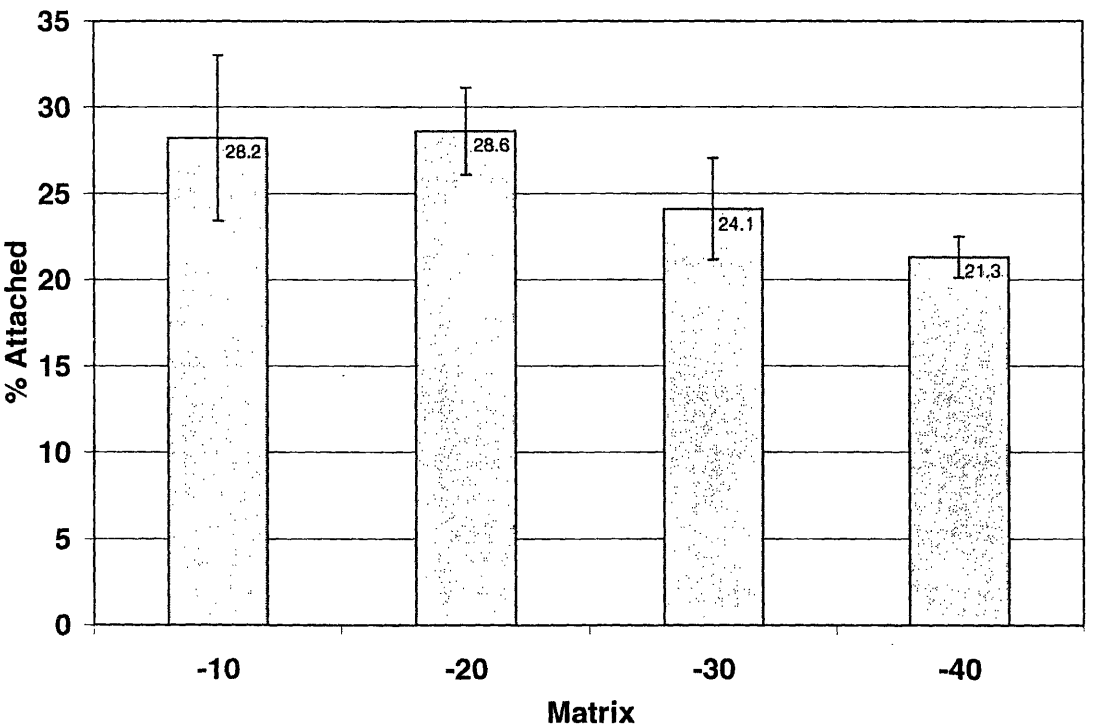

Figure 3.6 24-hour rabbit dermal fibroblast cell seeding

Error bars in Figure 3.6 point to a marked spread in the -10 scaffold measurements, with SEM decreasing with decreasing average pore size. Statistical analysis via ANOVA was done on the experimental results (n = 5). For the 24-hour results, no significant difference (P=0.33) was found between the attachment percentages for any of the different matrices.

48-Hour Attachment Study, Rabbit Dermal Fibroblast

Plotted percentages in Figure 3.7 are expressed in terms of percentage of seeded cells attached after 48 hours vs. the four scaffold types examined.

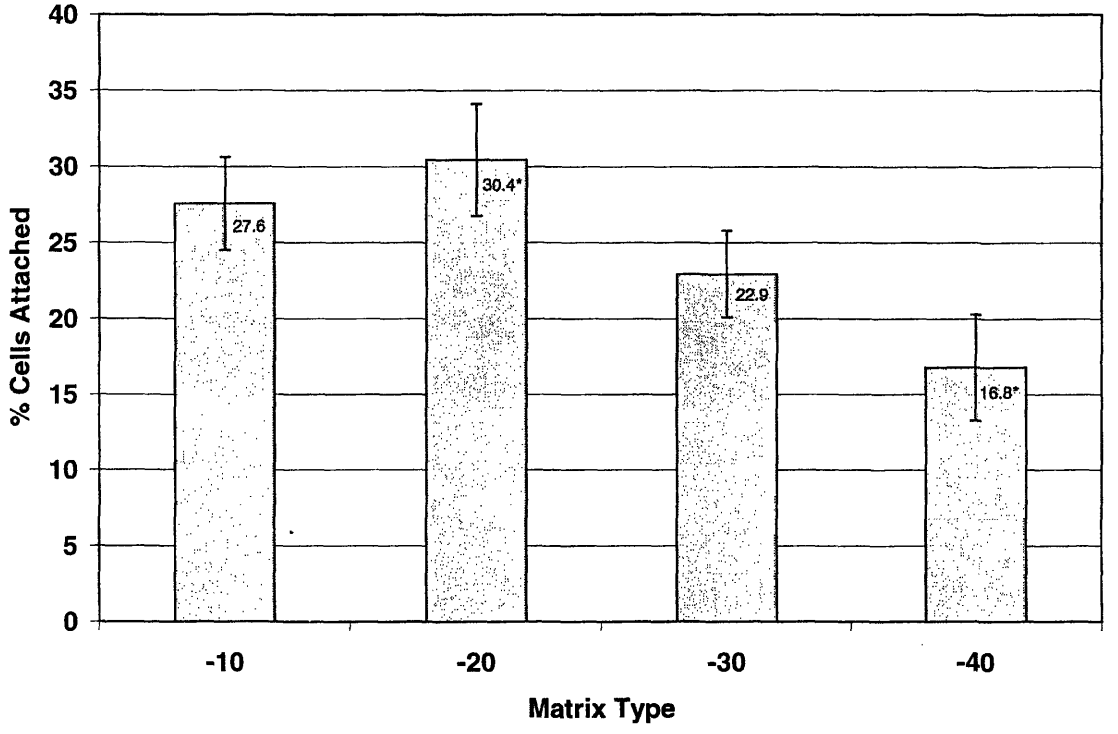

Figure 3.7 48-hour attachment, rabbit dermal fibroblast

Error bars (SEM) in Figure 3.7 point to a marked spread in all of the scaffold measurements at the 48-hour mark. Statistical analysis via ANOVA was done on the experimental results (n = 5). A statistically significant difference (P=0.048) was found in attachment percentage between the -20 and -40 scaffolds. It should also be noted that the SEM

spread in the 48-hour tests stayed relatively constant across all scaffold types, as opposed to the decreasing trend seen in the 24-hour measurements.

24-Hour Attachment Study, Rat Dermal Fibroblast

Plotted percentages in Figure 3.8 are expressed in terms of percentage of seeded cells attached after 24 hours vs. the four scaffold types examined.

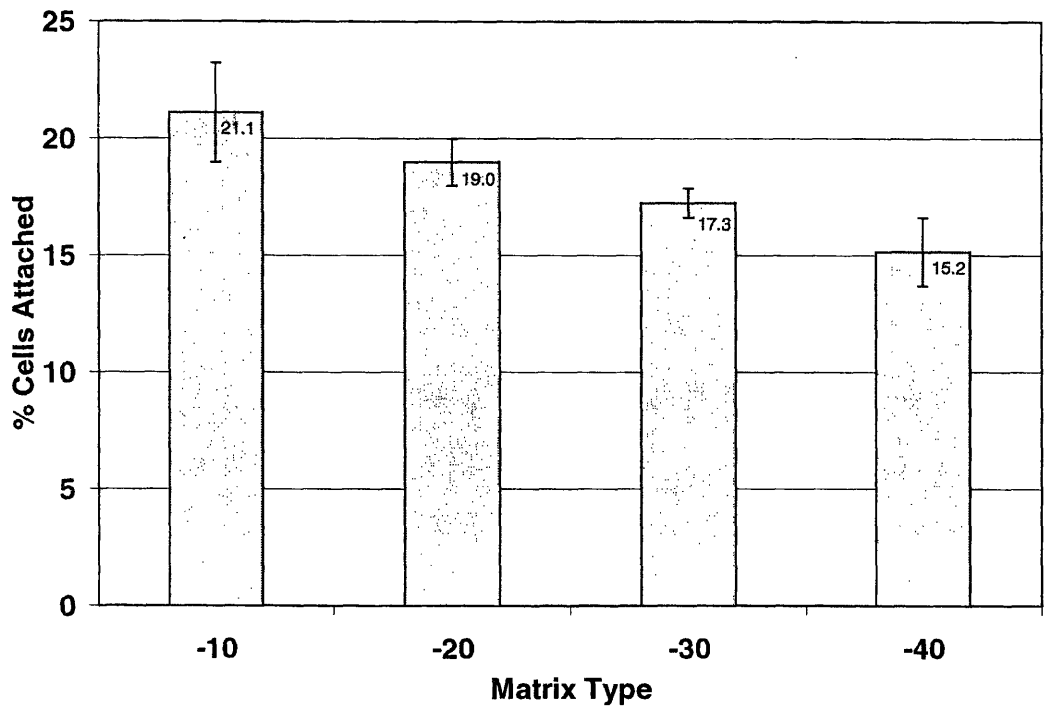

Figure 3.8 24-hour rat fibroblast attachment

Statistical analysis via ANOVA was done on the experimental results (n = 4 or 5). While there was not a statistically significant difference (P=0.064) in the attachment percentage of rat dermal fibroblasts between different scaffold types, the gross attachment percentages for all four scaffolds were shown to be lower across the board compared to the rabbit dermal fibroblast runs.

Rat vs. rabbit attachment percentages were analyzed via ANOVA and a significant difference (P=0.002) was found to exist between the mean attachment percentages of the 12

different groups (four matrix types in three different attachment scenarios: rabbit 24, rabbit 48, and rat 24). In order to compare the variation between individual groups, a Tukey post-test was done to search for possible significant differences in attachment percentage between species and incubation time. For all 12 categories the only significant difference found between species was the "-20 rabbit 48-hour" attachment and the "-40 rat" attachment. A significant difference between -20 and -40 scaffolds was also seen in the rabbit 48-hour testing, as reported earlier. There was no significant difference between any combination of the "-40 rabbit 24", "-40 rabbit 48" and "-40 rat" values, so the results, while significant in one of the tests, were not used in explaining the mechanism for overall cellular behavior in the scaffolds.

3.5 Cell Seeding on CFM Scaffolds

CFM runs were done on -10 and -40 scaffolds to examine the contractile behavior of fibroblasts as discussed earlier. The seeding done on the scaffolds was initially carried out in the same fashion as with the above seeded scaffold experimentation, but low attachment numbers led to the need for examination of a different technique. The blotting technique was tested in an effort to increase cell infiltration into the matrix, and the results are shown below.

Runs were done at different concentrations for different tests due to ongoing optimization aimed at increasing gross cellular number inside the scaffold. Results shown in Table 3.3 below are compared to previous results of -10 and -40 scaffold from rat fibroblast seeding runs.

Scaffold	Static Original (rat)	n	CFM static blot	n
-10	21.1±4.8 %	5	28.5±7.7 %	8
-40	15.2±3.3 %	5	25.1±3.7 %	7

Table 3.3 Cell seeding 22-hour attachment information from CFM runs

CFM runs with cells from P3V-P5 were used in calculating the -10 and -40 scaffold attachment for the blot numbers above. An ANOVA was done on the CFM seeding efficiency results to check for significant differences in attachment efficiency between static and CFM static blot techniques and also for seeding efficiencies between -10 and -40 scaffolds. A significant difference (P=0.003) was found between the four treatment groups. A Tukey post-test was then done to look for differences between individual groups. As reported earlier, no difference was found between the -10 and -40 static seeding results. For the CFM blot seeding, no significant difference was found between the -10 and -40 scaffolds. When comparing the static to the blot techniques, however, a significant difference in attachment percentage was found. A significant difference was found between the "-10 blot" and the "-40 static" values (P=0.002). In comparing only scaffolds of the same surface area, the "-40 blot" technique was found to have a significantly higher attachment percentage than the "-40 static" values presented earlier (P=0.027).

3.6 Cellular Distribution Through Scaffolds

Previous results published by O'Brien, et. al. (2004a) using scaffolds produced in the same fashion and exhibiting the same physical characteristics showed that cellular attachment was directly related to specific surface area (SSA). The O'Brien study was done using the MC3T3 cell line, an immortalized pre-osteoblast cell type with a general fibroblast morphology, and showed an increase in seeding efficiency as the available surface area inside the scaffold increased. Given that the results from the current study presented above do not show any correlation between fibroblast attachment and surface area, additional scaffolds were subsequently seeded, embedded, sectioned, and stained to examine the cellular distribution through the thickness of the scaffolds. Results are presented below.

Through-thickness Distribution of MC3T3 Cells

The image below shows the results of sectioning and staining of a -10 scaffold seeded with MC3T3 cells at the same density as the fibroblast study.

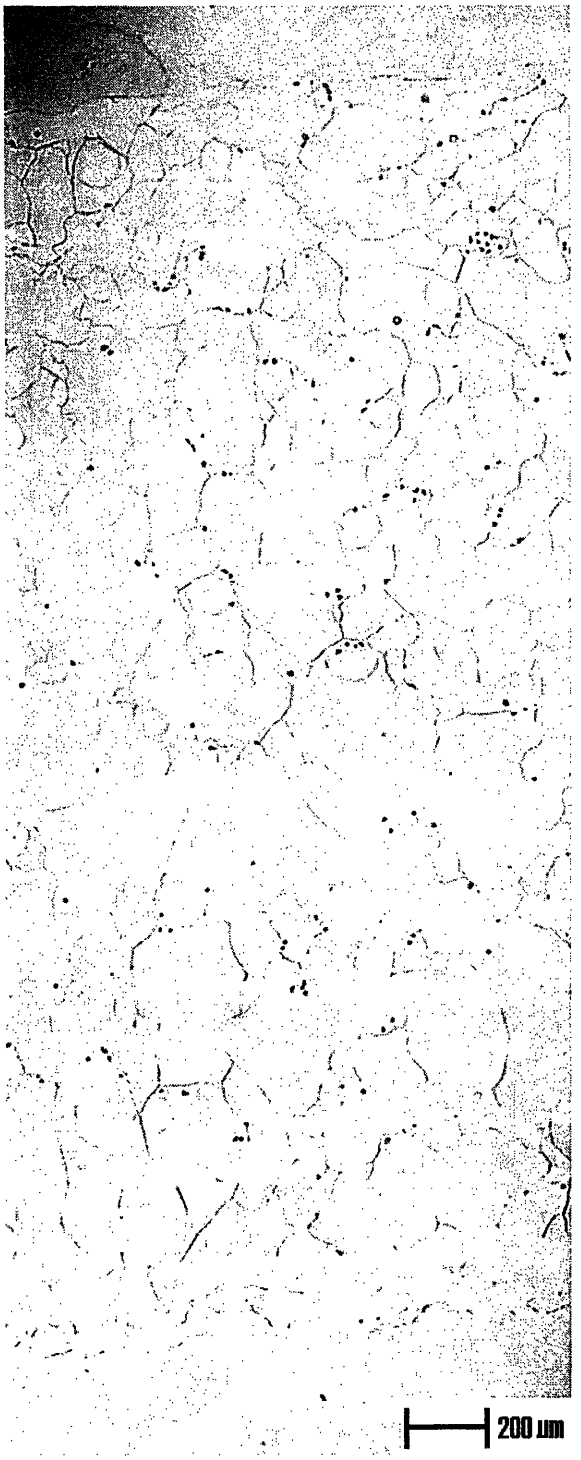

Figure 3.9 MC3T3 through-thickness micrograph of -10 scaffold at t = 0 hr.

The dark spots are stained cells and the lighter lines are stained collagen scaffold struts. Given that the through-thickness distribution of cells within the scaffold was relatively uniform at t = 0 hr., micrographs of 24-hour through-thickness distribution for MC3T3 cells are not included and were assumed to be similar to initial observations. It should also be noted that, while the cells do appear to be uniformly distributed through the scaffold, the first side to be seeded was not marked, and so can not be confirmed as the "shiny" or "non-shiny" side.

Rat Dermal Fibroblast Through-thickness Distribution

As shown above, the fibroblast seeding behavior did not follow the results reported by O'Brien et al. To examine the rat fibroblast distribution through the thickness of the scaffolds after static seeding, sections were obtained through the methods described in Chapter 2. In the staining procedure, the nucleus of the cell stains a dark brown, the cytoplasm a medium pink, and the collagen scaffold a lighter pink. Greyscale hues correspond directly to the original colors. Results are shown below for -10 and -40 scaffolds at t = 0 (sacrificed immediately after the second 10-minute incubation) and t = 24 hr.

For Images 3.10-3.13, composite pictures were assembled to illustrate the through-thickness distribution of rat fibroblast cells within the scaffolds. Given that initial embedding runs showed a marked difference in cell density with respect to scaffold top/bottom, scaffolds were re-embedded so the dry-seeded (1^{st} seeded) side was distinguishable from the wet-seeded (2^{nd} seeded) side. In Figures 3.10-3.13 below, the dry-seeded "shiny" side is shown at the top of each image.

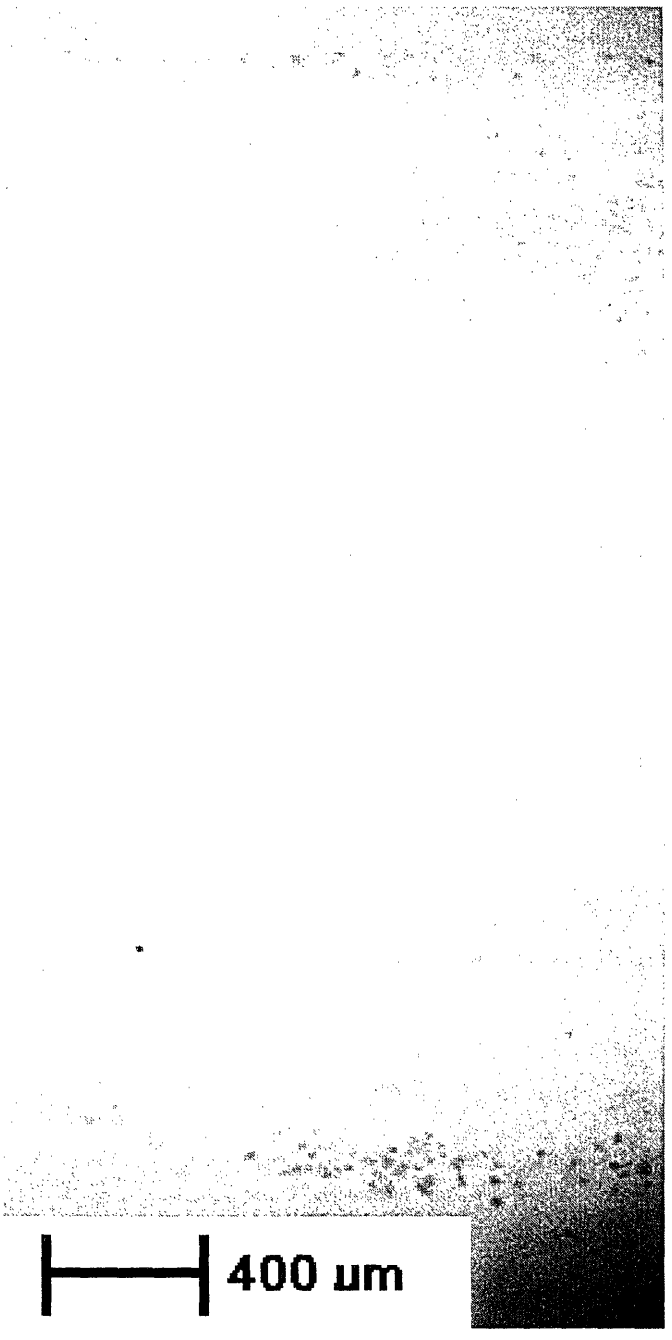

Figure 3.10 Rat dermal fibroblast -10 scaffold, t = 0 hr.

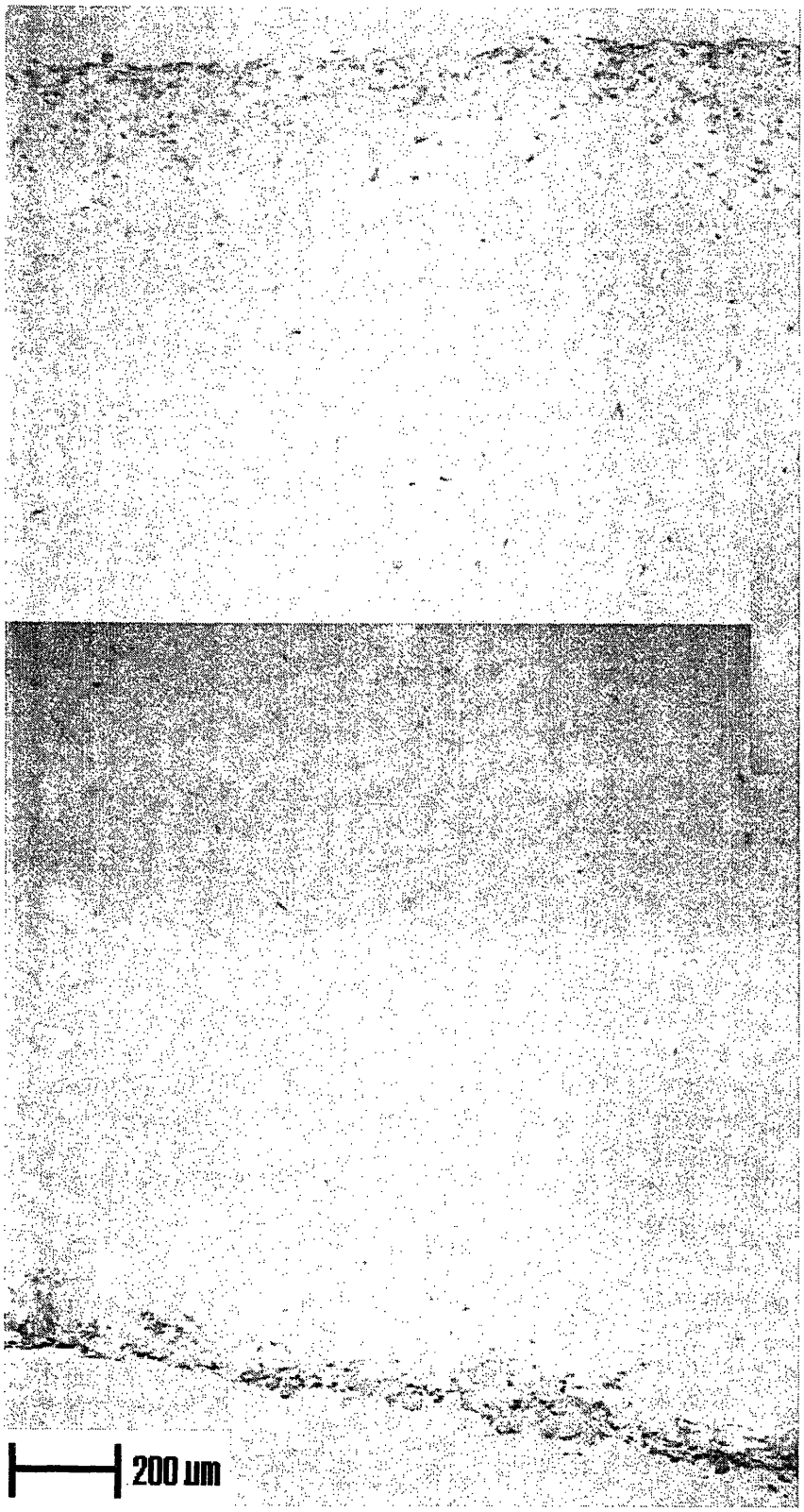

Figure 3.11 Rat dermal fibroblast -10 scaffold, t = 24 hr.

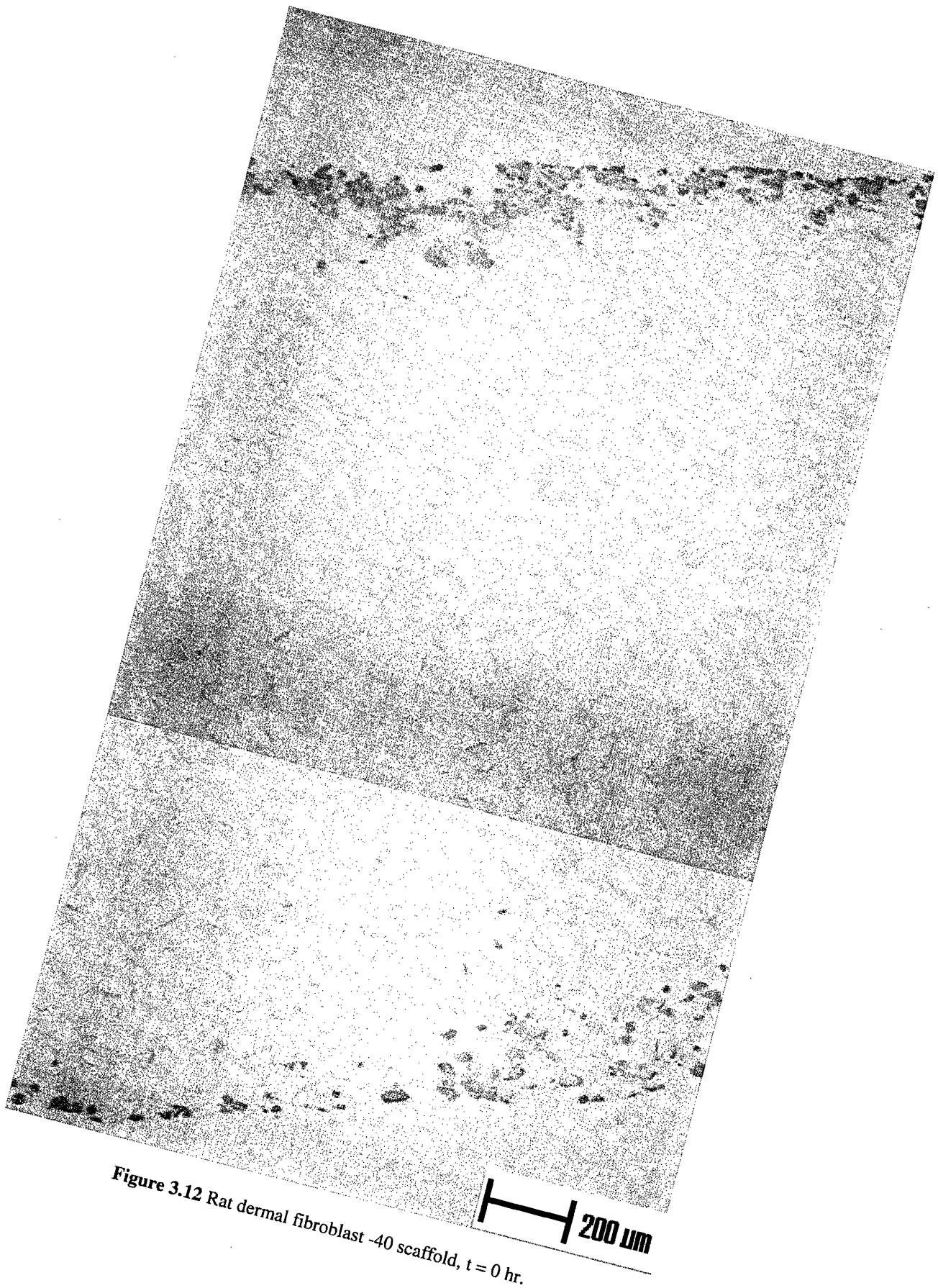

Figure 3.12 Rat dermal fibroblast -40 scaffold, t = 0 hr.

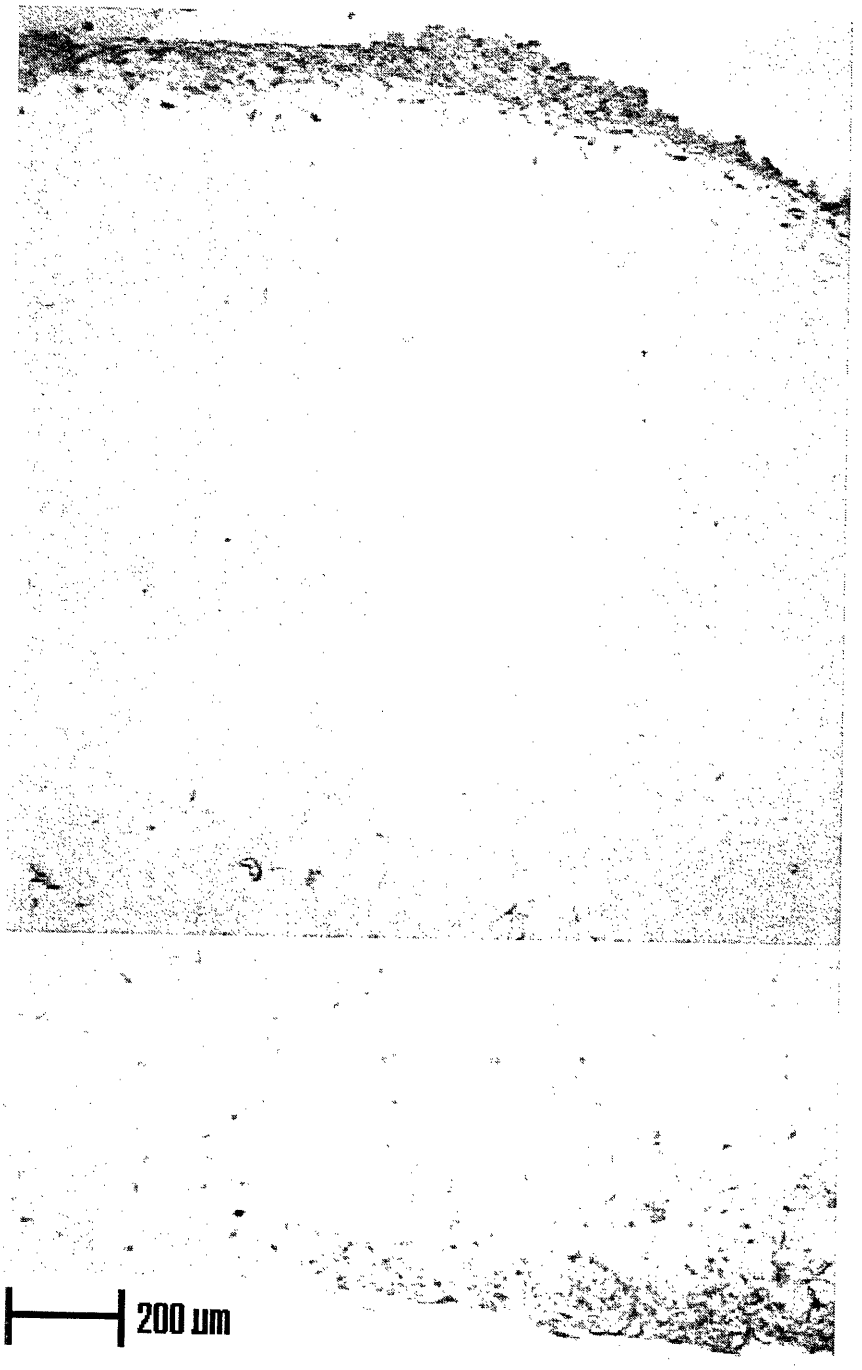

Figure 3.13 Rat dermal fibroblast -40 scaffold, t = 24 hr.

To show the cellular bunching that was observed on the surface of the scaffolds during seeding, several detail shots were taken of different scaffolds. Figures 3.14-3.16 show how cell distribution at the edge of the scaffold strongly differs from the inside of the scaffold.

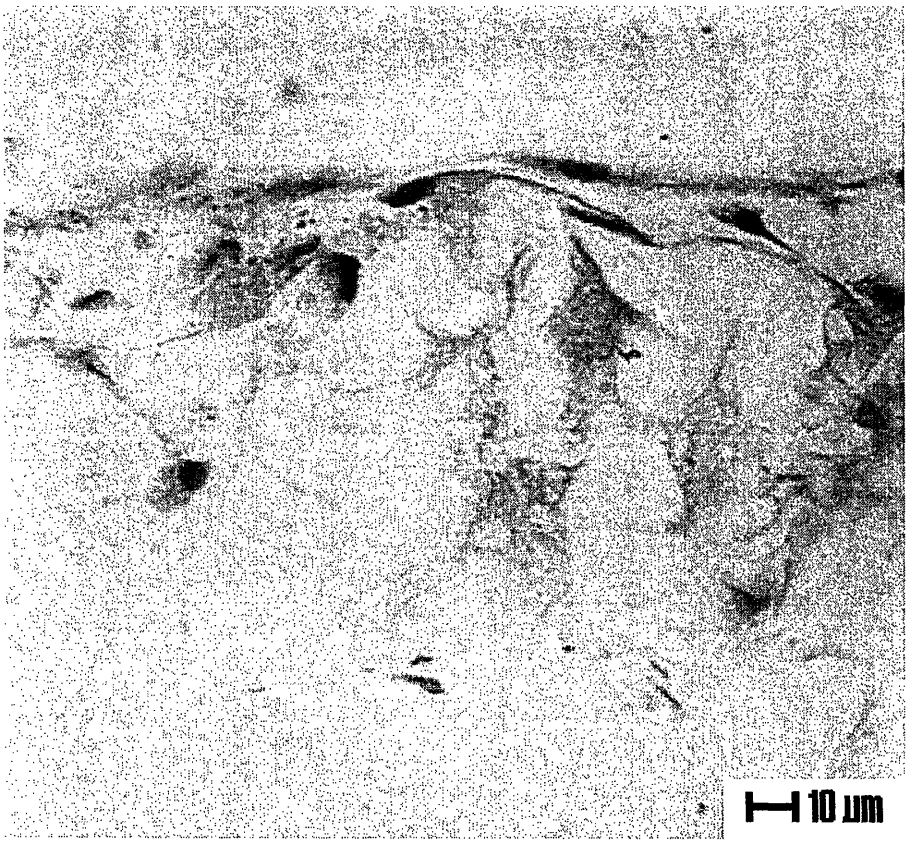

Figure 3.14 Rat dermal fibroblast -10 scaffold, t = 24 hr. ("non-shiny side")

Figure 3.15 Rat dermal fibroblast -40 scaffold, t = 0 hr. ("shiny" side)

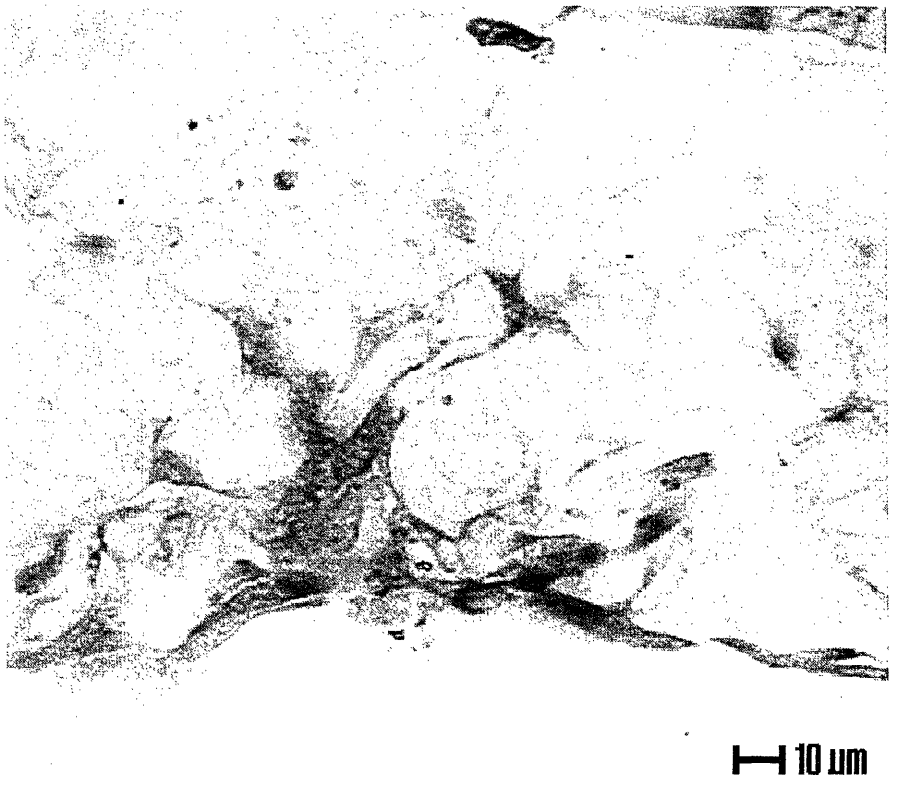

Figure 3.16 Rat dermal fibroblast -40 scaffold, t = 24 hr. ("shiny" side)

3.7 SEM Imaging of Scaffolds

Due to the irregular cellular distribution found within the scaffold, a scanning electron microscope (SEM) was used to obtain high-resolution images of the surfaces of the scaffolds. As noted earlier, the "shiny" and "non-shiny" sides were distinguishable to the naked eye. Images taken with the SEM help to give a better understanding of the micro-scale differences between the scaffold sides.

In order to compare the architectural differences between the current generation of scaffold and the previous generation of "quenched" scaffold, images were taken of both sides of the "quenched" matrix. This is shown in Figure 3.17.

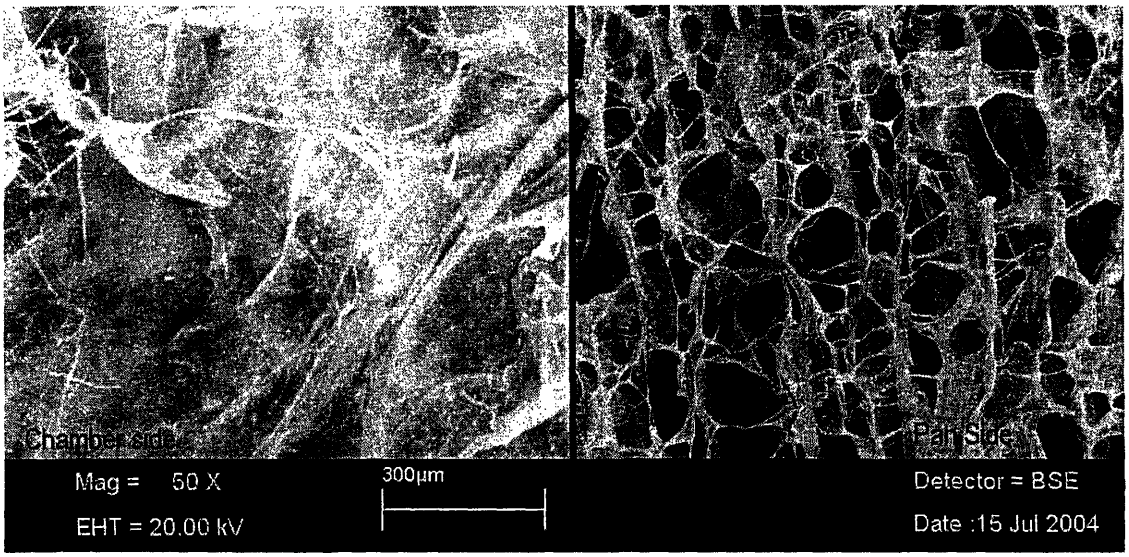

Figure 3.17 Quenched Matrix scaffold surfaces

The -10 and -40 scaffold surfaces, represented in Figures 3.18-21 below, show that the two sides, one exposed to the chamber atmosphere during freeze drying and one exposed to the pan during freeze drying, do differ in structure. For the new -10 and -40 scaffold fabrication procedures, the "chamber" side is referred to as the "shiny" side, and the "pan" side is referred to as the "non-shiny" or "fuzzy" side.

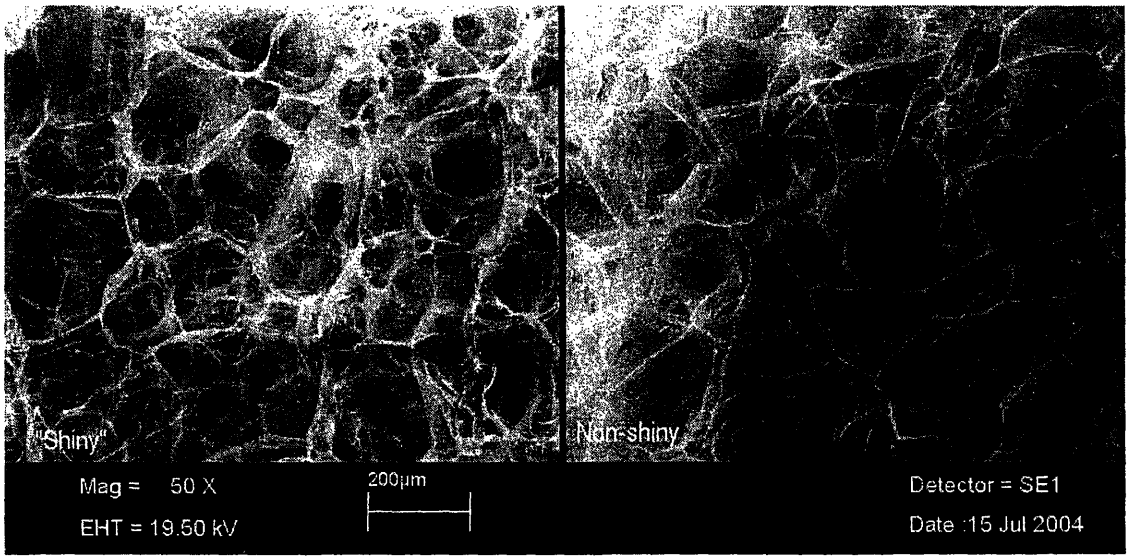

Figure 3.18 -10 Scaffold surfaces, uncoated

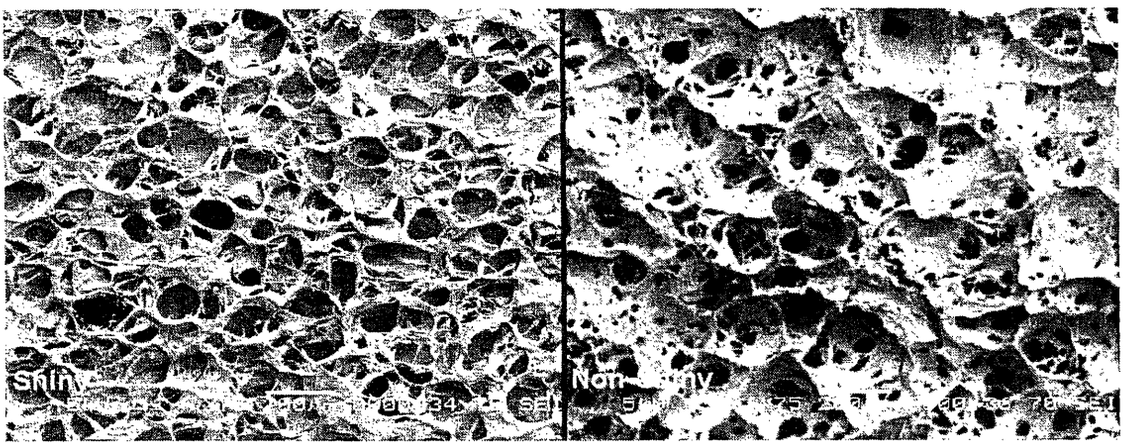

Figure 3.19 -10 Scaffold gold-coated (Images courtesy Amanda Blackwood, Olin College)

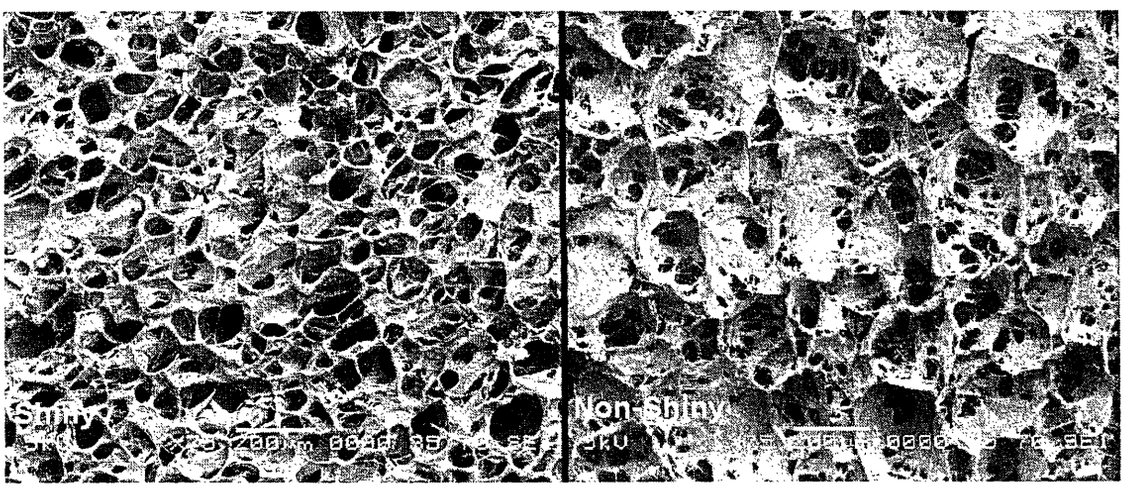

Figure 3.20 -40 Scaffold, gold-coated (Images courtesy Amanda Blackwood, Olin College)

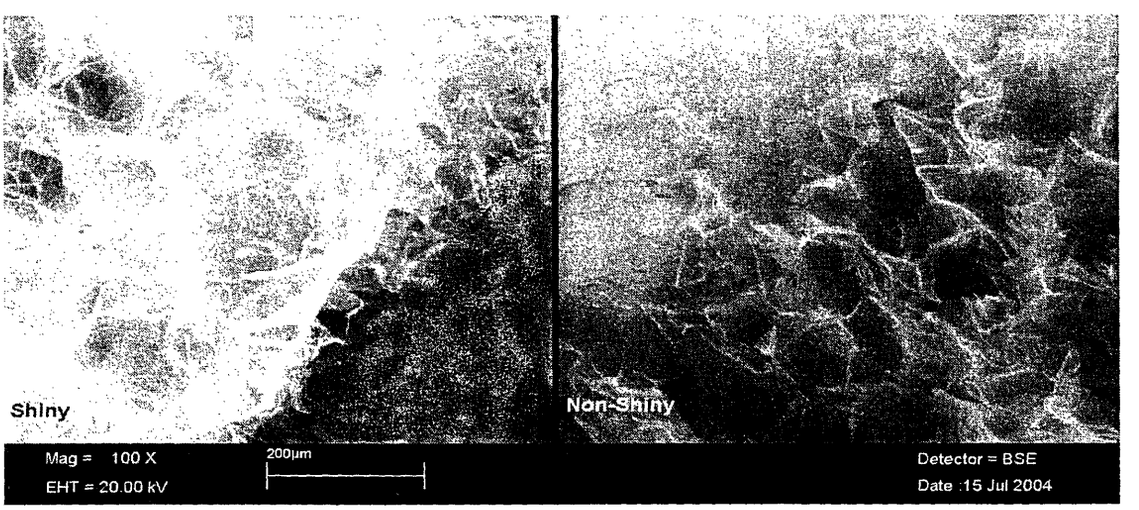

Figure 3.21 -10 Scaffold, uncoated- detail of cross-section edges

(Note: Lower right corner of "shiny" image airbrushed to remove reflection, scaffold unaltered)

3.8 Contractile Behavior in Scaffolds

CFM Runs

Individual CFM runs actually contain two data sets, with one curve corresponding to "CFM L" data and one curve corresponding to "CFM R" data. Calibration, grip, and matrix zeroing runs were done for both CFM's "L" and "R." Individual data sets/curves are considered to be directly comparable because of the similar calibration and zeroing behaviors observed on both CFM setups. Cell attachment numbers were also counted for both "L" and "R" for each CFM run, so the normalized cell contractile force is considered unique for all runs. This also applies to Aspect Ratio runs.

For different scaffold types, a new scaffold-only baseline was taken when a new sheet of prepared scaffold was used. Each sheet supplied enough scaffold to perform 3-4 CFM runs (7-8 data points).

In most CFM zeroing runs, the difference in scaffold-only response between CFM "L" and "R" was negligible (2 - 3.5% on average). In the case of the last sheet of -10 scaffold, the scaffold-only response deviated ~6% on average between the two sheets, so the two curves were combined to form a single scaffold-only response curve that was applied to both CFM "L" and "R."

In the aspect ratio scaffold-only runs, the 3:1 aspect ratio scaffold-only baselines showed an average voltage difference of 7.6%, so the two values were averaged and the resulting curve was used as the scaffold-only baseline for all 3:1 aspect ratio runs (n=4).

The 1:3 aspect ratio scaffold proved difficult to zero because the scaffold-grip setup extended across almost the entire length of the well. For this scaffold-only zero, two separate CFM zeroing runs were attempted. Three of the four zeroing curves produced a characteristic response, but a large voltage variation was seen between the three curves. In order to minimize the variation, the three curves were averaged and the single curve was used as the baseline response for all 1:3 aspect ratio runs (n=4).

CFM Zeroing

Grip-only baseline voltages were determined as detailed in Methods section above. Calibration curves can be found in Appendix 4. An example of a scaffold-only calibration curve is shown below in Figure 3.22. Figures are expressed in voltage (displacement) vs. time.

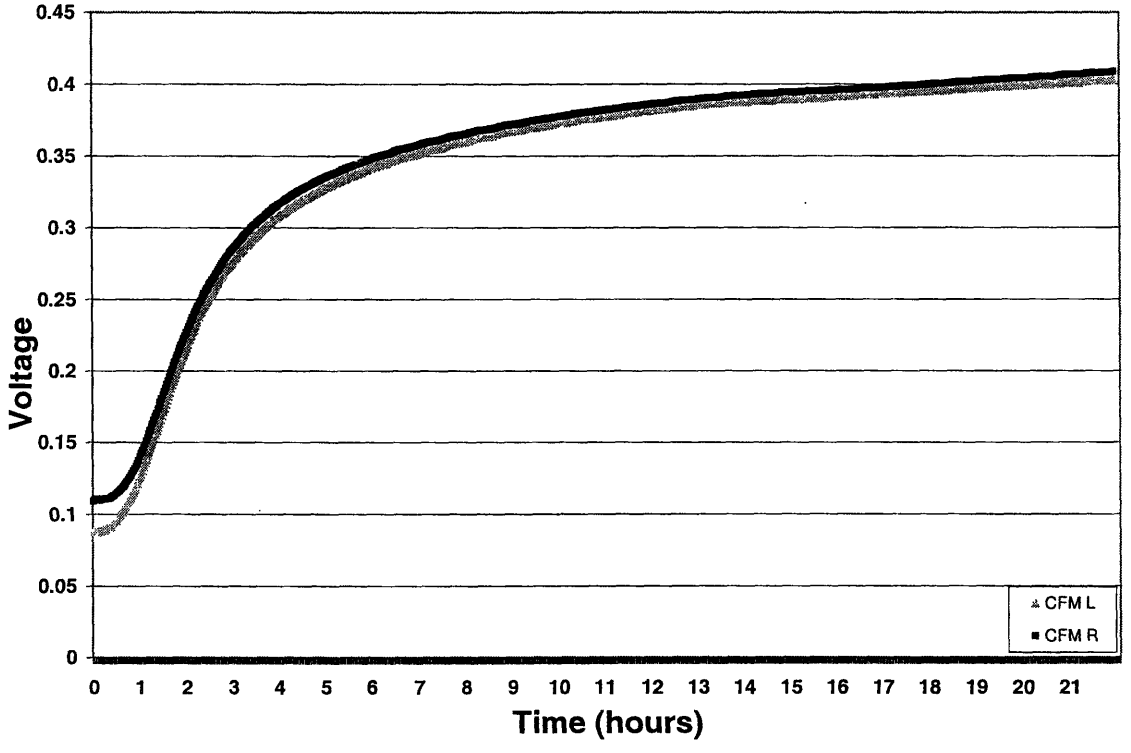

Figure 3.22 Typical CFM scaffold-only response

Cell-Only Contractile Response

The general results for all -10 and -40 seeded scaffold runs are shown in Figures 3.23-24. Note that the shaded area represents the standard error of the mean (SEM).

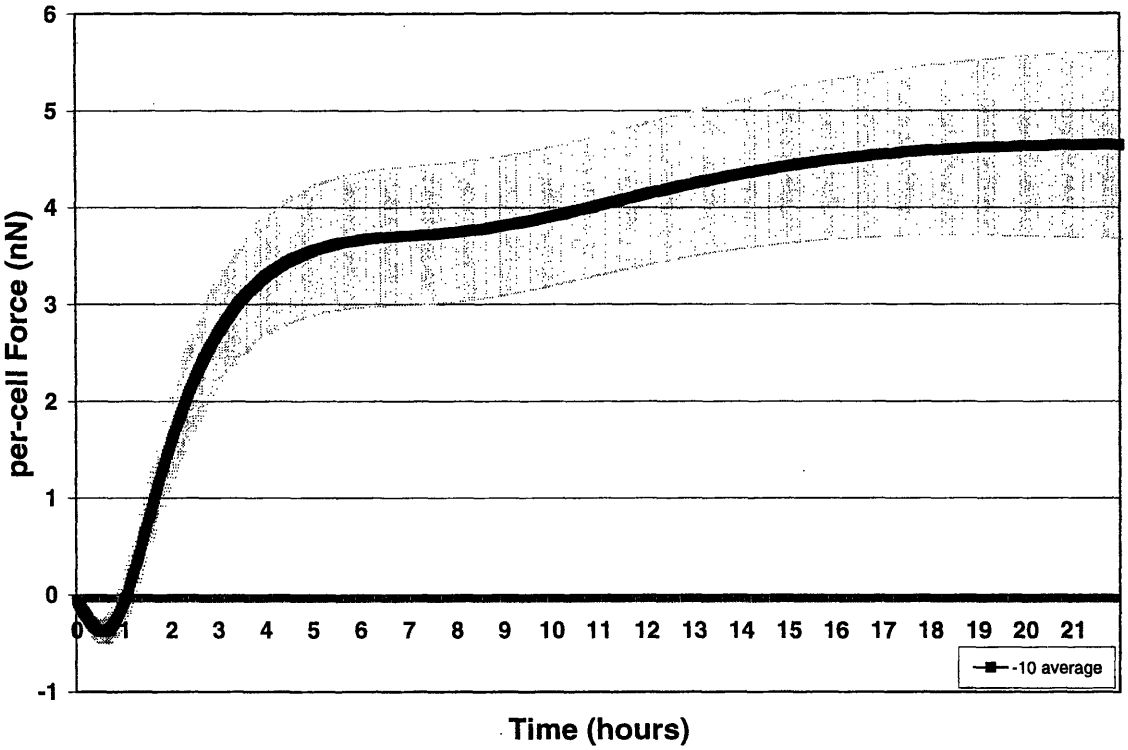

Figure 3.23 CFM rat fibroblast-only contractile response for all -10 matrix runs (n=8)

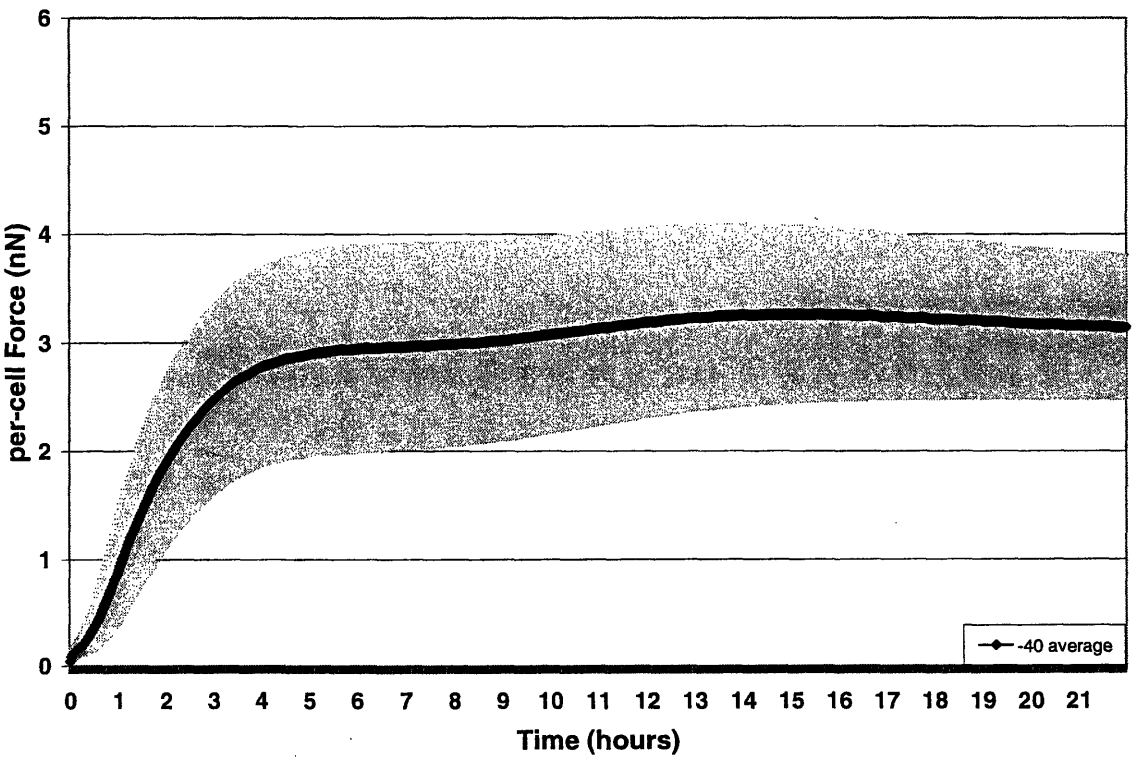

Figure 3.24 CFM rat fibroblast-only contractile response for all -40 matrix runs (n=7)

In all runs, a two-stage contractile mechanism was observed. The per-cell contraction force curve reached either a maximum point (1st derivative zero) or an inflection point (2nd derivative zero) between 4-9 hours. This was taken to be a characteristic response of the cell behavior in the scaffolds.

All results were re-grouped by scaffold type and by passage number to see whether contractile response significantly depended on scaffold type or passage number. The "P3V" and "P4V" passage labels refer to cells grown with the new passaging technique (see Chapter 2.3). The "P4" and "P5" passage labels refer to the cells cultured using standard splitting ratios.

The rate of generation of initial contractile force (initial contraction curve slope) is presented in Figures 3.25-26. For all runs, the most linear section of the initial contraction curve was selected by inspection. The same number of timesteps were selected from each curve to calculate the average slope. The slopes presented show the initial rate of contraction, up to 6 hours, for both scaffold types and all passage numbers. An ANOVA was performed on the gross slope value data represented by the linear trendlines shown in Figures 3.25-26. A significant difference ($P<0.001$) was found to exist between all slope values for both scaffold types and all passage values. When broken down into individual scaffold types, a significant difference ($P=0.024$) was found between the different passage numbers in the -10 scaffold runs. A significant difference ($P=0.012$) was also found between the different passage numbers in the -40 scaffold runs. A Tukey post-test was then used to check for significant differences between specific passage numbers within the ANOVA ($P<0.001$) performed on all -10 and -40 runs. For the -10 scaffold, a significant difference was found between the P5 and the P3V scaffold ($P=0.002$), as well as between the P4 and the P3V scaffold ($P=0.01$). For the -40 scaffold, a significant difference was found between the P5 and the P4 scaffold ($P=0.005$) and between the P5 and the P3V scaffold ($P=0.003$).

It should be noted in Figures 3.25-26 that the "minutes" scale is not absolute, and does not represent total elapsed time from the beginning of the experiment. Also, the linear trendlines presented correspond to the curve of the same shade.

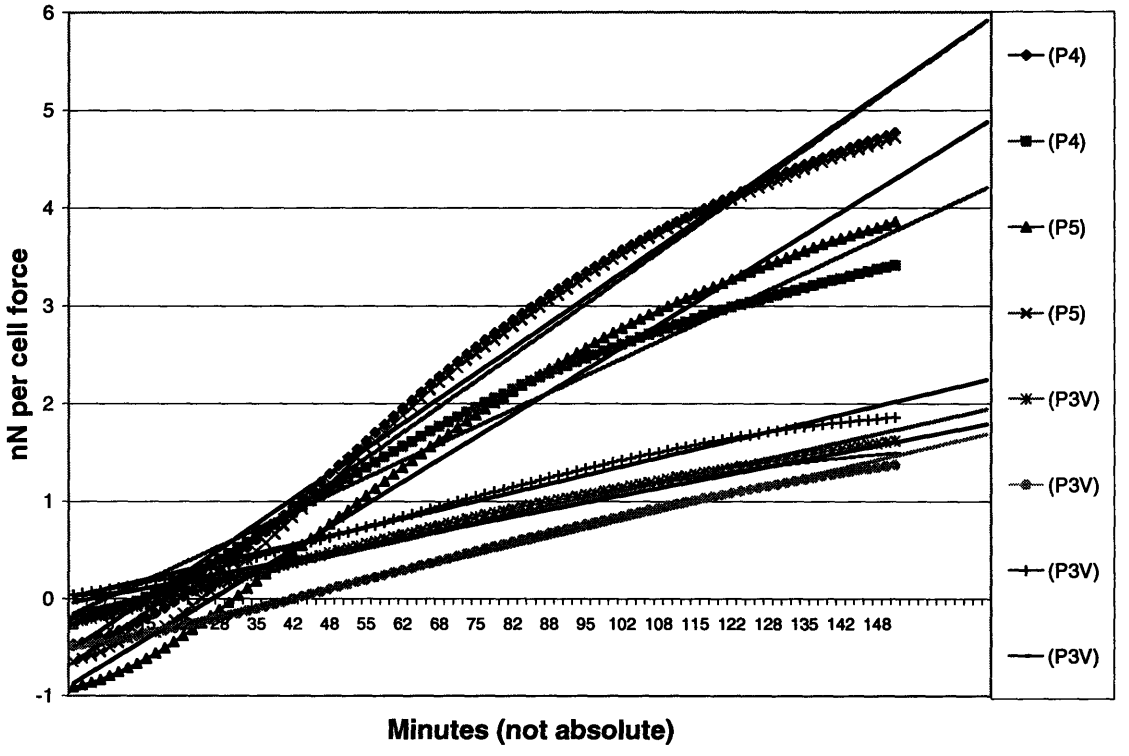

Figure 3.25 Initial contraction rate for -10 scaffold

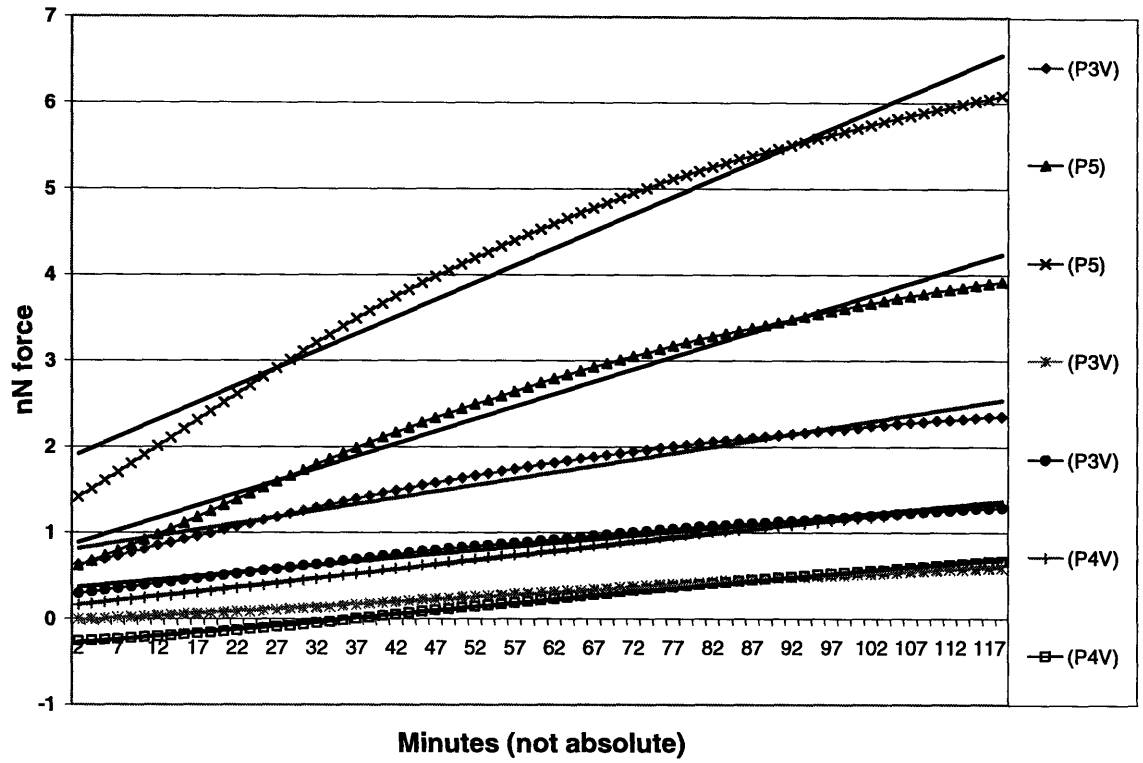

Figure 3.26 Initial contraction rate for -40 scaffold

CFM Inflection Point and End-of-run Force Value Determination

The difference in behavior between passages and matrix types for three critical parameters were measured for this study. The initial slope, inflection point contractile force value, and 22-hour (final) per-cell contractile force value were determined to be characteristic parameters of the individual runs. The inflection point where the slope of the force curve went to zero (1st derivative zero) was determined by inspection of the generated data columns. In the runs where the slope of the force curve did not go to zero, a best-fit curve (3rd order polynomial) was calculated (R^2 value of >0.995) and the roots of the second derivative were calculated to obtain the inflection point, measured in terms of the timestep of the curve. The corresponding force value was extracted from the data spreadsheets once the inflection point timestep was known. An ANOVA was done to compare the inflection point force values between passage numbers as well

as the final contractile force values between passage numbers. Results are shown in Table 3.4 below with SEM as error.

Scaffold/ Passage	Initial Contractile Slope (nN/Timestep)	Inflection Point Force (nN)	Final 22-hour Force (nN)
-10 (all)	0.0393±0.007 (n=8)	3.72±0.73 (n=8)	4.64±0.96
P3V	0.0208±0.0009 (n=4) *@	1.91±0.087 (n=4)	2.47±0.55 *
P4	0.0539±0.010 (n=2) @	4.98±0.82 (n=2)	5.23±0.42
P5	0.0616±0.004 (n=2) *	6.07±0.73 (n=2)	8.38±0.26 *
-40 (all)	0.0276±0.008 (n=7)	3.01±0.94 (n=7)	3.14±0.67
P3V	0.0160±0.005 (n=3) #	1.57±0.55 (n=3)	2.36±0.40 #
P4V	0.0157±0.002 (n=2) $	1.82±0.38 (n=2)	2.01±0.31 $
P5	0.0478±0.009 (n=2) #,$	6.34±1.4 (n=2)	5.44±1.1 #,$

Table 3.4 Initial contractile slope, inflection point force, and 22-hour contractile per-cell force value (Significant difference denoted by *,@,#,$ for respective groups)

As shown above in Table 3.4, the initial contractile slope, inflection point force, and final contractile force are similar when comparing the same passage number between scaffolds. This observation is based on the lack of a significant difference between P3V values for -10 and -40 scaffolds and P5 values for -10 and -40 scaffolds for the characteristic parameters measured (statistical analysis between -10 and -40 scaffolds not shown, $P>0.5$ in all cases). A transition in contractile behavior in passage 4 can be seen in the -10 and the -40 scaffold data. The difference between the passage numbers 4 and 4V was due to a change in culture technique. This transition in behavior between the P4 and P4V values seems to indicate a difference in the rate of contractile behavior change due to the changes made in the culture conditions. Given this

transition behavior, CFM runs were grouped according to observed contractile behavior for further statistical analysis. In the case of the -10 scaffolds, the P4 and P5 runs were shown to be statistically similar in all categories, so the results were grouped together as P3V and P4/P5. In the -40 scaffold runs, the P4V cells behaved more like the P3V cells, so results were grouped as P3V/P4V and P5. This grouping helps to show the completion of the implied trend through evaluation of the inflection point contractile values, as shown in Table 3.5 below.

Passage	Inflection Point Contractile Value (nN)	
-10 P3V	1.91±0.087 (n=4)	*(P=0.001) $(P=0.001)
-10 P4/P5	5.52±0.55 (n=4)	* @(P<0.001)
-40 P3V/P4V	1.67±0.32 (n=5)	#(P<0.001) @
-40 P5	6.34±1.4 (n=2)	# $

Table 3.5 Inflection point force grouped by passage contractile behavior (significant difference denoted by *,$,#,@)

For the 22-hour final contractile force values, the observed trend holds nearly constant across the different passage numbers. Overall, a significant difference was found between the different passage numbers for the final contractile force magnitude ($P<0.001$). A Tukey post-test was then run on the data to check for significant differences between individual passage numbers. A significant difference was found in the -10 scaffolds between the P3V and P5 runs ($P<0.001$), as well as in the -40 scaffolds between the P3V and P5 runs ($P=0.044$) and between P4V and P5 runs ($P=0.041$).

When the runs are grouped together as -10 P4/5 and -40P3V/4V, overall statistical significance still holds ($P=0.016$) when performing an ANOVA on ranks. The equal variance test, used as a measure of variation within a sample group, was performed in the SigmaStat software package before running ANOVA analyses. When the equal variance test fails, as in this case, an ANOVA on ranks is performed on the data. A Dunn's post-test was used in conjunction with the ANOVA on ranks to check for differences between individual groups. It was found that

statistical significance disappeared between all individual groups except between the -10P4/5 and -40P3V/4V ($P<0.05$).

3.9 Aspect Ratio Results

Cells used in the aspect ratio study for 3:1 and 1:3 data were P4V and P5V, utilizing the new cell passaging technique. The results from the runs done with these cells were compared to P4 and P5 data from -10 scaffold experimentation detailed in the previous section. The data used was separated out from other -10 scaffold runs and is presented below.

The contractile force generation curves for the 1:1, 3:1, and 1:3 aspect ratio runs with -10 scaffold are shown in Figures 3.27-29. In all figures, error is represented by SEM.

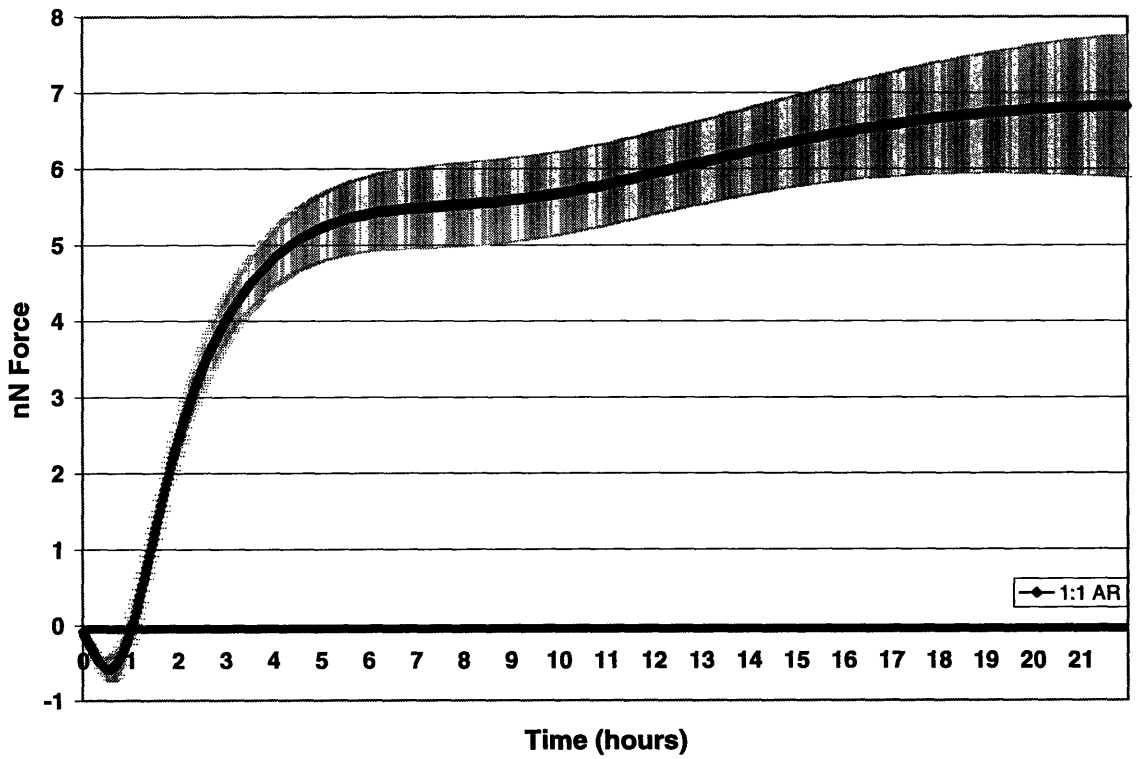

Figure 3.27 1:1 aspect ratio run results, rat dermal fibroblasts (n=4)

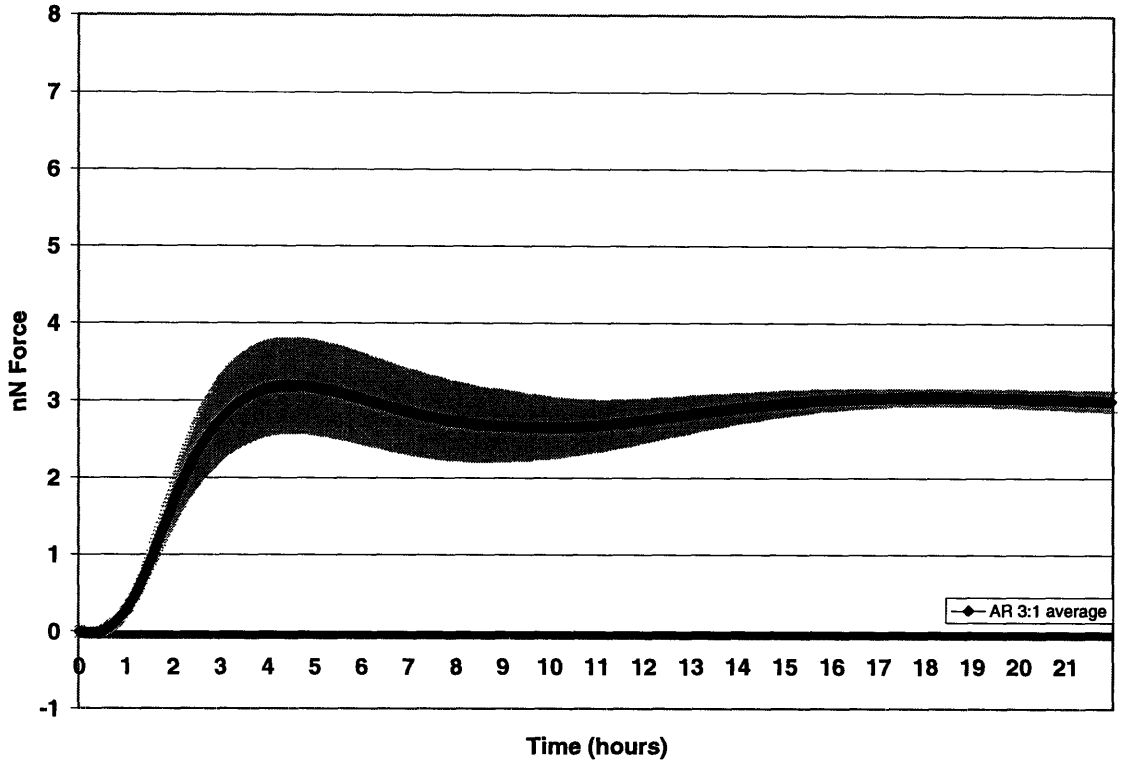

Figure 3.28 3:1 aspect ratio run results, rat fibroblast (n=4)

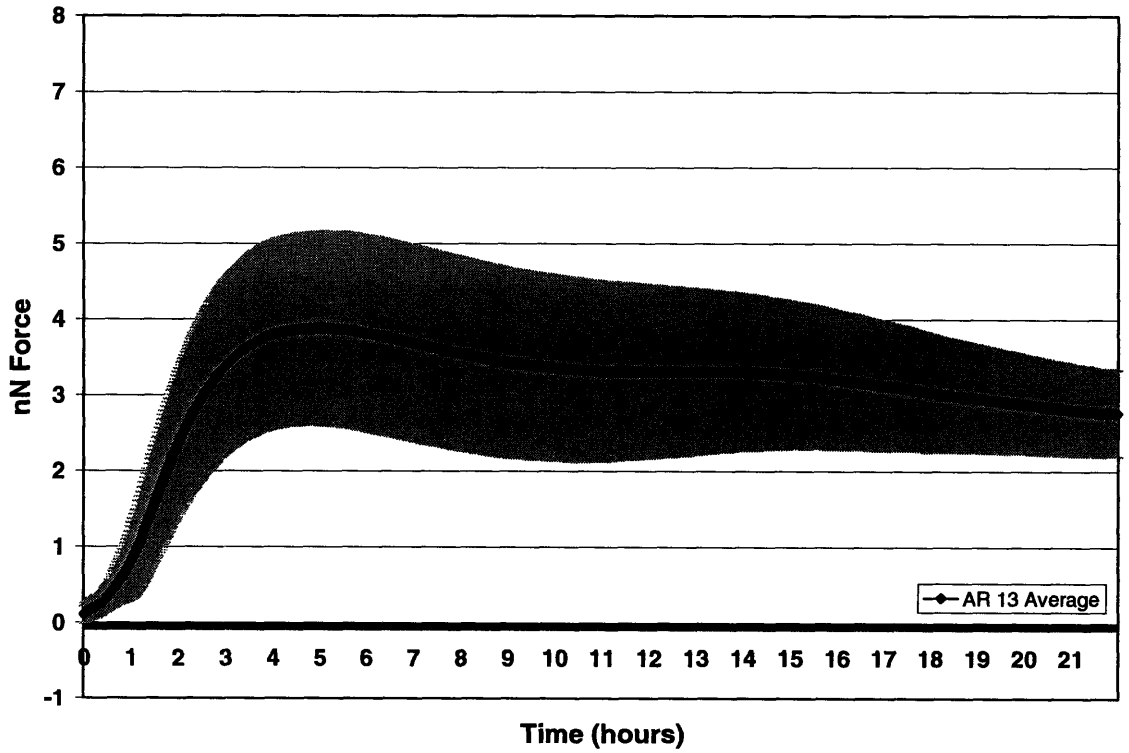

Figure 3.29 1:3 aspect ratio run results, rat fibroblast (n=4)

The same characteristic hump behavior as seen in the original CFM runs was also seen in the aspect ratio samples.

A comparison between 1:1, 1:3, and 3:1 aspect ratios was then carried out using the averaged -10 scaffold data as the basis for the 1:1 values. Statistical analysis via ANOVA was performed on the data to check for differences in initial contractile slope value. No significant difference was found between the initial contractile slope values for the aspect ratio runs (P=0.148). Due to the large data spread within the small number of runs done with each respective aspect ratio size, statistical analysis proved difficult to perform. An equal variance test was performed before running all ANOVA analyses. When comparing the inflection point force values and final contractile force values for the aspect ratio runs, the equal variance test failed. Statistical analysis performed on samples with a wide intra-sample variation utilized Mann-Whitney rank sum tests and ANOVA on ranks. Overall, no significant difference was found between the inflection point force values (P=0.296) when performing an ANOVA on ranks. A significant difference was found overall between the final contractile force values (P=0.015) when performing an ANOVA on ranks. No significant differences were found between groups within individual ANOVA analyses for any of the three measured characteristic values.

It should be noted that the same cell population was used (P4V and P5V) for the 1:3 and 3:1 aspect ratio runs. The 1:1 aspect ratio runs, taken from the original CFM runs presented earlier, represented P4 and P5 passages. This most likely describes the difference in average contractile force seen between the 1:1 runs and the other two aspect ratio setups. Results of the measured characteristics for the three aspect ratio types are reported in Table 3.6.

Aspect Ratio	Initial Slope (nN/timestep)	Inflection point force (nN±SEM) (#)	Final Force (nN±SEM) (#)
1:1	0.058±0.005	5.52±0.55	6.81±0.93
3:1	0.040±0.008	3.20±0.61	3.00±0.13
1:3	0.037±0.008	3.89±1.28	2.77±0.57

Table 3.6 Results for Aspect Ratio CFM runs

(Note: * or $ denotes statistical significance between groups, # denotes failed variance test)

The amount of data available, coupled with the problems with intra-sample variation, preclude any useful comparison of the effects of passage number on aspect ratio contraction, so no comparison is made in this study.

Chapter 4 Discussion

4.1 Scaffold Fabrication

As found by O'Brien, et al. (2004b), the pores created in this fabrication method were found to be more equiaxed compared to the previous quenching method of scaffold fabrication devised by Yannas, et al.(1980a). The standard deviation of pore size was also found to be smaller in the new technique. The surface area calculation shows that, as predicted by considering the ice particles as packed spheres, as the average pore size decreases, the available surface area increases (Funk and Dinger 1994). If cellular migration is not inhibited by geometry, cell size, scaffold pore size, or pore interconnectivity, then the cellular attachment values should depend on the number of binding sites available to the cells. The surface area consideration is valid only if the cells can freely migrate through the structure upon initial seeding.

As reported earlier, the scaffolds produced appear to have differing surface pore characteristics on the "shiny" and "non-shiny" sides. The creation of this "shiny" surface is most likely due to a surface tension effect on the top of the slurry exposed to the chamber atmosphere during freeze-drying. As evidenced by Figures 3.9 and 3.12, the pore characteristics appear to differ between the shiny surface and the non-shiny surface. If the surface tension created a less permeable pore structure at the immediate surface of the scaffold, this could be a possible mechanism explaining the inconsistent behavior between different cell types. The combination of this surface effect with the larger size of the fibroblasts compared to the MC3T3 cells may explain the different infiltration and attachment phenomena observed in the scaffolds.

4.2 Harvesting of Dermal Tissues

The work undertaken in this study was aimed at further characterizing the behavior of different cell types within mechanically and physically similar collagen-GAG scaffolds. The dermal fibroblast was chosen as an important cell type because the behavior of the dermal

fibroblast in a collagen-GAG scaffold has been well characterized in this lab (Yannas, Lee et al. 1989; Freyman, Yannas et al. 2001; Freyman, Yannas et al. 2001; Freyman, Yannas et al. 2002). The dermal fibroblast continues to be used in ongoing work with the characterized Collagen-GAG scaffolds fabricated in this lab and partner labs, so information obtained from this study can be directly compared to results obtained in future studies.

The methods for harvesting tissue used by Freyman, et al. (2001c) involved one to two weeks of migration of cells from the minced tissue to the culture flask. All Dutch Belted rabbit tissue harvests were performed according to this explant outmigration procedure. In all cases the cells, upon migrating to the tissue culture flask, would remain clumped around the tissue fragments. Fears that the "stacking" of cells in such a localized orientation was causing to premature phenotype changes led to the exploration of other harvest procedures.

In addition to preservation of cell phenotype, it was desired that new protocols liberate viable cells in a shorter time span than two weeks. Protocols used in the liberation of chondrocytes from articular cartilage were attractive because of the possibility of obtaining viable cells in less than 24 hours (Nehrer, Breinan et al. 1998).

The vortex method, adapted from Troxel (1994), was investigated because aggregates of cells were found to be floating in the solution after Trypsin treatment with the serial digestion method. In most observed cases, the cells were found to be clumped around undigested tissue fragments. The hypothesis for this behavior was that the cells were never fully liberated from the tissue during Collagenase treatment. In some cases, the clumped cells and tissue fragments would settle to the bottom of the flask after centrifugation, resuspension, and seeding. In this case the cells would often eventually adhere, but the same bunching problems, as seen with the explant outmigration procedure, were observed for the cells in culture. In other cases, the clumps of cells never settled to the bottom of the flask and were lost.

To disrupt the cellular adhesion to the ECM fragments, it was reported by Troxel that brief vortexing could help to disaggregate cells from remaining tissue fragments. The basic

theory was that the vortexing was similar to Trypsin treatment, but would achieve the same objective by mechanical instead of chemical means. Given the limited success in seeing individual cells liberated from tissue clumps by Trypsin in the serial digestion method, the vortexing method was tried and found to be successful in producing viable cells. However, the success rate of this method was similar to the serial digestion method. In some harvests, even though the same vortex protocol was followed, no viable cells were liberated from the tissue. The assumption is that the shear forces created by excessive vortexing actually tear the cell membranes, destroying cells instantly. Excessive Trypsin treatment during tissue digestion (the chemical analog to vortexing), due either to enzyme concentration or duration of cellular exposure, can chemically alter the cell membrane and receptor behavior and also destroy cells (Mediatech Technical Information 2004).

4.3 Cell Culture

Results reported by Freyman (2001a)show that previous culturing techniques yielded 3-5 million cells / 75cm^2 flask. This is substantially larger number than the quantities obtained in this study as described above.

From a geometric standpoint, the number of cells per confluent flask would seem to be dependent on gross cell size. While this effect may account for part of the story, the attachment behavior of cells to substrates may offer an additional mechanism for the decreasing cell counts with increasing time in culture. As modeled in a study of the kinetics of fibroblast attachment (Frisch and Thoumine 2002), as the adhesion energy per area, w_a, of the cell increases, the asymptote of the contact radius of the cell with the substrate will increase as well. If this study is coupled with the work of Hinz, et al. (Hinz, Celetta et al. 2001), amongst others, who found that α-SMA increased the strength of cellular adhesion of myofibroblasts, along with the work of Kinner and Spector, who found that α-SMA expression increased with increasing passage and time in culture for articular cartilage cells (Kinner and Spector 2001), then it is possible to

hypothesize that the *in vitro* culturing conditions led to a phenotype change in the cells. By this argument, the changing behavior of the dermal fibroblasts with increased *in vitro* culturing and passaging is in line with other experimental results. The parameter that needs to be determined, however, is whether or not the phenotypic change that occurred within the cells was significant enough to make grouping of all test results, from P2-P6 in the rabbit fibroblasts and P3V-P5 in the rat fibroblasts, valid as having come from the same cellular population. For the cell seeding study, this assumption was made and all results were assumed to be based on "identical" cells. As shown from the results of the CFM study in Chapter 3, a case can be made from the data that the different cell culturing procedures (differing in passaging procedure only) induced partial differentiation at different passage numbers.

4.4 Cell Seeding Considerations

Previous results reported by O'Brien, et. al. (2004a) using scaffolds produced according to the same protocols and exhibiting the same physical properties showed that increased cellular attachment directly correlated to an increase in specific surface area (SSA). The study was done using the MC3T3 cell line, an immortalized pre-osteoblast cell type with a general fibroblast morphology. Preliminary data from Chachra, also done in the same laboratory with the same characterized scaffolds but using primary osteoblast cells harvested from mouse calvaria, yielded results that showed no significant difference in attachment percentage due to changes in average pore size/SSA of the scaffold (Chachra, unpublished). The osteoblast seeding data from Chachra shows the same trend as the rabbit and rat fibroblast seeding data from this study, though the average attachment percentages varied between the two cell types.

The behavioral inconsistencies between the MC3T3 and fibroblast cell types within the same environment can be explained by a number of mechanisms.

From a mitotic and phenotypic standpoint, the respective cell types exhibit different behaviors. The MC3T3 cell is, as previously stated, an osteoblast progenitor cell. It is also an

immortalized cell line, meaning that the characteristics of the cell (including cell size, integrin behavior within the ECM, and rate of senescence) do not change with passaging. As shown in Chapter 3, the rat dermal fibroblasts were observed to undergo behavioral changes with increasing passage number. The gross cell size was observed to increase and the number of cells found in confluent flasks was found to decrease with increasing passage number for both rabbit and rat fibroblasts. This behavior hints at a passage-dependent phenotype change, though specific quantification of the changing cellular characteristics was considered to be beyond the scope of this study. As stated earlier, the observed trend leads to a hypothesis of increased α-SMA expression in the fibroblast cells used in this study with progressive passaging and increased time in culture. For the primary osteoblast experimentation, the cells were only expanded, not passaged, before use, so phenotypic changes were likely to be minimal within the week between harvest and experimentation. Cellular behavior of the primary osteoblasts was assumed to be similar to *in vivo* cellular behavior due to the short residence time in culture.

It should also be noted that the three cell types were of different origin with respect to life cycle of the host animal. The primary osteoblasts were taken from newborn mouse calvaria. The MC3T3 cell line also originated from newborn mouse calvaria, but had been immortalized through successive passaging (ATCC 2004). The rat and rabbit dermal fibroblasts were taken from both adolescent and full-grown adult tissues. Cells are well known to behave differently in different stages of life. This is evidenced by studies of embryonic, neonatal, and adult cells of similar tissue types, which have been shown to exhibit different levels of mitotic activity, contractile activity, and regenerative behavior (Yannas 2001).

It is not known what effect initial dry seeding on the "shiny" side of the scaffold had on cell seeding efficiency. All samples used in both the seeding study and the CFM study were seeded shiny-side first. The apparent change in scaffold structure at the shiny surface, qualitatively observed in Figures 3.9 and 3.12, may explain the inconsistency of seeding results

between the smaller MC3T3 and larger dermal fibroblast cell types. However, this mechanism can not be used as a complete explanation for the differing cellular attachment behaviors.

The most plausible argument on differing attachment results between cell types may come from the observation that the cell size differed largely between the cell types, as shown in Figures 3.3-3.5. The rabbit and rat dermal fibroblasts were observed to be up to three times larger in diameter compared to MC3T3 cells. A slight change in cell size was also qualitatively seen between passaging technique, as shown in Figures 3.4 and 3.5. Effects of changing cell size due to increased Passage number were not quantified in the seeding results described in Chapter 3.

If the rabbit and rat fibroblasts were larger than the MC3T3 cells, it is possible that the larger cells simply were not able to penetrate through the boundary pore layer on the shiny side of the scaffold as easily as the smaller cells. This size consideration may not have affected the seeding efficiency to such an extent on the other (non-shiny) side of the scaffold in a dry-seeding configuration. However, as the non-shiny side of the scaffold was always seeded after initial rehydration, the fact that the scaffold was already saturated with media may have negated any possible influence of a different boundary layer structure on seeding efficiency. The CFM runs (explained below) that utilized the "blot" technique may well have been able to use the capillary action phenomena of media infiltration into the bulk of the scaffold, due to the reduced saturation of the non-shiny side when seeding.

If the fibroblasts were simply adhering to the outside edges of the scaffold, then the internal specific surface area differences between scaffolds would not be expected to affect the attachment percentage. Since all scaffold pieces were cut to the same size (22mm x 15mm x 3mm) in the initial attachment study, the external surface area would theoretically be approximately the same. Given that both the rabbit and rat dermal fibroblast seeding runs showed no significant variation in attachment percentage between scaffolds, the surface agglomeration theory of attachment seemed most likely.

CFM attachment numbers were based on scaffolds that were twice the size (22mm x 30mm x 3mm) of the attachment scaffolds, seeded with twice the gross number of cells in most cases. The "blot" technique in the CFM runs helped to increase cellular attachment percentages, as shown by Table 3.3. This is most likely due to the fact that the blotting occurred on the non-shiny side of the scaffold, reducing the saturation of the scaffold and enabling more cell suspension to penetrate deeper into the scaffold upon secondary seeding by means of capillary action.

To investigate the theory of surface agglomeration, the scaffolds were seeded with rat fibroblast cells and sacrificed as described in Chapter 2. The scaffolds used for the sectioning study were 8-mm diameter punches seeded to the same concentration of cells per volume of scaffold as the larger cell seeding and CFM pieces. The smaller scaffold samples were used due to the limited amount of fibroblasts available for seeding and also because of the ease of handling smaller pieces during the embedding dehydration and infiltration process. It was assumed that the behavior of the rat fibroblasts in these smaller scaffold pieces mimicked the behavior of the cells in the larger pieces. The results of the embedding and sectioning procedures, shown in Figures 3.10-3.13, give a picture of the surface agglomeration effects as expected.

In investigating results that were counterintuitive to the proposed theory of surface agglomeration of fibroblasts, only one case stands out. A significant difference was found in the rabbit dermal fibroblast seeding percentage between the -20 and -40 scaffold ($P = 0.048$). The lack of correlation of this result to the rest of the rabbit or rat seeding data suggests the source of the variation to be in cell counting anomalies or scaffold cutting irregularities rather than a repeatable trend in seeding characteristics.

The lack of a statistically significant difference in attachment percentages between the scaffold types in the rat 24-hour seeding runs does not indicate a lack of value in having performed the test with the same dermal fibroblast cells from a different species. On the contrary, performing the experiments on similar cell types from different species acted as a check on the

validity of specific tissue harvesting procedures as well as experimental procedures. In this case, the similarity of results between dermal fibroblasts of two different species helped to solidify the hypothesis that the fibroblasts were clumping on the surface. The analysis of the physical size of both the rabbit and rat fibroblasts, compared to the MC3T3 cells, helps to support that argument.

The examination of Figures 3.14-3.16 shows how the cellular clumping on the surfaces of the scaffold evolves over the course of the 24-hour incubation. While cells on the surface of the scaffold initially have a rounded morphology as shown in Image 3.15, the cells are observed to elongate and contract after 24 hours, as shown in Images 3.14 and 3.16. This contraction, however, is not observed in all of the agglomerated cells on the surface, leading to further questions of phenotypic behavior and α-SMA content of individual cells. The issue of individual cell phenotype changes and their subsequent behavior was not examined in these experiments, but quantification of contracting cells and their associated α-SMA content may be of interest in future projects.

4.5 SEM Image Analysis

The Images taken with the SEM contribute useful data to the surface agglomeration argument. As shown in Figure 3.17, the previous generation "quenched" scaffolds had different surface characteristics on respective sides. The surfaces of this scaffold are seen to differ greatly from the new generation of scaffolds utilizing the new freeze drying protocol of O'Brien et al. (2004b). The images in Figures 3.18-21 show a marked difference in the surface characteristics of the new scaffolds from one side to the other. While the "shiny" side appears qualitatively to have smaller pores compared to the non-shiny side, the non-shiny side seems to have more of a general closed-cell pore structure at the surface. The detailed cross sections of the shiny and non-shiny edges shown in Figure 3.21 further confirm the different structures found at the two surfaces. When comparing the cell size of the dermal fibroblasts used in this study and the MC3T3 cells used in the previous O'Brien study to the actual size of the pores encountered by the

cells during seeding, the phenomenon of surgace agglomeration with fibroblast cells becomes more plausible. The smaller size of the MC3T3 cells may simply allow easier infiltration through the differing surface pore structures. This leads to the conclusion that seeding technique employed when working with the larger dermal fibroblasts is a critical factor in the resulting cellular infiltration into the scaffolds.

4.6 Cell Force Monitor Considerations

The cell force monitor, based on a design previously used by Freyman (2001a) and Eastwood, et al. (1994), is capable of measuring bulk force generation in an *in vitro* environment. While the test is performed on a bulk level, the results are reported on a per-cell basis. The assumption of this interpolation is that all cells are equally involved in cellular contraction. As shown by Figures 3.14 and 3.16 in Chapter 3, however, the scaffolds were observed to be contracted by only a fraction of the seeded cells. So, the contractile values calculated in the Results are most likely under-representing the per-cell force generation capabilities of individual cells.

The CFM contractile results can not be fully interpreted without also taking into account the complication of the seeding phenomena detailed earlier. Since the fibroblasts are observed to agglomerate on the surface of the scaffold and only infiltrate a minimal amount, the contractile behavior of cells within these scaffolds is assumed to be different from other cellular contraction results found with previous CFM experimentation. The scaffolds used in this study were also fundamentally different from previous matrices used in contractile experimentation (Freyman, Yannas et al. 2001), with different average pore size and much smaller pore size variation in each new, characterized scaffold than the previous generation. This change in scaffold fabrication procedure, however, is not necessarily responsible for the observed change in cellular behavior. As demonstrated by Figure 3.9 and previous work utilizing MC3T3 cells (O'Brien 2004a), cellular infiltration is possible through the thickness of the new, characterized scaffolds.

If the mechanism of contraction is fundamentally different in the fibroblast-seeded characterized (new) scaffolds, the presence of the inflection point in all contractile curves may suggest a possible explanation for this behavior. Every CFM run completed in this study exhibited a characteristic inflection point at 4-8 hours into the experiment. In roughly half of the runs, the cellular contractile value decreased after reaching this inflection point. In the other half of the runs, the curve rebounded and increased further with increasing time, to a global maximum contractile value at the end of the run (t=22 hours). There was no apparent correlation between a force increase/decrease after the inflection point and the Passage number of the cells, nor was there a correlation between post-inflection point behavior and gross cell attachment number at the end of the run.

As shown in the Results, the initial contractile slope, inflection point force, and final contractile force were similar when comparing the same passage number between scaffolds. The ANOVA results in Table 3.4 show the lack of a significant difference between P3V values for -10 and -40 scaffolds and a lack of a significant difference between P5 values for -10 and -40 scaffolds for the characteristic parameters measured. Statistical analysis between -10 and -40 scaffolds was not shown, but P-values were greater than 0.1 ($P>0.1$) in all cases. A transition in contractile behavior in Passage 4 can be seen between the -10 and the -40 slope and force data. The difference between the passage numbers 4 and 4V was due to a change in culture technique, as described earlier. This transition in behavior between the P4 and P4V values seems to indicate that the new culture technique can delay the phenotypic change that is assumed to lead to increased contractile behavior in all three of the measured characteristics. The grouping of the results as P3V and P4/5 in the -10 scaffolds and P3V/P4V and P5 in the -40 scaffolds shows this trend to hold over the majority of the data. The passage-dependent contractile behavior offset due to the new passaging technique is potentially useful in future experimentation. As stated earlier, consistent cellular behavior is desired over a range of passage numbers in order to obtain large quantities of cells for use in various experiments. By employing the new passaging technique, it

was possible to prolong the onset of increased contractile behavior by a full passage number. This new passaging technique allows larger overall quantities of cells to be cultured for use before phenotype changes due to culture residence time become a factor.

Inflection Point Behavior and Origins

Data from Zaleskas et al. (2004) reports using collagen-GAG scaffolds with uniform pore sizes of approximately 85μm in diameter in a CFM with a similar setup to the one used in this experimentation. In the CFM runs presented, the chondrocytes were observed to contract the scaffold with a three-stage contraction mechanism. The initial curve and inflection point graphs for the chondrocyte contraction runs are strikingly similar to the fibroblast data from this study.

An additional inflection point (local minimum) was also observed in the reported chondrocyte contraction data at a later timestep in the 22-hour run, and the initial inflection point force plateau was much lower in magnitude than the fibroblast data presented in this study, but the initial shape of the curve for both chondrocytes and fibroblasts is similar in different scaffolds with uniform pore size distributions. The fact that both scaffolds reported a more uniform pore size distribution compared to earlier-generation scaffolds (Freyman, Yannas et al. 2001) may potentially point to an architecture-dependent contraction mechanism for cells in the new, characterized scaffolds. Whether this contractile behavior is due to more uniform pore size, more uniform strut thickness, or some other characteristic is unknown. Further experimentation is needed to specifically show how dermal fibroblasts interact differently with the new, characterized scaffolds compared to earlier results.

It should be noted that the above comparison between current results, Freyman results, and Zaleskas results is based on cellular infiltration into the bulk of the scaffolds resulting in the cells actually "seeing" the different pore sizes in different CFM runs. While the "blot" seeding technique done for all reported CFM runs in this study helped to significantly increase cellular attachment percentage in the -40 scaffold, it is not known to what extent the cells were able to

penetrate into the scaffolds as a result of this different seeding technique. As such, direct comparison of pore size-dependent contractile behavior may require further investigation.

Contractile Force as a Function of Available Surface Area

Interestingly, a significant difference was not found for the inflection point force or the initial contractile slope between the -10 and -40 scaffolds. The initial force generation slope value appears to be dependent on the cell phenotype, since contractile force generation has been correlated to time in culture as previously discussed. Since the same passage number and passaging technique were used for the comparison of initial force generation slope value, phenotype changes in the cells can be discounted. The observation that the cells are generally located along the surface of the scaffolds, coupled with data that shows no correlation of seeding or contractile behavior to scaffold type, leads to the conclusion that the attachment surface area utilized by cells in this study can be considered roughly equivalent.

Contractile Force as a function of Passage Number

While the post-inflection point force increase or decrease may not show any correlation to passage number or scaffold type, there is a definite trend of force magnitude correlating to the passage number. In fact, as shown in the Results, an increase in passage number led to higher contractile force values in the initial contractile slope, inflection point force, and final force value. The observed increase in fibroblast contractile behavior as a function of passage number agrees well with previous experimentation detailing cell phenotype changes observed with increased time in culture (Kinner and Spector 2001). As stated earlier with the discussion on cell spreading and α-SMA generation in culture, the evolving phenotype of the cell will contribute to changing contractile behavior. This effect, while explained previously for culture conditions, is applicable for cellular behavior in the scaffolds as well.

A correlation between passage number and initial contractile behavior (slope) can also be seen in Figures 3.20-3.21. The increase in slope correlates directly to increased residence time in culture (larger passage number). This observed phenomenon of more rapid force generation, coupled with larger gross cell contraction as discussed in the previous paragraph, makes the basis for an interesting future study dealing with the phenotype changes associated with increased residence time. Since no specific staining procedures were done on cells to test for α-SMA or Actin in general, further quantification or discussion of the chemical processes of force generation in these fibroblasts is not possible.

Post-Inflection Point Cellular Behavior

There was no correlation between a change in cellular contractile value and passage number or scaffold type after the inflection point. The increase or decrease in contractile value was not dependent on attached cellular density in the scaffolds, either. This unexplained behavior leads to questions of the origin of the experimental variability in individual CFM runs. If gross contraction decreases after the inflection point, it is possible that the decrease is due to cell death. The cause of this cell death would most likely be due to contamination during the scaffold seeding and grip mounting process. A contamination in the incubator used is not a likely suspect due to the diffusion required to reach the seeded scaffolds inside the media-filled wells. If contamination is indeed playing a part in the sporadic results of the run, either the beam or the grips are primary suspects. All involved pieces were sprayed or wiped with 70% ethanol solution before every run, so the chances of infection were reduced. The media also contains 1%Antibiotic-Antimycotic, which should also help to prevent rapid infection and cell death. No testing for mycoplasma or other infectious agents was ever done for the cultured cells, so no definitive answer can be given about the chances of infection and cell death leading to the decrease in contractile behavior in select runs.

4.6 Aspect Ratio Considerations

In a contractile study by Brown, et al. (Brown, Prajapati et al. 1998) using a culture force monitor similar to the CFM, it was shown that cells reached a "tensional homeostasis" in force generation that was dependent on both the internal and external mechanical characteristics of the measurement system. In that study, it was shown that directional orientation of cells within the scaffold was influenced by geometry of the scaffold as well as external cyclical mechanical stimuli.

The current study did not utilize any cyclical mechanical stretching, but it did seek to test whether or not cells would have a different contractile response based on the geometry of the scaffold itself. The aspect ratio study was done with scaffolds containing the same scaffold volume and cellular seeding density as with the present CFM experimentation, but different aspect ratios as measured by the dimensions between the grips. The results of the CFM contraction study presented in Chapter 3 show that passage number had a stronger effect on contractile response than average scaffold pore size.

The results of the aspect ratio study show that no discernible difference in contractile response could be seen by varying the geometric orientation of the scaffold. While scaffold architecture and orientation in the CFM may have an effect on cellular contraction in scaffolds with through-thickness seeding, the current results did not correlate any physical scaffold characteristics to changes in contractile behavior. The seeding technique used in the aspect ratio study was the same "blot" technique as employed in the CFM runs, so the surface agglomeration phenomenon seen with static seeding in Chapter 3 may still be occurring to an extent in these scaffolds. As such, definitive conclusions on fibroblast behavior due to geometric scaffold constraints are not possible at this time.

Chapter 5 Conclusions

Cell culture techniques can greatly influence the behavior of cells *in vitro*. It was shown that preserving the cell's immediate environment by seeding cells to the same density in the culture flasks with each passage number could delay cellular differentiation into what is assumed to be a myofibroblastic or similar phenotype that exhibits increased α-SMA activity. However, this change in passaging technique only helped to delay the onset of intensified contractile behavior by a single passage. Cells exhibited behavioral changes in all culture techniques by the fifth passage.

While the new passaging technique allows for greater quantities of cells to be cultured, it is recommended that larger amounts of tissue be harvested from individual animals. By taking larger numbers of primary cells, the exponential splitting capabilities of the cells can be increased and more cells can be grown in culture through the fifth passage to complete planned experimentation.

Seeding

Cellular behavior in Collagen-GAG scaffolds is highly dependent on the cell seeding technique employed. Current techniques of hand-pipetting onto dry scaffold surfaces exhibited attachment percentages of only 15-30%. In order to increase cellular attachment efficiency, it is recommended that alternative seeding techniques be examined and implemented. The "blot" technique employed in seeding the CFM scaffolds showed significantly increased attachment efficiency in the -40 scaffolds. Further work needs to be done to quantify the through-thickness distribution of cells when utilizing this new technique.

The methods of centrifugal seeding or spinner-flask seeding from the literature seem to be viable prospects given the mechanical properties of the scaffold and the behavior of the cultured cells.

Different cell types can exhibit dramatically different behavior under similar culture and seeding conditions, as evidenced by the difference between the dermal fibroblast and MC3T3 behavior in the characterized scaffolds in this study and the O'Brien study (2004b). In order to facilitate increased seeding efficiency in the characterized scaffolds for the cultured dermal fibroblasts, it is recommended that future work focus on finding a seeding technique that improves the through-thickness distribution of cells within the scaffold. Improvement of this aspect of the seeding process should lead to an increase in seeding attachment efficiency as desired.

CFM

For all of the contraction-based experiments performed in this study, the same overall trend was observed with regard to fibroblast behavior: as passage number increased, the size of the fibroblasts increased and the contractile behavior of the fibroblasts increased. This increase in contractile behavior was attributed to an increase in α-SMA expression by the cells, though direct staining for α-SMA was not performed in this study.

Experimentation with new, characterized scaffolds in the Cell Force Monitor led to the discovery that cell culture techniques had a much larger effect on cellular contractile behavior than the structural architecture or geometrical characteristics of the scaffolds. The per-cell contractile force generated varied from 1-9nN after a 22-hour run, with asymptotic levels of contraction only occurring in a small percentage of the runs. Further experimentation should focus on seeding scaffolds with improved through-thickness cellular distribution in order to ascertain the true effect of pore characteristics and scaffold geometry on contractile behavior.

Additional CFM runs with longer data acquisition times (>24 hours) may be beneficial in determining whether asymptotic force levels are reached in the new, characterized scaffolds.

For future CFM runs, it may be beneficial to see if cells that pull faster and with more force (higher passage number) interact differently with the scaffold than lower passage number cells. This could be accomplished through staining procedures for α-SMA or by *in vitro* confocal microscopy.

Once the scaffold seeding complications are resolved, further aspect ratio studies may be enhanced by additional staining and sectioning procedures aimed at illustrating how cellular orientation in the scaffold changes as a function of scaffold geometry, seeding density, and time.

References:

ATCC (2004). MC3T3 Information Sheet.

Bates, R. C., A. Buret, et al. (1994). "Apoptosis Induced by Inhibition of Intercellular Contact." Journal of Cell Biology **125**(2): 403-415.

Beningo, K. A., M. Dembo, et al. (2001). "Nascent focal adhesions are responsible for the generation of strong propulsive forces in migrating fibroblasts." Journal of Cell Biology **153**(4): 881-887.

Brown, R. A., R. Prajapati, et al. (1998). "Tensional homeostasis in dermal fibroblasts: Mechanical responses to mechanical loading in three-dimensional substrates." Journal of Cellular Physiology **175**(3): 323-332.

Brown, R. A., K. K. Sethi, et al. (2002). "Enhanced fibroblast contraction of 3D collagen lattices and integrin expression by TGF-beta 1 and -beta 3: Mechanoregulatory growth factors?" Experimental Cell Research **274**(2): 310-322.

Cacou, C., D. Palmer, et al. (2000). "A system for monitoring the response of uniaxial strain on cell seeded collagen gels." Medical Engineering & Physics **22**(5): 327-333.

Campbell, B. H., W. W. Clark, et al. (2003). "A multi-station culture force monitor system to study cellular contractility." Journal of Biomechanics **36**(1): 137-140.

Chachra, D. Unpublished data, personal communications.

Chen, G. P., T. Ushida, et al. (2001). "Development of biodegradable porous scaffolds for tissue engineering." Materials Science & Engineering C-Biomimetic and Supramolecular Systems **17**(1-2): 63-69.

Clark, R. A. F., J. Q. An, et al. (2003). "Fibroblast migration on fibronectin requires three distinct functional domains." Journal of Investigative Dermatology **121**(4): 695-705.

Delvoye, P., P. Wiliquet, et al. (1991). "Measurement of Mechanical Forces Generated by Skin Fibroblasts Embedded in a 3-Dimensional Collagen Gel." Journal of Investigative Dermatology **97**(5): 898-902.

Dembo, M. and Y. L. Wang (1999). "Stresses at the cell-to-substrate interface during locomotion of fibroblasts." Biophysical Journal **76**(4): 2307-2316.

Desmouliere, A., A. Geinoz, et al. (1993). "Transforming Growth-Factor-Beta-1 Induces Alpha-Smooth Muscle Actin Expression in Granulation-Tissue Myofibroblasts and in Quiescent and Growing Cultured Fibroblasts." Journal of Cell Biology **122**(1): 103-111.

Dvir-Ginzberg, M., I. Gamlieli-Bonshtein, et al. (2003). "Liver tissue engineering within alginate scaffolds: Effects of cell-seeding density on hepatocyte viability, morphology, and function." Tissue Engineering **9**(4): 757-766.

Eastwood, M., D. A. Mcgrouther, et al. (1994). "A Culture Force Monitor for Measurement of Contraction Forces Generated in Human Dermal Fibroblast-Cultures - Evidence for Cell-Matrix Mechanical Signaling." Biochimica Et Biophysica Acta-General Subjects **1201**(2): 186-192.

Eastwood, M., V. C. Mudera, et al. (1998). "Effect of precise mechanical loading on fibroblast populated collagen lattices: Morphological changes." Cell Motility and the Cytoskeleton **40**(1): 13-21.

Freyman, T. M. (2001). Development of an In Vitro Model of Contraction by Fibroblasts. Dept. of Materials Science and Engineering. Cambridge, Massachusetts Institute of Technology.

Freyman, T. M., I. V. Yannas, et al. (2001). "Cellular materials as porous scaffolds for tissue engineering." Prog. Mat. Sci. **46**: 273-282.

Freyman, T. M., I. V. Yannas, et al. (2001). "Fibroblast contraction of a collagen-GAG matrix." Biomaterials **22**(21): 2883-2891.

Freyman, T. M., I. V. Yannas, et al. (2002). "Fibroblast contractile force is independent of the stiffness which resists the contraction." Experimental Cell Research **272**(2): 153-162.

Frisch, T. and O. Thoumine (2002). "Predicting the kinetics of cell spreading." Journal of Biomechanics **35**(8): 1137-1141.

Funk, J. and D. Dinger (1994). Predictive Process Control of Crowded Particulate Suspensions, Kluwer Academic Publishers.

Giancotti, F. G. and E. Ruoslahti (1999). "Transduction - Integrin signaling." Science **285**(5430): 1028-1032.

Godbey, W. T., B. S. S. Hindy, et al. (2004). "A novel use of centrifugal force for cell seeding into porous scaffolds." Biomaterials **25**(14): 2799-2805.

Grande, D. A., C. Halberstadt, et al. (1997). "Evaluation of matrix scaffolds for tissue engineering of articular cartilage grafts." Journal of Biomedical Materials Research **34**(2): 211-220.

Grinnell, F., C.-H. Ho, et al. (2003). "Dendritic Fibroblasts in Three-dimensional Collagen Matrices." Mol. Biol. Cell **14**(2): 384-395.

Harper, R. A. and G. Grove (1979). "Human-Skin Fibroblasts Derived from Papillary and Reticular Dermis - Differences in Growth-Potential Invitro." Science **204**(4392): 526-527.

Hebel, R. (1976). Anatomy of the Rat. Baltimore, MD, Williams and Wilkins.

Hersel, U., C. Dahmen, et al. (2003). "RGD modified polymers: biomaterials for stimulated cell adhesion and beyond." Biomaterials **24**(24): 4385-4415.

Hinz, B., G. Celetta, et al. (2001). "Alpha-smooth muscle actin expression upregulates fibroblast contractile activity." Molecular Biology of the Cell **12**(9): 2730-2741.

Hinz, B., V. Dugina, et al. (2003). "alpha-smooth muscle actin is crucial for focal adhesion maturation in myofibroblasts." Molecular Biology of the Cell **14**(6): 2508-2519.

Hutmacher, D. W. (2000). "Scaffolds in tissue engineering bone and cartilage." Biomaterials **21**(24): 2529-2543.

Invitrogen (2001). Invitrogen Product Guide. **2004**.

Kinner, B. and M. Spector (2001). "Smooth muscle actin expression by human articular chondrocytes and their contraction of a collagen-glycosaminoglycan matrix in vitro." Journal of Orthopaedic Research **19**(2): 233-241.

Kisiday, J., M. Jin, et al. (2002). "Self-assembling peptide hydrogel fosters chondrocyte extracellular matrix production and cell division: Implications for cartilage tissue repair." Proceedings of the National Academy of Sciences of the United States of America **99**(15): 9996-10001.

Knezevic, V., A. Sim, et al. (2002). "Isotonic biaxial loading of fibroblast-populated collagen gels: a versatile, low-cost system for the study of mechanobiology." Biomechanics and Modeling in Mechanobiology **1**(1): 59-67.

Lee, C. R., A. J. Grodzinsky, et al. (2001). "The effects of cross-linking of collagen-glycosaminoglycan scaffolds on compressive stiffness, chondrocyte-mediated contraction, proliferation and biosynthesis." Biomaterials **22**(23): 3145-3154.

Lee, S. H., B. S. Kim, et al. (2003). "Elastic biodegradable poly(glycolide-co-caprolactone) scaffold for tissue engineering." Journal of Biomedical Materials Research Part A **66A**(1): 29-37.

Malmstrom, J., H. Lindberg, et al. (2004). "Transforming growth factor-beta(1) specifically induce proteins involved in the myofibroblast contractile apparatus." Molecular & Cellular Proteomics **3**(5): 466-477.

Marieb, E. (2003). Essentials of Human Anatomy and Physiology. San Francisco, CA, Benjamin Cummings.

Marty-Roix, R., J. D. Bartlett, et al. (2003). "Growth of porcine enamel-, dentin-, and cementum-derived cells in collagen-glycosaminoglycan matrices in vitro: expression of alpha-smooth muscle actin and contraction." Tissue Engineering **9**(1): 175-186.

McGlohorn, J. B., L. W. Grimes, et al. (2003). "Characterization of cellular carriers for use in injectable tissue-engineering composites." Journal of Biomedical Materials Research Part A **66A**(3): 441-449.

Mediatech Technical Information (2004). Dissociation of Cell Monolayers using Trypsin Solutions.

Munevar, S., Y. L. Wang, et al. (2001). "Distinct roles of frontal and rear cell-substrate adhesions in fibroblast migration." Molecular Biology of the Cell **12**(12): 3947-3954.

Nehrer, S., H. A. Breinan, et al. (1998). "Chondrocyte-seeded collagen matrices implanted in a chondral defect in a canine model." Biomaterials **19**(24): 2313-2328.

Nehrer, S., H. A. Breinan, et al. (1997). "Matrix collagen type and pore size influence behaviour of seeded canine chondrocytes." Biomaterials **18**(11): 769-776.

Nien, Y. D., Y. P. Han, et al. (2003). "Fibrinogen inhibits fibroblast-mediated contraction of collagen." Wound Repair and Regeneration **11**(5): 380-385.

O'Brien, F., Harley, BA, Yannas, IV, Gibson, LJ (2004). "The effect of pore size on cell adhesion in collagen-GAG scaffolds." Biomaterials **TBD**(in press): xxxx-xxxx.

O'Brien, F. J., B. A. Harley, et al. (2004). "Influence of freezing rate on pore structure in freeze-dried collagen-GAG scaffolds." Biomaterials **25**(6): 1077-1086.

Orban, J. M., L. B. Wilson, et al. (2004). "Crosslinking of collagen gels by transglutaminase." Journal of Biomedical Materials Research Part A **68A**(4): 756-762.

Park, J. C., B. J. Park, et al. (2001). "Comparative study on motility of the cultured fetal and neonatal dermal fibroblasts in extracellular matrix." Yonsei Medical Journal **42**(6): 587-594.

Pek, Y. S., M. Spector, et al. (2004). "Degradation of a collagen-chondroltin-6-sulfate matrix by collagenase and by chondroitinase." Biomaterials **25**(3): 473-482.

Pelham, R. J. and Y. L. Wang (1999). "High resolution detection of mechanical forces exerted by locomoting fibroblasts on the substrate." Molecular Biology of the Cell **10**(4): 935-945.

Perets, A., Y. Baruch, et al. (2003). "Enhancing the vascularization of three-dimensional porous alginate scaffolds by incorporating controlled release basic fibroblast growth factor microspheres." Journal of Biomedical Materials Research Part A **65A**(4): 489-497.

Reyes, C. D. and A. J. Garcia (2003). "A centrifugation cell adhesion assay for high-throughput screening of biomaterial surfaces." Journal of Biomedical Materials Research Part A **67A**(1): 328-333.

Rhee, S. H. and J. Y. Choi (2002). "Preparation of a bioactive poly(methyl methacrylate)/silica nanocomposite." Journal of the American Ceramic Society **85**(5): 1318-1320.

Ruoslahti, E. and M. D. Pierschbacher (1987). "New Perspectives in Cell-Adhesion - Rgd and Integrins." Science **238**(4826): 491-497.

Sachlos, E., N. Reis, et al. (2003). "Novel collagen scaffolds with predefined internal morphology made by solid freeform fabrication." Biomaterials **24**(8): 1487-1497.

Salem, A. K., R. Stevens, et al. (2002). "Interactions of 3T3 fibroblasts and endothelial cells with defined pore features." Journal of Biomedical Materials Research **61**(2): 212-217.

Salzman, N. P. (1961). "Animal Cell Cultures." Science **133**(3464): 1559-1565.

Sethi, K. K., V. Mudera, et al. (2002). "Contraction-mediated pinocytosis of RGD-peptide by dermal fibroblasts: inhibition of matrix attachment blocks contraction and disrupts microfilament organisation." Cell Motility and the Cytoskeleton **52**(4): 231-241.

Sheu, M. T., J. C. Huang, et al. (2001). "Characterization of collagen gel solutions and collagen matrices for cell culture." Biomaterials **22**(13): 1713-1719.

Silver, F. H., L. M. Siperko, et al. (2003). "Mechanobiology of force transduction in dermal tissue." Skin Research and Technology **9**(1): 3-23.

Spector, M. (2002). "Novel cell-scaffold interactions encountered in tissue engineering: Contractile behavior of musculoskeletal connective tissue cells." Tissue Engineering **8**(3): 351-357.

Strobel, J. L., S. G. Cady, et al. (1986). "Identification of Fibroblasts as a Major Site of Albumin Catabolism in Peripheral-Tissues." Journal of Biological Chemistry **261**(17): 7989-7994.

Tamariz, E. and F. Grinnell (2002). "Modulation of Fibroblast Morphology and Adhesion during Collagen Matrix Remodeling." Mol. Biol. Cell **13**(11): 3915-3929.

Tampieri, A., G. Celotti, et al. (2001). "Porosity-graded hydroxyapatite ceramics to replace natural bone." Biomaterials **22**(11): 1365-1370.

Tan, J. L., J. Tien, et al. (2003). "Cells lying on a bed of microneedles: An approach to isolate mechanical force." Proceedings of the National Academy of Sciences of the United States of America **100**(4): 1484-1489.

Torres, D. S., T. M. Freyman, et al. (2000). "Tendon cell contraction of collagen-GAG matrices in vitro: effect of cross-linking." Biomaterials **21**(15): 1607-1619.

Troxel, K. (1994). Delay of Skin Wound Contraction by Porous Collagen-GAG Matrices. ME. Cambridge, MA, MIT.

Veilleux, N. H., I. V. Yannas, et al. (2004). "Effect of passage number and collagen type on the proliferative, biosynthetic, and contractile activity of adult canine articular chondrocytes in type I and II collagen-glycosaminoglycan matrices in vitro." Tissue Engineering **10**(1-2): 119-127.

Vunjak-Novakovic, G., B. Obradovic, et al. (1998). "Dynamic cell seeding of polymer scaffolds for cartilage tissue engineering." Biotechnology Progress **14**(2): 193-202.

Vunjak-Novakovic, G. a. R., M (2003). Cell Seeding of Polymer Scaffolds. Biopolymer Methods in Tissue Engineering. A. a. H. Hollander, PV. Totowa, NJ, Humana Press: p.131-145.

Wang, J. H. C., G. G. Yang, et al. (2004). "Fibroblast responses to cyclic mechanical stretching depend on cell orientation to the stretching direction." Journal of Biomechanics **37**(4): 573-576.

Werner, J., B. Linner-Krcmar, et al. (2002). "Mechanical properties and in vitro cell compatibility of hydroxyapatite ceramics with graded pore structure." Biomaterials **23**(21): 4285-4294.

Williamson, A. K., A. C. Chen, et al. (2001). "Compressive properties and function-composition relationships of developing bovine articular cartilage." Journal of Orthopaedic Research **19**(6): 1113-1121.

Worthington Biochemical Corporation (2003). Cell Isolation Theory. **2004**.

Wrobel, L. K., T. R. Fray, et al. (2002). "Contractility of single human dermal myofibroblasts and fibroblasts." Cell Motility and the Cytoskeleton **52**(2): 82-90.

Yang, J., G. X. Shi, et al. (2002). "Fabrication and surface modification of macroporous poly(L-lactic acid) and poly(L-lactic-co-glycolic acid) (70/30) cell scaffolds for human skin fibroblast cell culture." Journal of Biomedical Materials Research **62**(3): 438-446.

Yang, Y., J. L. Magnay, et al. (2002). "Development of a 'mechano-active' scaffold for tissue engineering." Biomaterials **23**(10): 2119-2126.

Yannas, I. V. (2001). Tissue and Organ Regeneration in Adults. New York, Springer.

Yannas, I. V. (2003). Class Notes. 2.79J Class Notes. Cambridge, MA.

Yannas, I. V. and J. F. Burke (1980). "Design of an Artificial Skin .1. Basic Design Principles." Journal of Biomedical Materials Research **14**(1): 65-81.

Yannas, I. V., J. F. Burke, et al. (1980). "Design of an Artificial Skin .2. Control of Chemical-Composition." Journal of Biomedical Materials Research **14**(2): 107-132.

Yannas, I. V., E. Lee, et al. (1989). "Synthesis and Characterization of a Model Extracellular-Matrix That Induces Partial Regeneration of Adult Mammalian Skin." Proceedings of the National Academy of Sciences of the United States of America **86**(3): 933-937.

Zaleskas, J. M., B. Kinner, et al. (2004). "Contractile forces generated by articular chondrocytes in collagen-glycosaminoglycan matrices." Biomaterials **25**(7-8): 1299-1308.

Zeltinger, J., J. K. Sherwood, et al. (2001). "Effect of pore size and void fraction on cellular adhesion, proliferation, and matrix deposition." Tissue Eng. **7**(5): 557-572.

Zhao, F., Y. J. Yin, et al. (2002). "Preparation and histological evaluation of biomimetic three-dimensional hydroxyapatite/chitosan-gelatin network composite scaffolds." Biomaterials **23**(15): 3227-3234.

Appendix 1

Dermal Fibroblast Isolation Procedure for Sprague-Dawley Rat

Supplies for both tissue harvest and dissociation:

- Surgical assistant (to hand off supplies during surgery)
- Pentobarbital
- Betadine solution
- 70% Isopropyl Alcohol
- Gauze pads
- Electric hair clippers
- Shaving cream
- Disposable Razor
- Sterile surgeon's gloves (1 pair)
- Sterile drape (1)
- Surgical Kit (All sterile)-
  - -Forceps
  - -Scalpel blade holder
  - -Scissors (Bandage and Surgical)
- Scalpel blades (#10 works well)
- 50mL Tube Top Filter- 0.22μm
- 50mL Centrifuge Tubes (4)
- 15mL Centrifuge Tubes (2+/-)
- Plastic weigh boat (~1 in^2 base)
- Straight pins, flame sterilized
- Sterile PBS supplemented with 2% Antibiotic/Antimycotic
- Collagenase (Type 1A)
- DMEM (unsupplemented)
- Complete DMEM
- Vortexer
- Cell Strainer (70μm)

All tissue dissociation protocols start with the same harvesting procedure presented below

Tissue Harvest Procedure-

Sacrifice rat with CO_2 chamber asphyxiation and subsequent overdose of pentobarbital. Place rat on clean disposable drape on surgical table.

a) Use hair clippers to shave half of the ventral anterior side of the rat. A spot about 4 inches down the length of the body by 2 inches wide from the base of the front leg to about halfway down the belly should be sufficient.
b) Use the disposable razor and shaving cream to remove remaining hair. Note: rat hair is difficult to completely remove- eliminate as much as possible and move on.
c) Clean the shaved area with Betadine scrub (several times up and down the exposed area is sufficient) followed by 70% Isopropyl Alcohol wipe to remove all Betadine. Repeat.
d) Put on sterile surgical gloves and pull out sterile bandage scissors. Cut appropriate size hole in sterile drape to match sterile area. Apply drape over rat, making sure to not touch any non-sterile areas.
e) Assemble scalpel and blade and pull out forceps. Visualize two squares, approximately one inch on a side, in the sterile area of the rat. Cut through the epidermal layer and carefully separate off from remaining attached dermis. The epidermis is easily identified as the non-vascularized layer of skin.
f) Once epidermis is removed, the remaining two layers of dermis are slightly more difficult to discern. The muscle layer beneath is characterized by a more striated appearance and a slightly different color. Separate off the dermal layers from the muscle layer in order to prevent multiple cell types in the harvested specimen.
g) Remove as many sections of dermis as desired, taking care to remain within the sterile field. Place sections in chilled DPBS tubes for transport (if transport is needed). Sections can be rinsed in a separate tube of sterile DPBS to remove any blood if necessary.

---Protocols diverge here---

Tissue Dissociation Procedures: Serial digestion, vortexing, and explant outmigration procedures continue on as presented in Chapter 2 previously.

Appendix 2

Cell Culture Protocol

Equipment:

NAPCO 6000 Series CO_2 Incubator, set to 37°C 5% CO_2 and 95% relative humidity (VWR Scientific/PrecisionNAPCO, Winchester, VA)

Water Bath, set to 37°C

Sterile Hood, laminar flow or traditional

Inverted Cell Culture Microscope (Nikon TMS-F)

Centrifuge [set to 900RPM] (Heraeus Labofuge 400)

Materials:

5mL, 10mL, 25mL Sterile Pipettes

PipetteAid Hand mechanical pipetting device

250mL waste beaker

Supplies / Stains:

500mL Bottle DMEM (Gibco 12320-032)

5mL Antibiotic-Antimycotic [containing 10,000U/mL penicillin G sodium, 10,000µg/mL streptomycin sulfate, and 25µg/mL Fungizone] (Gibco 15240-062)

50mL Characterized Fetal Bovine Serum (Hyclone, Logan, UT)

Trypan Blue Stain (Gibco 15250-061)

Trypsin-EDTA (0.05%Trypsin) (Gibco 25300-062)

Media Preparation

a) Place all media supplies in a water bath at 37°C to thaw/warm.
b) Spray down 2x25mL and 1x5mL pipettes with 70%EtOH and place in a sterile hood.
c) When media supplies are ready, wipe down all bottles and spray with 70% EtOH before placing in sterile hood.
d) Remove 55mL of DMEM from a full sterile bottle of media and discard.
e) Add 50mL FBS and 5mL Antibiotic-Antimycotic.
f) Cap and gently swirl to mix.

Cell Feeding

a) Warm media in water bath at 37°C.
b) Spray down 2x25mL pipettes, PipetteAid, and waste beaker with 70% EtOH. Place in sterile hood.
c) When media is warm, wipe dry with paper towel and spray with EtOH before placing in sterile hood.
d) Using 25mL pipette, remove all liquid from all flasks, taking care not to scrape cells with pipette tip.
e) Replace with 17mL complete media at 37°C using a new, sterile pipette tip.

Passaging

a) Warm complete media, DPBS, and 4mL Trypsin (per flask to be passaged) in water bath at 37°C.
b) Spray down 2x25mL 2x10mL, and 1x5mL pipette, PipetteAid, and waste beaker with 70% EtOH and place in sterile hood.
c) When media, PBs, and Trypsin is warm, wipe dry with paper towel and spray with EtOH before placing in sterile hood.
d) Using 25mL pipette, remove all liquid from all flasks, taking care not to scrape cells with pipette tip.
e) Add 5mL DPBS per flask and set horizontally for 30 seconds. Swirl gently to remove any remaining media from edges.
f) Remove DPBS and add 4mL Trypsin per flask.
g) Incubate for 7 minutes to facilitate detachment. (If necessary, allow cells to sit for 3-4 additional minutes if not detached.)
h) Add 6mL complete media to each flask.

Old passaging technique:

i) Split each 10mL flask into five (5) new, sterile flasks, with 2mL cell suspension each.
j) Top off with 15mL additional complete media per flask and return to incubator.

New "V" passaging technique

i) Combine all flask cell suspension into 50mL centrifuge tube(s).
j) Perform cell count on sample from tube (see below).
k) Spin down cells and resuspend in complete media at a density of 5E5 cells/mL.
l) Add 1mL cell suspension to each new flask.
m) Top off each flask with 16mL complete media. Return to incubator.

Cell Counting Procedure

a) Remove 100 µL from cell suspension while maintaining sterile conditions.

b) Mix 100 µL of cell suspension with 100 µL Trypan blue. Pipette several times to mix stain and cell suspension.

c) Place cover slip on hemacytometer and pipette 10 µL of stain/cell suspension into notch.

d) Cell counts were done in all 5 boxes shown below. Average cell number per box (total number of cells counted / total boxes counted) was used in the calculation of cell quantities, as shown in the equation below. (Note: "10,000" is a volumetric multiplier used to convert from the volume above each square (0.1µL) to the "# cells / mL" quantity desired.

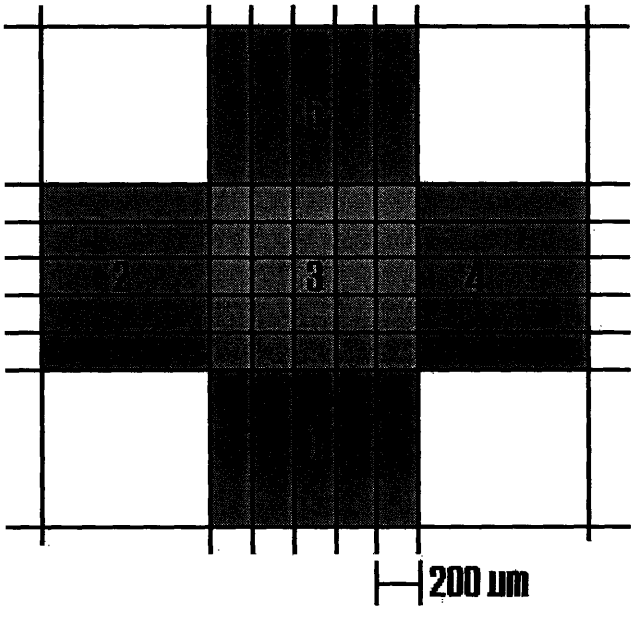

(In order to prevent double counting of cells at the junction of two or more squares, cells were counted as being in a square only if more than half of the cell was lying on either the bottom or right edge of the square in question.)

$$\frac{\text{\# cells counted}}{\text{\# squares counted}} \times 2^{*} \times 10{,}000 \times \text{mL cell suspension} = \text{Total \# cells}$$

(* = dilution factor used only when cells were stained with Trypan Blue)

Appendix 3

Glycomethacrylate (GMA) Embedding Protocol (Adapted From Freyman 2001a)

For embedding collagen-GAG matrix samples (seeded or unseeded) in Glycomethacrylate.

Equipment

Plastic Embedding Mold (16643A, Polysciences, Warrington, PA)

Plastic Block Holders (15899, Polysciences)

Solutions

10% Neutral Buffered Formalin solution (from raw materials or purchased)

JB-4 Embedding Kit (Polysciences):

Catalyzed Solution A:

100mL Solution A

1.25g Catalyst (mixed well for 20 minutes)

Solution B

Embedding Protocol

a) Fix cell-seeded samples in 10% neutral buffered formalin for 24-48 hrs at room temperature. For non-cell-seeded samples, start directly with step (b). For dry, unseeded matrix samples, it is possible to start directly with 100%EtOH for several hours after step (b).
b) Cut samples along desired axes into pieces no larger than 5mm on a side and place in a 24-well plate.
c) Dehydrate samples as follows for 30 minutes each: dH_2O, dH_2O, 50% EtOH, 70% EtOH, 80% EtOH, 95% EtOH, 100% EtOH, 100% EtOH, 100% EtOH.
d) Create a 50:50 solution of Catalyzed Solution A and 100%EtOH. Add ~1mL to each well, enough to submerge each sample. Incubate samples overnight at 4°C.
e) Infiltrate samples with Catalyzed Solution A at 4°C for 24-72 h under vacuum, replacing Solution every 12 hours.
f) Combine 25ml Catalyzed Solution A and 1ml Solution B. Mix well.
g) Place each sample into a well in the plastic embedding mold. The JB-4 mixture will polymerize rapidly after ~30 minutes. Make sure samples are oriented correctly after this time. Mixture will darken as polymerization proceeds.
h) After the JB-4 mixture becomes viscous enough that the samples do not float, place plastic stubs over each well. Store tray at 4°C overnight.
i) Remove embedded samples from mold and store at 4°C.

Hematoxylin and Eosin Staining Protocol (taken directly from Freyman 2001a)

Protocol for staining formalin-fixed, cell-seed, collagen-GAG matrix samples which been GMA embedded and sectioned at 5 μm thickness. Cell nuclei will stain a dark red-brown, cytoplasm a salmon pink, and the matrix a lighter shade of salmon pink. Over staining with Eosin will result in high background staining. Eosin is water soluble so background will rinse out in tap water.

Solutions

Eosin Y (Sigma-Aldrich, St. Louis, MO)

Eosin Stock Solution

Weak Ammonium Hydroxide Water

Tap water, 200 ml

Ammonium hydroxide, 2-4 drops

Acid-Alcohol

70% EtOH, 200 ml

Hydrochloric Acid, 1 ml

Harris's Hematoxylin (HHS-16, Sigma)

Cytoseal 60 Mounting Medium (8310-16, Stephens Scientific)

Staining Procedure

1. Place slides to be stained in staining rack and place in Harris's Hematoxylin for 90 m.
2. Rinse in running tap water for 2 m.
3. "Blue" with weak ammonium hydroxide water for 2 m.
4. Rinse in running tap water for 2 m.
5. Differentiate in acid-alcohol for 2 m.
6. Rinse in running tap water for 5 m.
7. Counterstain with Eosin for 3 m.
8. Rinse in running tap water 3 m. Check that the matrix and cytoplasm are stained and the background staining is not too strong. If matrix or cytoplasm are not stained repeat step 7 and rinse again for a shorter period of time. If the background is too strong rinse, continue to rinse, checking at 1 m intervals, until an acceptable level is reached.
9. Air dry and then mount with mounting medium.

Appendix 4
CFM Materials and Calibration

CFM Components Replaced:
(Based on design from Freyman 2001a)

Edmund Optics, Barrington, NJ
X-Y positioner, # NT38-971
Rack and pinion support post, # NT03-650
Stainless Steel Mounting Post, 1.5" #L36-494

Goodfellow, Berwyn, PA
Be-Cu beams, # CU070350 (custom milled to 24mm wide, 0.125mm thick)

(Note: The thickness of the beam compared to previous experimentation by Freyman (2001a) was changed in order to keep the Moment of Inertia of the beams as similar as possible between the two generations.)

Kaman Aerospace and Instrumentation, Colorado Springs, CO
Proximity sensors, model number KD2300-2S

McMaster-Carr, Dayton, NJ
Polysulfone sheet, 3/8"

Drawings of refurbished milled pieces follow:

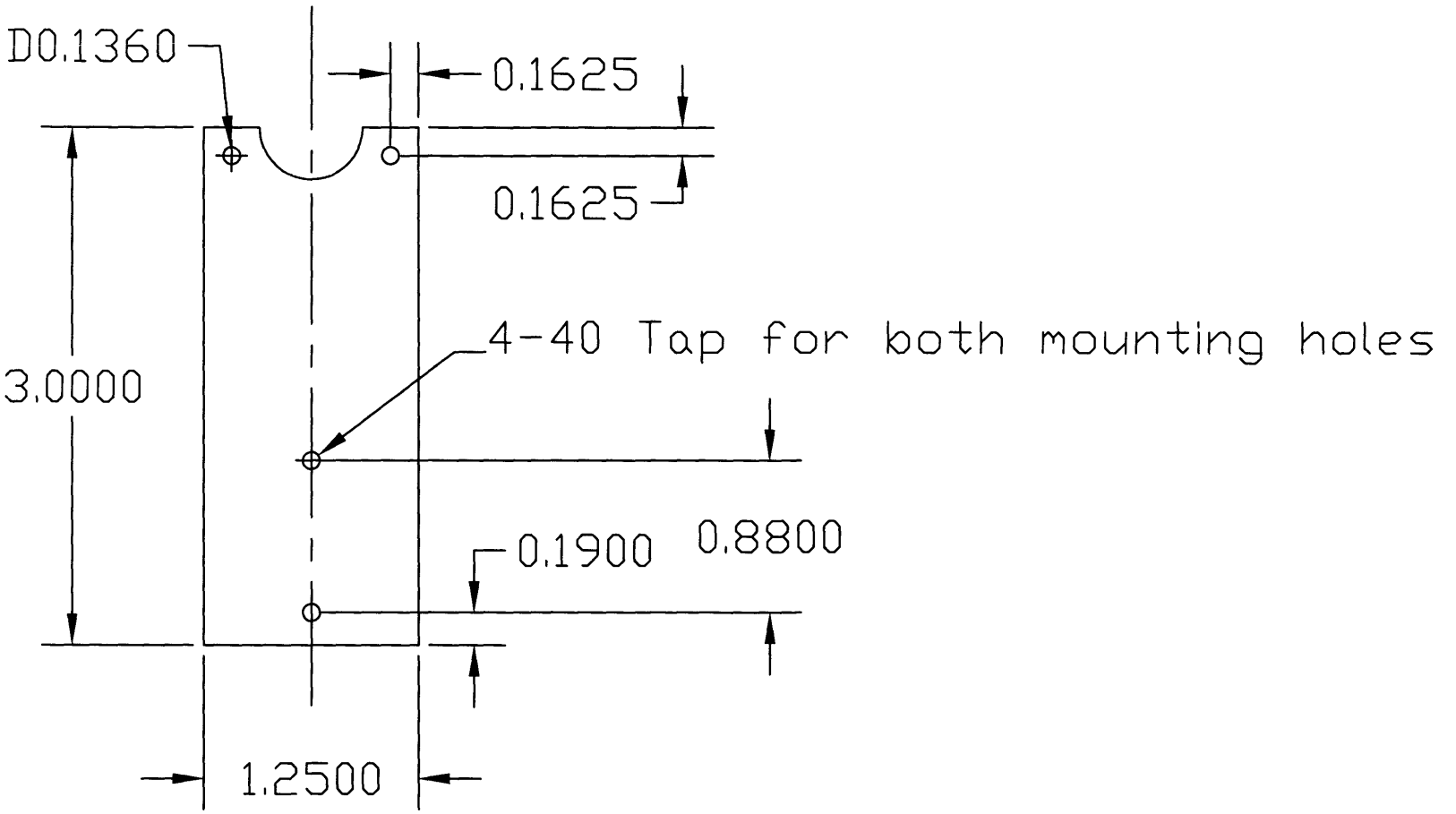

Part: Translation Stage Grip Holder	Material: Polysulfone
Notes: Polysulfone milled to 1/4" thick for piece	Scale: 1:1 (in.)

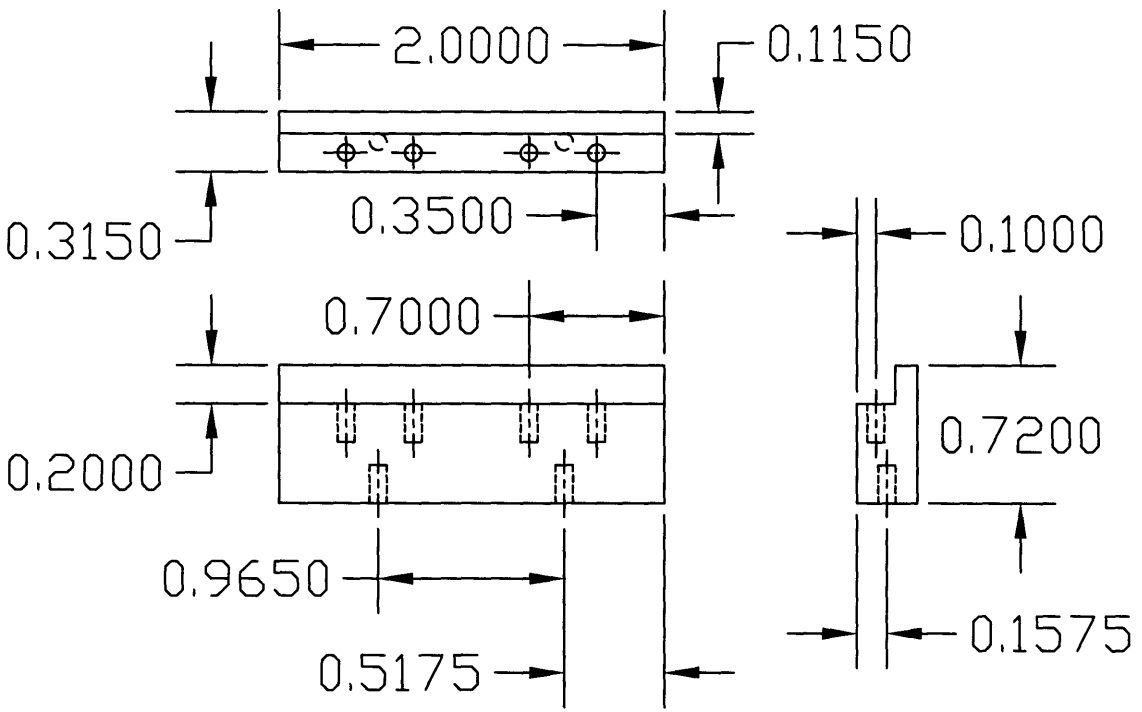

Part: Grips	Material: Polysulfone
Notes: All holes 4-40 Tap and 0.200 in. deep	Scale: 1:1 (in.)

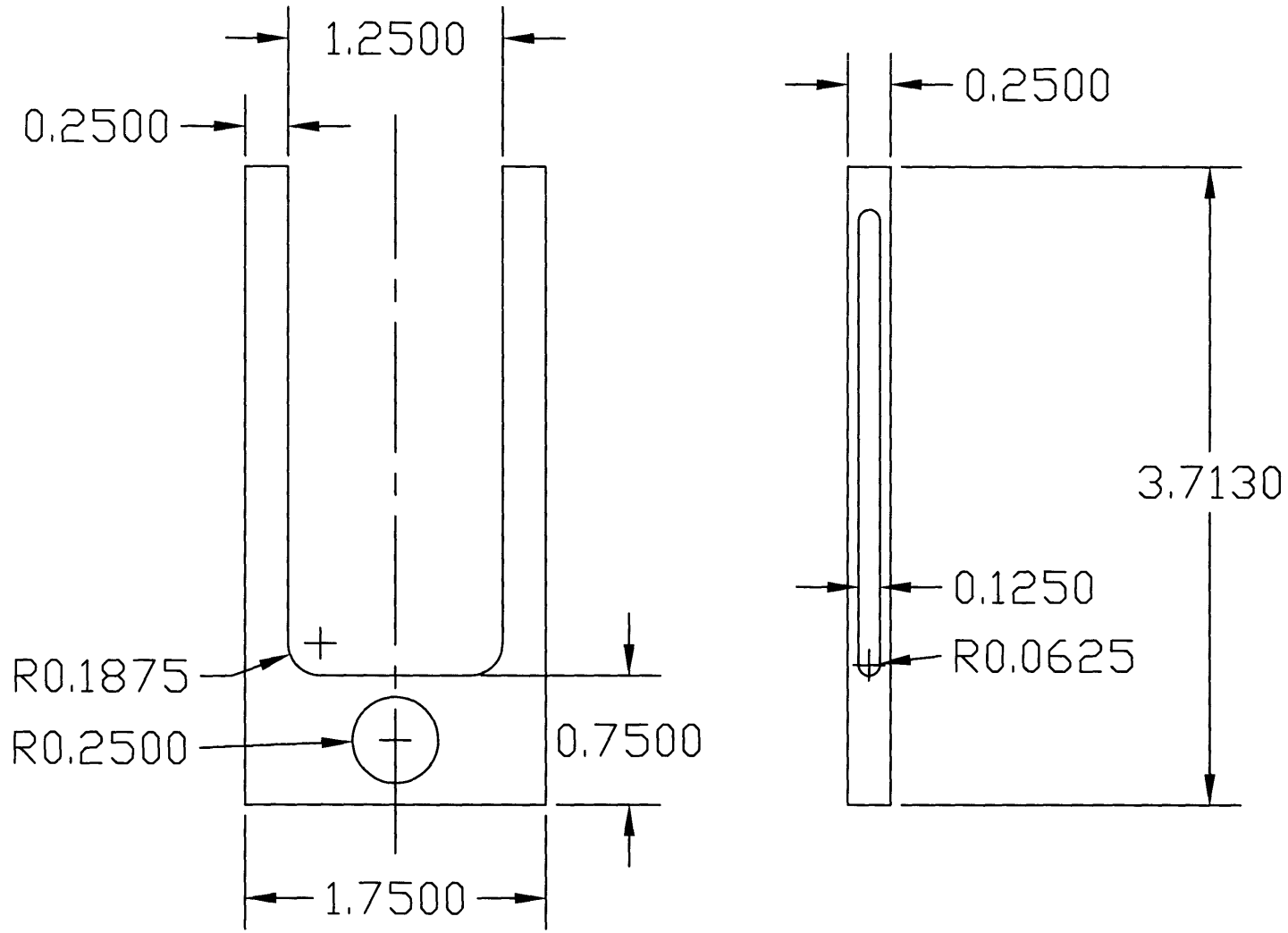

Part: Sensor Bracket	Material: Aluminum 1/4" stock
Notes: none	Scale: 1:1

Calibration Charts:

Voltage vs. Force

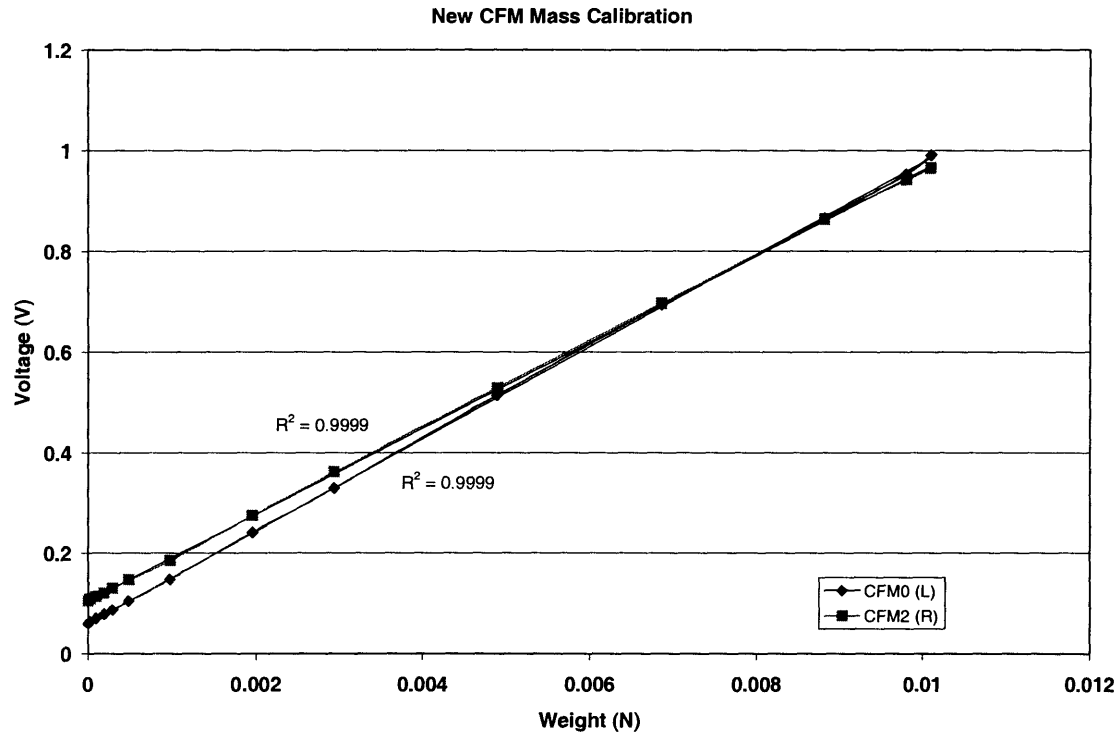

CFM L Force Slope: C_{force} = 0.010094N/0.9308V = 0.010844N/V

CFM R Force Slope: C_{force} = 0.010094N/0.8610V = 0.0117236N/V

Voltage vs. Displacement

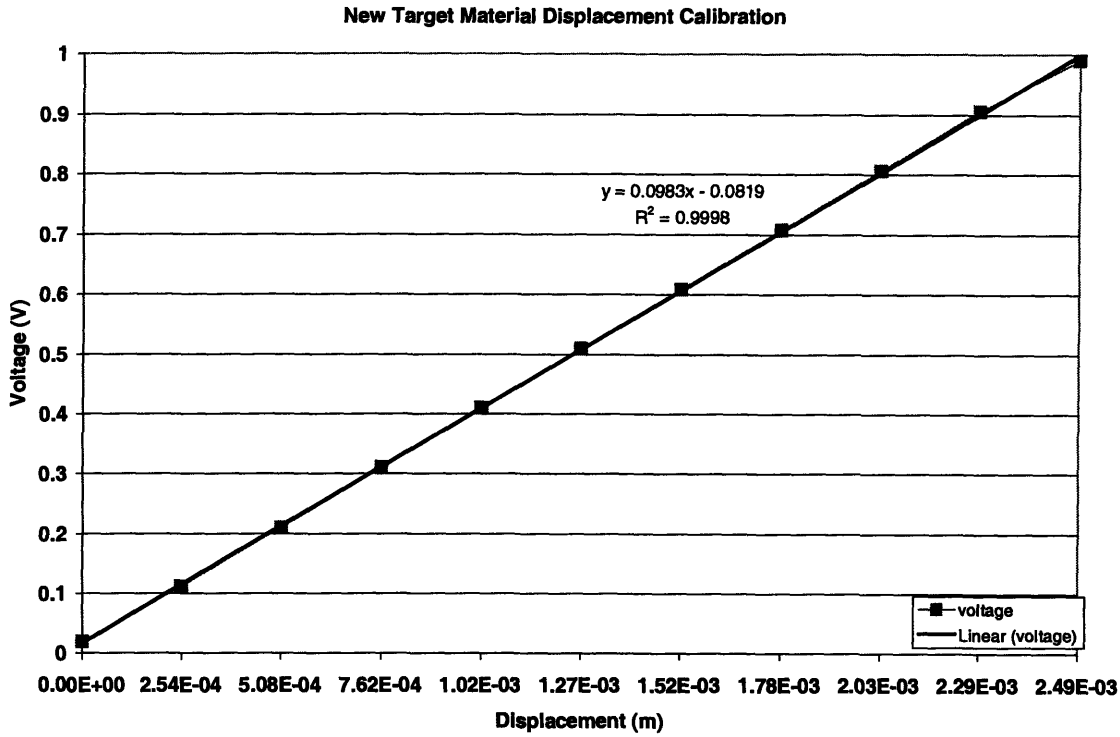

$C_{displ.}$ Used for both CFM's L and R: 0.002489m / 0.9706 V = 0.002564m/V

Biography

Andrew Albers grew up in Northern Indiana under the shadows of Notre Dame's Golden Dome and a lot of really tall corn. Given the opportunity to escape the cold winters and lake-effect snow, he chose Clemson University for an education in engineering and southern cuisine.

With the stress-relieving assistance of amusing roommates, mountain bikes, waffles, black coffee, and midnight trail runs, he graduated with a B.S. in Ceramic Engineering from Clemson University in May 2001. He worked as a Manufacturing Engineer with Corning Optical Fiber in Concord, North Carolina from June 2001 to October 2001. After a spirited bout with unemployment in the fall and winter of 2001-2002, he returned to Clemson, South Carolina in March 2002 and worked at the National Brick Research Center setting up an ASTM-based quality control system for one of the Center's member companies.

You have just completed reading the fruits of his year spent doing research for Professor Lorna Gibson at MIT. In addition to his research, he worked as a teaching assistant for 3.094 (Materials in Human Experience) in the Spring of 2003 and also helped to start an alternative energy journal club on campus in the Spring of 2004. He was a representative of the Graduate Materials Council to the Graduate Student Council for the 2003-2004 school year.

While he has no immediate employment obligations, he looks forward to the possibilities wrapped up in the vast expanse of a thousand tomorrows.

"In the motions and the things that you say, it all will fall, fall right into place."
-Modest Mouse